4-22-2021 10:00 AM

Catechol-Containing Copolymers As An Active Ingredient for Denture Adhesives

Vincent Ying Wun Kong, *The University of Western Ontario*

Supervisor: Charpentier, Paul A., *The University of Western Ontario*
Co-Supervisor: Rizkalla, Amin, *The University of Western Ontario*
A thesis submitted in partial fulfillment of the requirements for the Master of Engineering Science degree in Chemical and Biochemical Engineering

Abstract

Moisture inside the mouth adds challenge to making denture adhesives formulations. Some formulations have zinc to enhance adhesion on wet skin despite knowing the health hazards. Inspired by mussel foot proteins' catechol unit's strong underwater adhesion, nine catechol containing copolymers (P1A-P3C) were synthesized by free radical polymerization of 3,4-dimethoxystyrene (3,4- DMS) with different styrene derivatives followed by deprotection. P1A-P3C were used to make Fn(P)-C-PBS denture adhesive formulations which had suitable shear stresses around ≥ 5 kPa satisfying ISO 10873. In-situ NMR studies of free radical polymerization of 3,4 - DMS and styrene derivatives allowed computation of their reactivity ratios showing all copolymers are random. This work has shown the potential of polystyrene-based catechol copolymers for next generation denture adhesives.

Keywords

Mussel-inspired polymer, free radical polymerization, reactivity ratio, catechol, adhesion, denture adhesive

Summary for Lay Audience

Dentures are commonly worn accessories by the elderly population upon losing their real teeth. In conjunction, denture adhesives under brand names Poligrip, Effergrip, and Fixodent, are applied to stabilize the denture fitting inside the oral mucosa. To function, the denture adhesive draws saliva to swell and generate a cushion between the denture and oral mucosa. This prevents food particles being entrapped in between. However, some formulations include zinc to better the adhesion properties despite knowing the health hazards it can present to the body. According to ISO 10873, a standard for all commercial denture adhesives, all formulations must be non-toxic, have shear stress of 5 kPa or higher, and prevents denture from displacing for 12-16 hours. To develop a denture adhesive that adheres effectively on wet surfaces, researchers have turned their attention to mussel foot proteins and drawn inspiration from their catechol chemistry.

In this work, nine polystyrene-based catechol copolymers were made by polymerizing 3,4-dimethoxystyrene (3,4-DMS) and different styrene building blocks. The resulting copolymers were then treated with tribromo boron to provide catechol units in the chain. Subsequently, the copolymers were used to make denture adhesive formulations which were evaluated by lap shear experiments. The shear stress values were around ≥ 5 kPa which satisfies ISO 10873. In addition to evaluating their potential as active ingredients, the polymerization of 3,4 – DMS and styrene building blocks were studied under in-situ NMR. Doing so provides insight on the chain sequence of the copolymer as structure dictates both chemical and physical properties. From the in-situ NMR studies, all copolymers have a random sequence. This work has shown the potential of polystyrene-based catechol copolymers for next generation denture adhesives.

Acknowledgments

First and foremost, I would like to extend my gratitude towards Dr. Paul Charpentier for allowing me to join his group as an M.Eng student and later MESc. His wealth of knowledge and enthusiasm for science has been helpful throughout this project. I want to extend my appreciation to my co-supervisor Dr. Amin Rizkalla. Not only did he teach me biomaterials, but he also invested his time to help me run my specimens on the Instron which was vital to Chapter 3. His constructive feed back towards my work and desire to help me succeed will always be remembered. Next, I would like to thank Dr. William Zhu who was a great mentor throughout the mid-COVID-19 months of my studies. He guided me in many core tasks such as polymer synthesis, and running major instrumentations such as TGA, DSC, FTIR, NMR. Lastly, he helped me complete Chapter 3 & 4 by obtaining PDI values by GPC and computing the reactivity ratios of my monomers, respectively. To the rest of the Charpentier group members Dr. Olabode Oyeneye, Dr. Anil Atwal, Dr. Hanna Qin, Dr. Dicho Zomaya, Satyam Dixit, Kazi Naziba Tahsin, Shaun Fraser, Harrison Ng, and Devon Machin: thank you for being excellent peers by exchanging scientific knowledge, talking about future, going on coffee breaks or simply just being there to listen to any concerns, frustration or worries which made everyday less stressful.

To friends outside of the group Chantal Walker, Rebeca Arambula, Alice Li, Glenn De Souza, Steve Kong, Sandra Lopez, Dennise Sosa Carrero, Ugur Gulmen, Zhaoran Xin, Mai Thanh, Harpreet Atwal, Anika Wong, Pradip Mondal, and Aishik Chakraborty: You are the reason why graduate school was fun and enjoyable. Thank you everyone for all the insightful conversations, encounters in the hallways, and tolerating my unending weirdness.

Finally, I must give my biggest thanks to all my family and friends back in Vancouver, BC. No one knew there was going to be a pandemic which changed our world. To be honest, there have been many times I cried, felt scared and wanted to give up. What made the difference was your continuous love, encouragement, video chats, and constant reminder that God is good in all situations.

Table of Contents

List of Tables

List of Figures

List of Schemes

List of Abbreviations

^{1}H-NMR – proton nuclear magnetic resonance

2,6-DMS - 2,6 dimethoxystyrene

3,4-DMS – 3,4 – dimethoxystyrene

3-VCA - 3-vinylcatechol acetonide

4ms - 4-methylstyrene

4tbs - 4-tert-butylstyrene

4-VCA - 4-vinylcatechol acetonide

AIBN - 2,2′-Azobis (2-methylpropionitrile)

ATRP - atom transfer radical polymerization

CBZs – carboxybenzyls

Ceof - cyclic ethyl orthoformates

CTA - chain transfer agent

DCM – dichloromethane

DI – deionized

DMA - Dopamine methacrylate

DMAA - N,N'-dimethylacrylamide

DMAPMAAm - N-3-(dimethyl amino)propyl methacrylamide

DMF – dimethylformamide

DOPA - 3,4-dihydroxyphenylalanine

DSC - differential scanning microscopy

F-R – Fineman- Ross

FRP - free radical polymerization

FTIR - Fourier Transformation – Infrared Spectroscopy

GPC - gel permeation chromatography

H-bonding – hydrogen bonding

K-T - Kelen-Tüdös

LAM – less active monomer

LFRP - living free radical polymerization

LLS – linear least squares

MA - methyl acrylate

MAEP – monoacryloxyethyl phosphate

MAM – more active monomer

Me – methyl

MeOH – methanol

Mfps - mussel foot proteins

MMA - methyl methacrylate

NaCMC - sodium carboxymethylcellulose

NCA - N-carboxyanhydride

NLLS – non-linear least squares

NMP - nitroxide-mediated polymerization

NMR – nuclear magnetic resonance

NSD – numerical solution differential

NVP - N-vinylpyrrolidone

p(3,4-DHS-co-4-R-S) - poly (3,4-dihydroxystyrene-co-4-R-styrene)

p(3,4-DHS-co-sty) – poly (3,4-dihydroxy-co-styrene)

p(3,4-DHS-co-Sty) - poly (3,4-dihydroxystyrene-co-styrene)

p(DHS/S-alt-MA) - poly (3,4-dihydroxystyrene/styrene-alt-maleic acid)

p(DMS/S-alt-MA) - poly (3,4-dimethoxystyrene/styrene-alt-maleic acid)

PAA-MA - polyacrylic acid-maleic acid

PBS - phosphate buffer solution

PBVE-MA - poly butyl vinyl ether-maleic acid

PDI - polydispersity index

PEG - polyethylene glycol

PEGMEMA – poly (ethylene glycol) methyl ether methacrylate

PG – polyglycerol

PMMA - polymethyl methacrylate

PMVEMA - polymethyl vinyl ether/maleic acid

PS-MA - polystyrene-maleic acid

RAFT – reversible additional fragment transfer

ROMP - ring opening metathesis polymerization

Sty - styrene

TBC - tert-butylcatechol

TBDMS - t-butyldimethylsilyl

t-Bu – tert-butyl

TGA - thermogravimetric analysis

THF – tetrahydrofuran

Chapter 1

1 Introduction

1.1 Adhesive Formulations and their Drawbacks.

1.1.1 Synthetic Adhesives

Adhesives are ubiquitous, especially in automotive, electronics, furniture, construction, and consumer goods industries [1]. They are used to bond two or more objects together such as metals, ceramics, and polymers. Polymeric adhesives are single use materials which are derived from petroleum-based monomers [2]. Examples of these materials include epoxies, urethanes, acrylates, and cyanoacrylates [3] which are commercially available in the market. However, using them frequently in continually growing civilization leads to health issues. Most adhesive formulations are based on formaldehyde [1,4], such as urea-formaldehyde, phenol-formaldehyde, and melamine-formaldehyde which can off-gas the carcinogen [5]. Additionally, as synthetic adhesives continue to burgeon, renewability and degradability is traded-off for better adhesion. The permanent and non-degradable characteristics prevent disassembling and recycling of metals in electronics [6], and contributes to landfill [1,7].

1.1.2 Dentures and Denture Adhesive Formulations

As humans age, our teeth degrade resulting in mechanical difficulties in the mouth leading to denture usage. Dentures are replacement gums containing artificial teeth that can be placed into and taken out with the mouth. All dentures are custom made to provide comfort and to match the individual’s mouth profile. Dentures come in three types [8]: conventional full denture, immediate full denture, and partial denture (Figure 1.1).

Figure 1.1 Full denture (left) [8] and partial denture (right) [9].

A conventional full denture is placed after remaining teeth are removed and tissues are healed and gain their support from the neighbouring teeth and underlying bone. Immediate full denture is placed after remaining teeth are removed, however, relining is required as tissue healing changes the shape of the oral mucosa and loosens the denture. Partial dentures rest on a metal framework and attaches alongside with the natural teeth Dentures are mounted onto oral mucosa and stabilized with adhesives. In conjunction to the denture, denture adhesives are applied between the oral mucosa and the denture to prevent unwanted displacement of the denture from the mouth due to actions such as running, jumping, and eating etc. The presence of saliva swells the adhesive to reduce the void between the denture and the tissue resulting physical retention of the dentures. Historically, denture adhesives were first used in the late eighteenth century and first mentioned in the dental literature by the American Dental Association, Council of Dental Materials, Instruments and Equipments in 1935 [10]. Today, they can be in forms such as pastes, powders or adhesive pads [11] sold under brand names such as Effergrip, Fixodent, and Poligrip. Denture adhesive formulations include petrolatum, mineral oil, flavoring, optional dyes, cellulose gum and finally the active ingredient polymethyl vinyl ether maleic acid (PMVEMA) (Figure 1.2)[4,12].

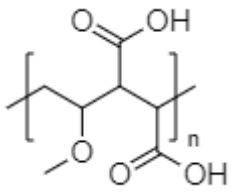

Figure 1.2 Polymethyl Vinyl Ether Maleic Acid (PMVEMA).

In some formulations, such as Fixodent, zinc is an additive to enhance adhesion [11]. Singh et al. [13] reported excessive zinc intake induces neuropathies such tingling, numbness, loss of mobility, poor coordination, abnormal blood pressure and heart rate, reduced perspiration, and both constipation and bladder dysfunction. ISO 10873, an international standard, classifies denture adhesives, specifies requirements, and test methods needed for all related commercial products [14]. According to ISO 10873, the ideal solution should be non-toxic, biocompatible, adhere well on wet tissue surfaces for 12-16 hours [14,15], decrease lateral and vertical movement of dentures and have a shear stress of ≥ 5 kPa . Developing tissue adhesives for the oral environment is challenging due to their moisture content [12].

1.2 Thesis Objectives

Catechol-containing copolymers based on polystyrene with increasing hydrophobic styrene co-monomers have yet to be reported. In Chapter 3, the polymeric system poly (3,4-dihydroxystyrene-co-styrene) (p(3,4-DHS-co-S)) will be evaluated for its potential as a denture adhesive. Advantages of this structure include accessible starting materials, no monomer synthesis, and it has been reported to be non-toxic [16]. Three sets of poly (3,4-dihydroxystyrene-co-4-R-styrene) (p(3,4-DHS-co-4-R-S)) derivatives (R = H (P1), Me (P2), and t-Bu (P3)) will be synthesized with 3,4-dimethoxystyrene (3,4- DMS) and the appropriate styrene derivative. Polymer analysis will include gel permeation chromatography (GPC) to determine molecular weights and dispersity, thermogravimetric analysis (TGA) for thermal stability, and differential scanning microscopy (DSC) for glass transition temperature. Additionally, the polymers will be included into a formula borrowed from Gill et al [12] and will be subjected to mechanical testing following the method outlined by Fallahi et al [14]. In Chapter 4, kinetic studies

will be carried out using in-situ NMR to monitor the free radical polymerization between 3,4-DMS and substituted styrene derivatives from Chapter 3 to compute their reactivity ratios to determine copolymer sequence. Finally, Chapter 5 will summarize all the results covered in chapters 3 and 4 along with suggested future works.

1.3 References

[1] H.M. Siebert, J.J. Wilker, Deriving Commercial Level Adhesive Performance from a Bio-Based Mussel Mimetic Polymer, ACS Sustainable Chem. Eng. 7 (2019) 13315–13323. https://doi.org/10.1021/acssuschemeng.9b02547.

[2] G. Schmidt, J.T. Woods, L.X.-B. Fung, C.J. Gilpin, B.R. Hamaker, J.J. Wilker, Strong Adhesives from Corn Protein and Tannic Acid, Advanced Sustainable Systems. 3 (2019) 1900077. https://doi.org/10.1002/adsu.201900077.

[3] G. Schmidt, B.R. Hamaker, J.J. Wilker, High Strength Adhesives from Catechol Cross-Linking of Zein Protein and Plant Phenolics, Advanced Sustainable Systems. 2 (2018) 1700159. https://doi.org/10.1002/adsu.201700159.

[4] N.L. Gilbert, D. Gauvin, M. Guay, M.-È. Héroux, G. Dupuis, M. Legris, C.C. Chan, R.N. Dietz, B. Lévesque, Housing characteristics and indoor concentrations of nitrogen dioxide and formaldehyde in Quebec City, Canada, Environmental Research. 102 (2006) 1–8. https://doi.org/10.1016/j.envres.2006.02.007.

[5] C.L. Jenkins, H.M. Siebert, J.J. Wilker, Integrating Mussel Chemistry into a Bio-Based Polymer to Create Degradable Adhesives, Macromolecules. 50 (2017) 561–568. https://doi.org/10.1021/acs.macromol.6b02213.

[6] V. Sahajwalla, V. Gaikwad, The present and future of e-waste plastics recycling, Current Opinion in Green and Sustainable Chemistry. 13 (2018) 102–107. https://doi.org/10.1016/j.cogsc.2018.06.006.

[7] J.M. Garcia, M.L. Robertson, The future of plastics recycling, Science. 358 (2017) 870–872. https://doi.org/10.1126/science.aaq0324.

[8] Collin, Understanding Dentures, Westermeier Martin Dental Care. (2018). https://wmsmile.com/understanding-dentures/ (accessed August 11, 2019).

[9] Partial Dentures: Costs, Types, & Benefits | DDS Dentures + Implant Solutions, (n.d.). https://www.dentalservice.net/dentures/partial-dentures/ (accessed April 7, 2021).

[10] J.E. Grasso, Denture adhesives, Dental Clinics. 48 (2004) 721–733. https://doi.org/10.1016/j.cden.2004.04.002.

[11] C. for D. and R. Health, Denture Adhesives, FDA. (2019). http://www.fda.gov/medical-devices/dental-devices/denture-adhesives (accessed November 18, 2019).

[12] S.K. Gill, N. Roohpour, P.D. Topham, B.J. Tighe, Tunable denture adhesives using biomimetic principles for enhanced tissue adhesion in moist environments, Acta Biomaterialia. 63 (2017) 326–335. https://doi.org/10.1016/j.actbio.2017.09.004.

[13] V.D. Singh, A. Chaturvedi, Denture Adhesive and Zinc Toxicity, 2 (2015) 2.

[14] A. Fallahi, N. Khadivi, N. Roohpour, A.M. Middleton, M. Kazemzadeh-Narbat, N. Annabi, A. Khademhosseini, A. Tamayol, Characterization, mechanistic analysis and improving the properties of denture adhesives, Dental Materials. 34 (2018) 120–131. https://doi.org/10.1016/j.dental.2017.09.015.

[15] 14:00-17:00, ISO 10873:2010, ISO. (n.d.). https://www.iso.org/cms/render/live/en/sites/isoorg/contents/data/standard/04/62/46254.html (accessed April 26, 2021).

[16] M.J. Brennan, H.J. Meredith, C.L. Jenkins, J.J. Wilker, J.C. Liu, Cytocompatibility studies of a biomimetic copolymer with simplified structure and high-strength adhesion, Journal of Biomedical Materials Research Part A. 104 (2016) 983–990. https://doi.org/10.1002/jbm.a.35633.

Chapter 2

2 Literature Review

2.1 Mussels

2.1.1 Mussel Foot Proteins

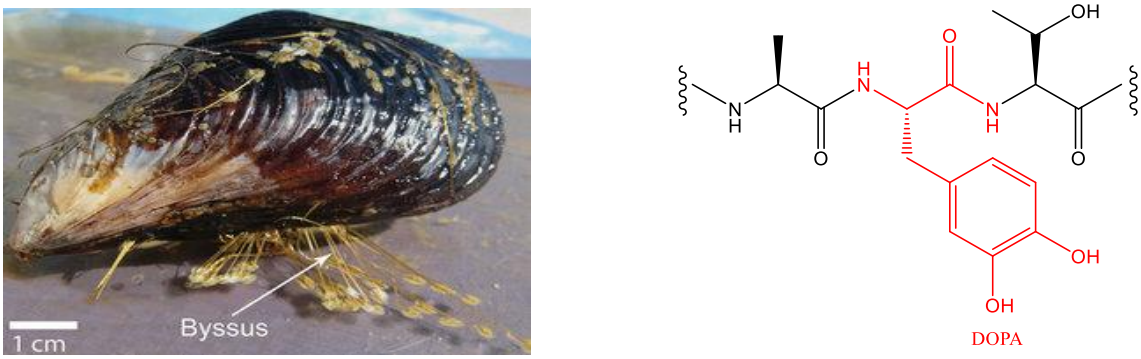

Figure 2.1 A mussel and its byssus threads (left) [13] and 3,4-dihydroxyphenylalanine (DOPA) in the polypeptide chain of mfps (right) [14].

Mussels (Figure 2.1) are marine creatures that are regarded as experts on adhering to surfaces under wet conditions using mussel foot proteins (mfps) [1,5,15–18] located in the byssus. Byssus' impressive adhesion properties come from the catechol unit of the amino acid 3,4-dihydroxyphenylalanine (DOPA) in the polypeptide chain [2–4] of mfps. To understand marine adhesion technology, it is important to look at the structure of a single byssal thread (Figure 2.2).

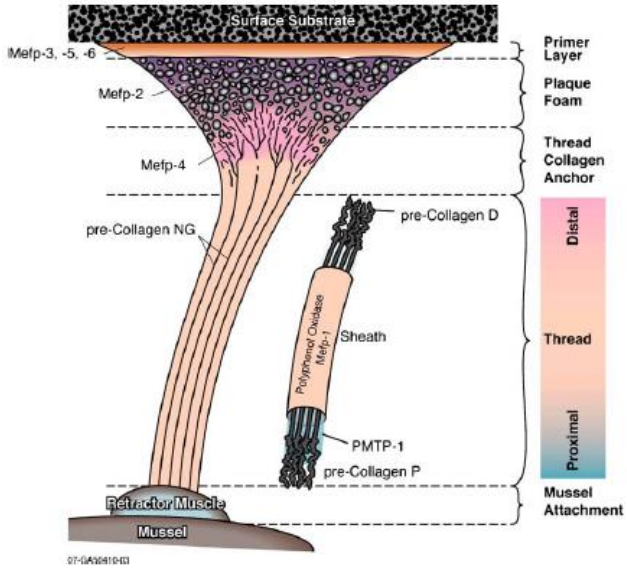

Figure 2.2 Structure of singular byssal thread containing mfps 2-6. Adapted from Silverman and Roberto [5]. Note that Mefp is used in [5] originally.

A single byssus contains two components, the byssal thread (distal and proximal) and the byssal plaque. A byssus consists of six mussel foot proteins named mfp-1 to mfp-6 [6,7], and their locations, mass, functions and DOPA contents are summarized on Table 2.1.

Table 2.1 Mfps and their location, mass, function, and DOPA contents [8].

Mfp	Location	Mass (kDa)	Function	DOPA (%)
1	Cuticle	108	Sheathing	10-15
2	Plaque	42-45	Structuring integrity	5
			Adhesion	> 20 (f)
3	Plaque	5-7		5-10 (s)
4	Plaque	90	Links plaque to shock-proof thread	2
5	Plaque	9	Adhesion, interfacial binding	30
6	Plaque	11	Controls redox chemistry	2

Mfp-1, a basic protein which is in the cuticle of the byssus thread and plaque. It has a high molecular weight of 108 kDa and serves as the protective sheath for the other mfps [7,9]. Mfp-2 is a smaller and most abundant protein in the plaque with 25 weight percentage and have with molecular weight of 42–47 kDa. Mfp-2 provides structural integrity to the byssal plaque by its high content of cysteine (6 mol %) in its protein chain joined by sulfur-sulfur (S-S) bonds [10] and given it is a secondary structure [6]. Mfp-4, a

decapeptide of 90 kDa, binds strongly onto metal ions due to the ligation effect of the rich histidine content within its chain [7]. Mfp-4 is found in between the byssal plaque and the distal portion of the byssal thread to effectively join the plaque proteins with distal collagen and proximal collagen [5,7,11]. The Col-P is a protein which provides the byssus the ability to absorb shock and extensibility. Mfp-3, 5, and 6 are found at the plaque of the byssus contributing to strong adhesion in wet environments. Mfp-3 is the smallest adhesive protein within the plaque with molecular weight of 5–7 kDa and has two polymorphic forms Mfp-3 fast (Mfp-3f) and slow (Mfp-3s) [12]. Both Mfp-3 proteins are rich in glycine and asparagine. Additionally, Mfp-3f exhibits higher contents DOPA (> 20 mol %) and 4-hydroxyarginine, and positively charged residues which makes it hydrophilic. On the other hand, Mfp-3s has lower DOPA content (5–10 mol %) alongside with a lower charge density compared to Mfp-3f, making it more of a hydrophobic protein [7]. Mfp-5 (9 kDa) contains the highest DOPA (30 mol %) content amongst all the plague protein and its hydrophilic character is attributed to the cationic amino acids present [12]. Additionally, Mfp-5 also contains variable amounts of post-translationally modified phosphoserine to bind to calcareous mineral materials suggesting it is an important role in interfacial binding [5,7]. Unlike Mfp-3 and 5, Mfp-6 contains the least amount of DOPA (3 mol %) content as the tyrosine residues in Mfp-6 are not efficiently converted to DOPA. To compensate for the lack of DOPA, Mfp-6 has the highest contents of charged residues along with cysteine present in the form of disulfide bonds. The thiols present gives Mfp-6 the unique ability to control the redox chemistry of DOPA present in other plaque proteins [13]. Redox control is vital especially when auto-oxidation of the catechol into its quinone form is detrimental to the adhesion performance of the proteins [6]. The DOPA content does not exceed over 30% within a byssus as it leads to excessive crosslinking which introduces extra cohesion in the system while reducing the surface adhesion as the trade off [4,14,15].

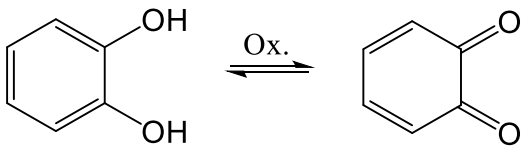

Figure 2.3 Catechol and quinone.

2.2 Catechol Chemistry

The abundant in DOPA content in mfps which contain catechol units which fulfill the dual role of interfacial binding and the solidification of the adhesive proteins [7,16]. Catechol can undergo a diverse range of chemistries to form reversible non-covalent (hydrogen bonding, π–π, cation – π, and metal coordination) or irreversible covalent (oxidative cross-linking and Michael addition) interactions to bind to both organic and inorganic surfaces.

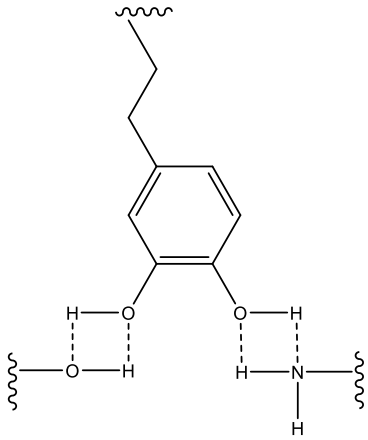

Figure 2.4 Hydrogen Bonding (H-bonding) of catechol.

The two hydroxy functional groups of catechol forms strong hydrogen bonds (H-bonds) (Figure 2.4) which enables the protein to adhere onto the surface of mucosal tissues [17] and hydroxyapatite [18]. H-bonds is a form of dipole–dipole bond which is stronger than van der Waals forces, but weaker than covalent bonds [19]. This dipole-dipole bond involves a hydrogen atom that bounds to a more electronegative atom/group with a lone pair. Some H-bonds are stronger than those formed by water. For example, when catechol binds to a surface through H-bonding, it forms bidentate hydrogen bonds that allows catechol groups to displace water from the surface [19,20].

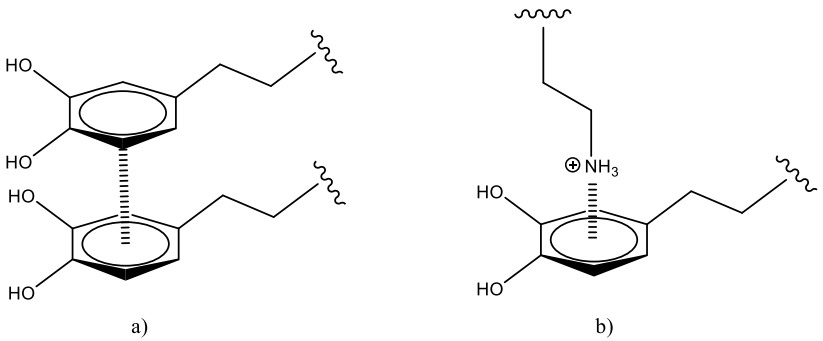

Figure 2.5 Catechol unit undergoing a) π-π and b) cation - π interactions.

The benzene ring of catechol contributes to the cohesive properties of catechol-containing polymers and enables them to attach to rich aromatic surfaces via π–π electron interactions (Figure 2.5 a) [7,21,22]. Additionally, catechol undergoes cation - π interactions to enhance absorption onto charged surfaces and contributes to cohesion property of materials abundant in both cationic and aromatic functional groups [7,23]. Cation - π interactions (Figure 2.5 b) are also important for coacervation, which is the fluid–fluid phase separation of ionic polymers or proteins from the aqueous solution [24]. The formed coacervate features water immiscibility, and low surface tension, allowing stability under water and spreadable on many submerged surfaces [25] which is important for mussel's bio adhesion [19]. Maier et al. [26] stressed the importance of catechol-cation synergy for underwater adhesion through the plant pathogen *Dickeya chrysanthemi*'s adjacent catechol–lysine within its structure and the lysine can repel hydrated cations at the mica surface allowing more catechol binding [27].

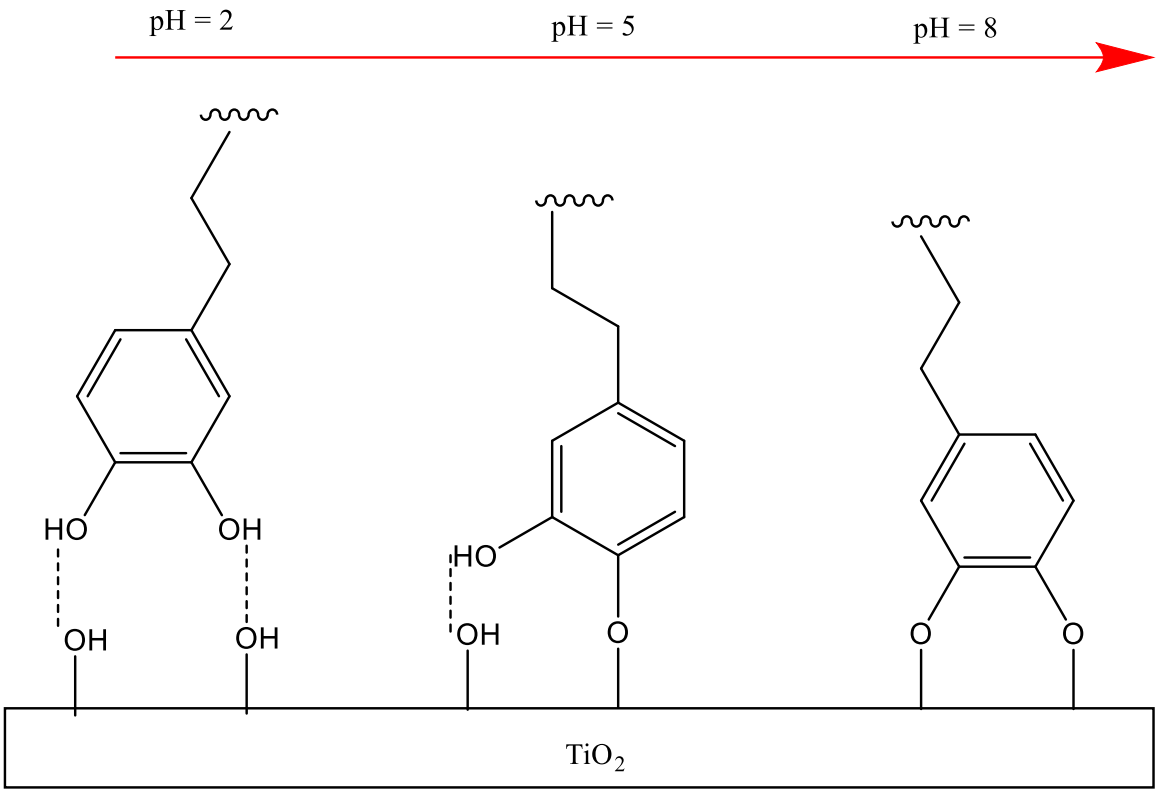

Figure 2.6 The effect of pH on catechol coordination on TiO_2 surface.

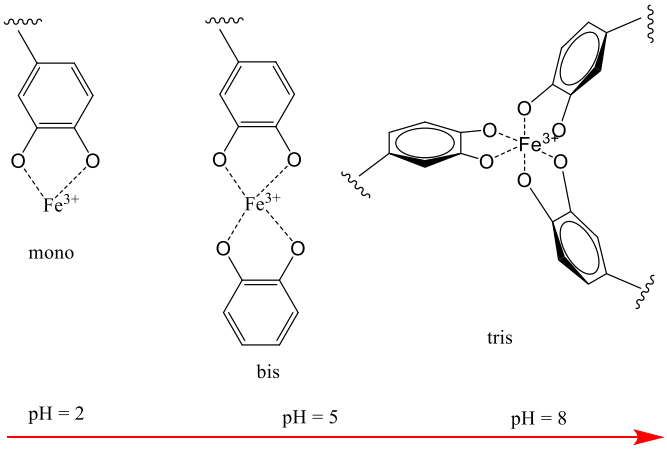

Figure 2.7 Stoichiometric catechol-Fe 3+ complexes from acidic to basic pH.

The catechol unit of DOPA is a bidentate ligand which can coordinate to metallic materials through the interactions between the two hydroxy groups and metal atoms of the surface. Hydrogen bonding in tandem with coordination bonding helps maintain the interfacial bonding, both which are dependent on the pH of the media [28]. For example,

on titania (TiO_2) the catechol coordination transitions from two H-bonds (pH = 2) to one H-bond plus monodentate coordination (pH = 5), and lastly, bidentate coordination (pH = 8) [29–32]. With regards to iron (Figure 2.7), catechol can stoichiometrically chelate to the metal forming mono-, bis and finally tris-catecholate–Fe3+ complexes as pH increase [20]. In sea water (pH ~ 8), more catechol in its deprotonated form giving rise to more ligation to form the tris- complex. The strength of catechol–Fe3+ pars with H-bonding, and reversible making it robust [33]. To promote catechol – metal complex formations, a reported strategy is to replace the para aromatic proton in the catechol side chain is with an electron withdrawing group such as chloro- [34] and nitro- [35]. These modifications enhance interfacial binding and lower the dissociation constants (pKa) of the catechol hydroxyl groups, allowing catechol–metal ion complexes formation at reduced pH and with a higher stoichiometry [36].

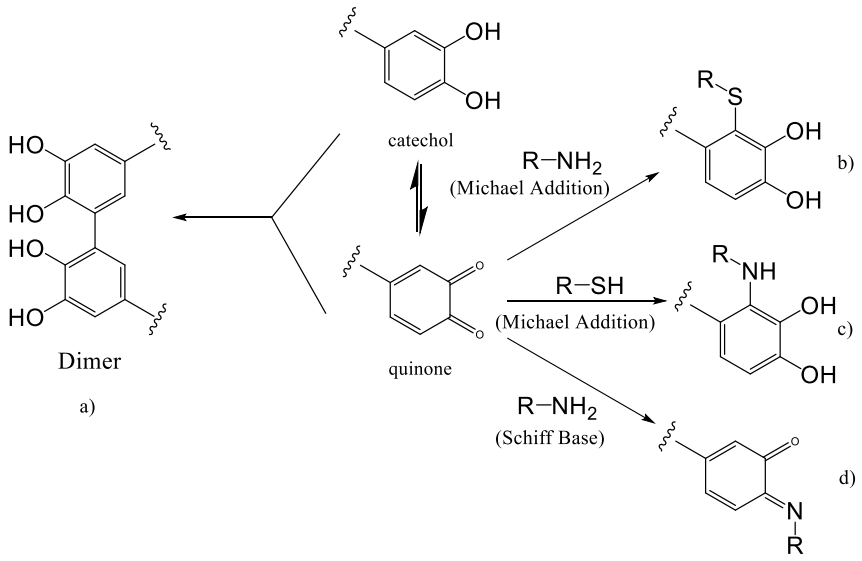

Figure 2.8 Catechol oxidation to quinone and its crosslinking pathways a) dimerization, b) Michael addition of -NH_2, c) Michael addition of -SH, and d) Schiff base formation.

As mentioned previously, auto-oxidation of the catechol unit reduces the performance of protein adhesions. Having control of catechol oxidations is also crucial for strong adhesion and cohesive strength of mussel proteins. Curing, which is defined as the hardening process of the mussel proteins leading to adhesion [5], can be controlled by

adjusting variables such as time, pH, choice of chemical oxidants [19]. Catechol oxidizes to the highly reactive quinone, which can undergo various covalent cross-linking reactions to enhance the strength of underwater adhesion [37]. The quinone and another catechol unit can dimerize (Figure 2.8 a) and subsequently polymerize resulting in the curing of catechol containing polymer under influences such as elevated pH, metal ions or oxidizing agents [5,38]. Through the Michael addition reaction, the quinone can react with functional groups such as $–NH_2$ (Figure 2.8 b) and –SH (Figure 2.8 c) to form amines and thiol ethers, respectively. The $–NH_2$ can also condense with one of the carbonyls of the quinone to form a Schiff base (Figure 2.8 d) [19].

2.2.1 Preparation of Catechol-Functionalized Polymers

There is a plethora of synthetic strategies to prepare of mussel - inspired polymers with various catechol derivatives possessing both strong wet adhesion and rapid curing abilities. These examples include i) direct functionalization of polymers with catechol, ii) polymerization of catechol-modified monomers, and the use of iii) catechol-functionalized initiator to polymerize synthetic monomers [7].

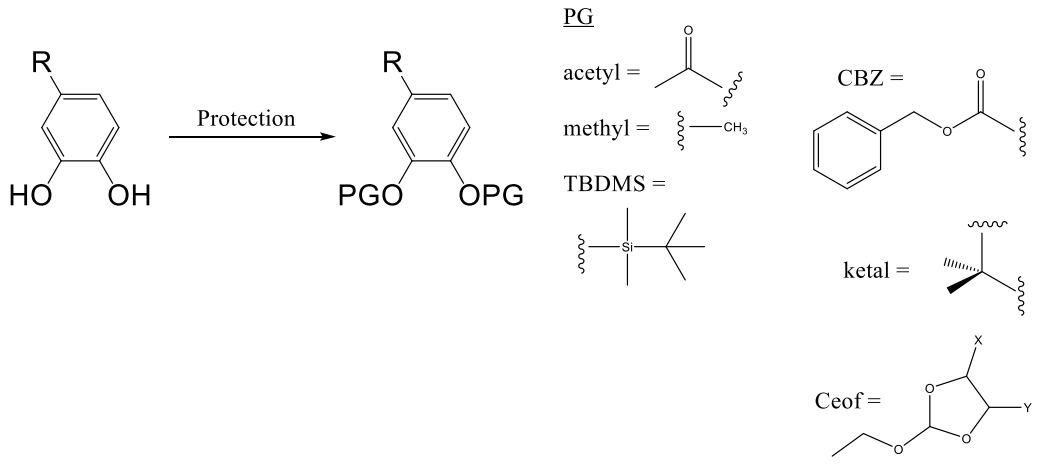

Figure 2.9 Protection of catechol with listed protecting groups (PGs).

Firstly, the protection of the catechol side chains is mandatory as oxidation and unwanted chemical reactions may affect their reactivity and properties. The presence of oxygen introduces issues such as quinone formation from auto-oxidation and inhibition of free radical polymerization [7,39]. A chemical protecting group [2] and elimination of oxygen

[40] can prevent such outcomes. The protecting group should remain stable during the entire synthetic process while the choice of the deprotection method should be relative to the type of protection group. Given catechol is an aromatic ortho-diol, suitable protecting groups (Figure 2.8) include acetyls [41], methyl ethers [2], t-butyldimethylsilyl (TBDMS) [42–44], carboxybenzyls (CBZs) or bridged protection groups such as ketals [45] and cyclic ethyl orthoformates (ceof) [46].

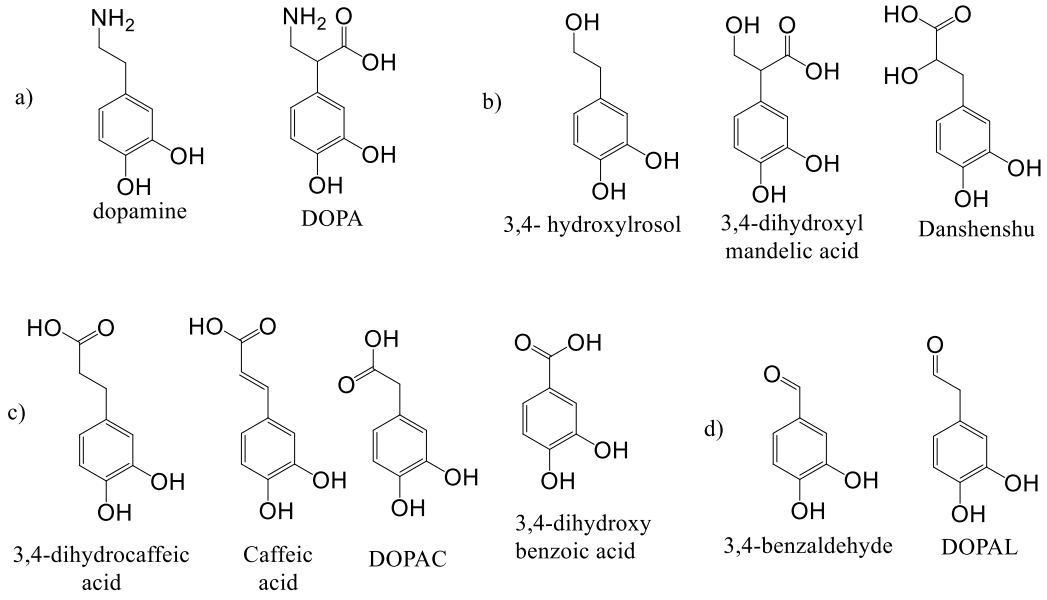

Figure 2.10 List of common catechol building blocks with functional groups such as a) -NH2 (amines), b) -OH (hydroxyls), c) -CO2H (carboxylic acid), and d) -CHO (aldehyde) to functionalize available polymers.

Direct catechol functionalization involves chemical conjugation between a catechol unit with functional group such as -NH_2 (Figure 2.10 a), -OH (Figure 2.10 b), -CO_2H (Figure 2.10 c), CHO (Figure 2.10 d) etc. onto readily available synthetic or natural polymers forming amides, esters and other linkages taking on side-chain or end-chain architectures [47].

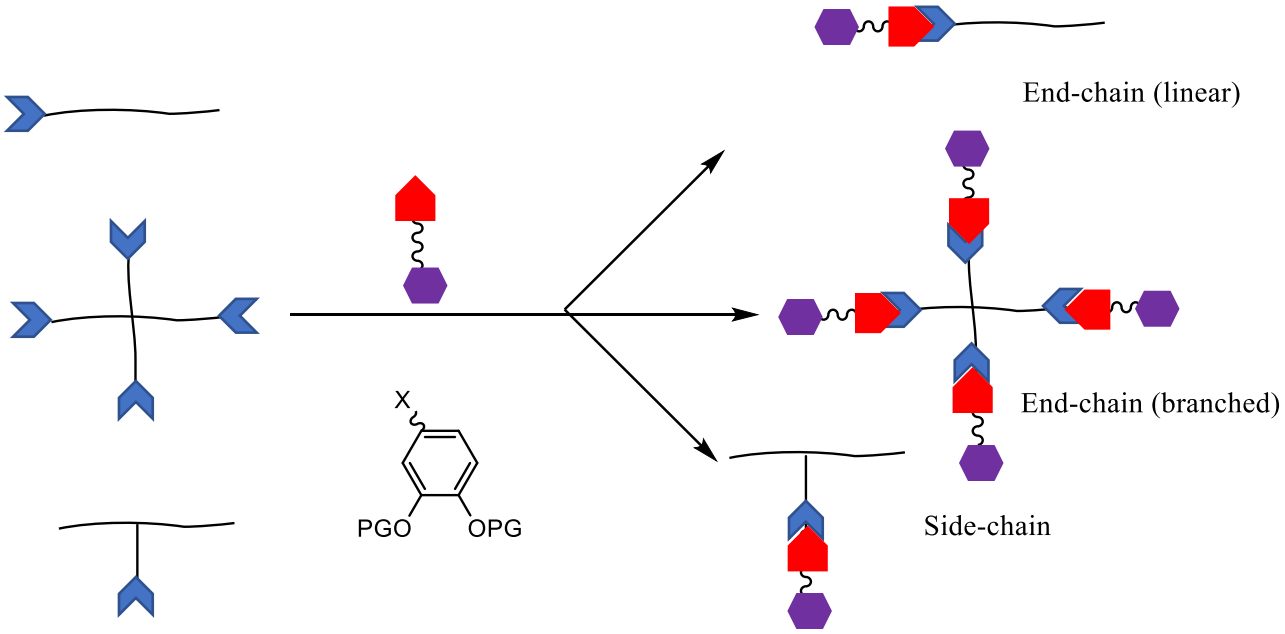

Figure 2.11 Architectures of direct catechol-functionalized polymers.

Regarding end-chained polymers, examples include -NH_2 or -CO_2H terminated 4-armed polyethylene glycol (PEG) and -NH_2 terminated polyglycerol (PG) which is biocompatible, hydrophilic, and inert making it appealing for various biomedical applications [7,47]. Barrett et al. [48] using -CO_2H terminated 4-armed PEG and functionalized with dopamine for negative-swelling tissue adhesives with heat-sensitivity. Holten-Anderson et al. [49] combined -NH_2 terminated 4 armed PEG with 3,4-dihydrocaffeic acid to generate self-healing hydrogels through Fe^{3+} coordination. Wei et al. [50] conjugated -NH_2 terminated PG with 3,4-dihydrocaffeic acid and the resulting material can adhere to TiO_2 and polystyrene surfaces providing anti-fouling properties. In brief, catechol functionalized side-chain polymers can be obtained by taking biopolymers such as alginate (anti-bacterial films) [51], gelatin (tissue adhesive) [52], p (L-glutamic acid) (biodegradable capsules for therapeutic releases) [53], heparin (cell culture medium) [54], hyaluronic acid (drug carrier) [55], and xanthan gum (injectable shear-thinning hydrogel) [56] can be conjugated with dopamine whereas chitosan (self-healing haemostatic needles) [57] can be conjugated with 3,4-dihydrocaffeic acid.

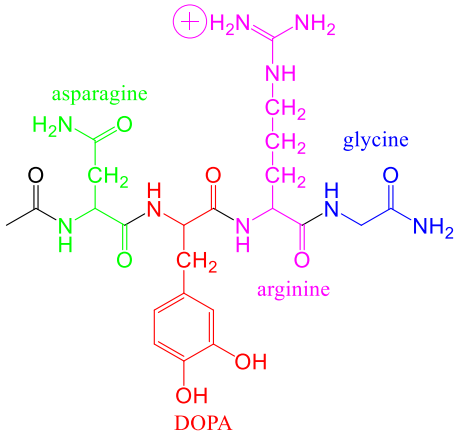

Figure 2.12 DOPA polypeptide with sequence asparagine-DOPA-arginine-glycine prepared through solid-phase synthesis by Sever and Wilker [58].

Catechol-containing monomers can be synthesized and polymerized subsequently. DOPA polypeptides were one of the earliest examples of mussel-inspired prepared by solid- or solution-phase peptide chemistry [47]. One example, Sever and Wilker [58] designed a biomimetic polypeptide containing the sequence asparagine-DOPA-arginine-glycine (Figure 2.12) by solid-phase method.

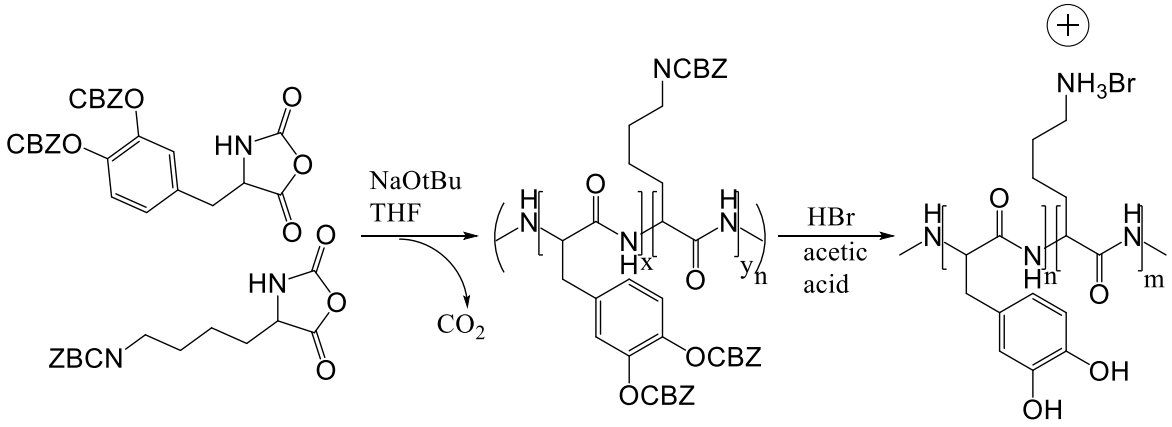

Figure 2.13 Yu and Deming's ring opening polymerization of catechol and lysine functionalized N-carboxyanhydrides (NCAs) followed by deprotection to yield co-polypeptide [59].

Later, co-polypeptides can be prepared using functionalized N-carboxyanhydride (NCA) monomers [47]. NCAs are prepared by subjecting amino acids to liquid phosgene and can be polymerized into polypeptides via ring-opening addition reactions that rids carbon dioxide as a by-product [59]. One example, Yu and Deming [59] prepared NCAs functionalized with CBZ-protected DOPA and lysine followed by their polymerization using sodium tert-butoxide (NaOtBu) in tetrahydrofuran (THF), and finished with their CBZ removal using hydrobromic acid (HBr) in acetic acid.

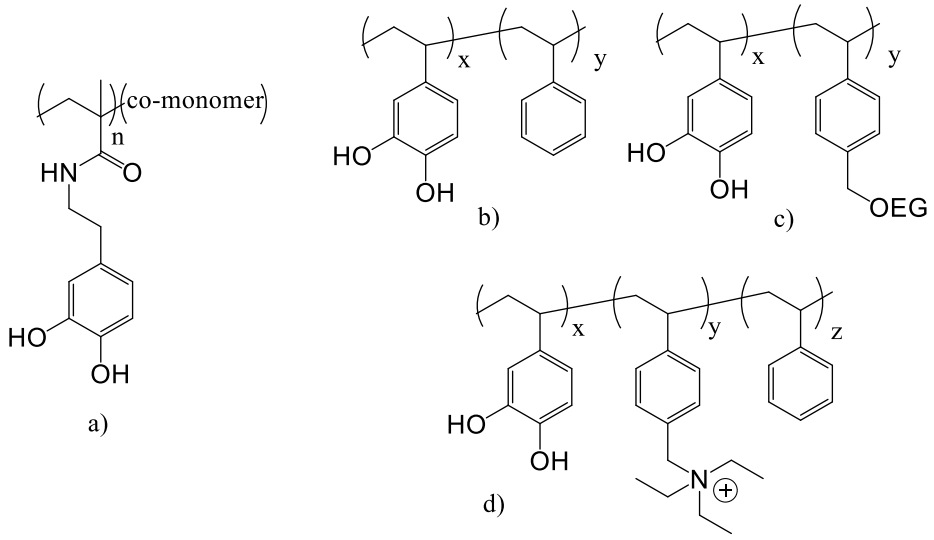

Figure 2.14 Mussel-inspired polymers based on a) poly (dopamine-co-monomers) and polystyrenes b) poly (3,4-dihydroxy-co-styrene), c) poly (3,4-dihydroxy-co-4-oligo-ethylene glycol styrene), and d) poly[(3,4-dihydroxystyrene)-co- (p-vinyltolyltriethylammonium chloride)-co-styrene].

Dopamine methacrylate (DMA), another commonly used catechol monomer has been copolymerized along with co-monomers (Figure 2.14 a) such as methyl methacrylate (MMA) [60], poly(ethylene glycol) methyl ether methacrylate (PEGMEMA) [60,61], N-3-(dimethyl amino)propyl methacrylamide (DMAPMAAm) [62], N,N'-dimethylacrylamide (DMAA) [63], cholic acid [63], and monoacryloxyethyl phosphate (MAEP) [64] to make mussel-mimetic polymers for protein repellency, bacterial binding, or drug release. Similarly, a polystyrene-base mussel polymer can be made using 3,4-DMS as the key component along with styrene [2,65,66] (Figure 2.14 b) and other

styrene-related monomers such as 4-vinylbenzylchloride [67] to be functionalized with oligo-ethylene glycols [68] (Figure 2.14 c) and cations (Figure 2.14 d).

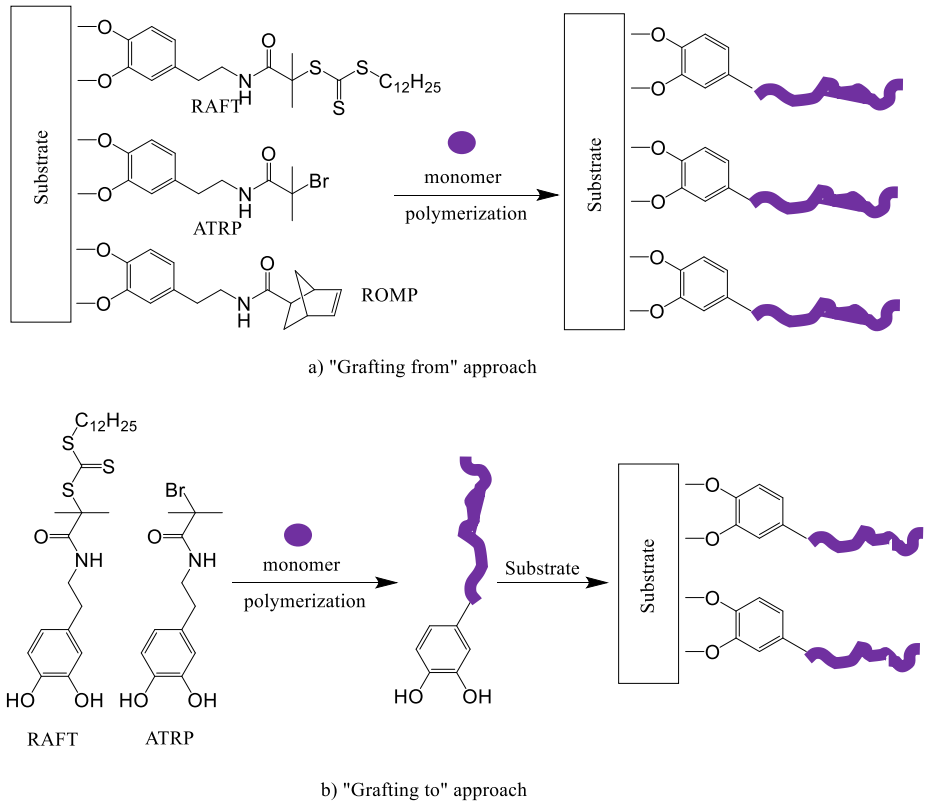

Figure 2.15 a) "Grafting from" and b) "Grafting to" approaches on substrates using catechol-functionalized initiators.

Extending from end-chained functionalized polymers, catechol-modified initiators have been developed to modify various surface substrates via “grafting from” or “grafting to” approach. Systems such as dopamine functionalized with a reversible addition-fragmentation chain transfer (RAFT) agent, or an alkyl bromine for atom transfer radical polymerization (ATRP), or lastly, a ring-opening moiety for ring opening metathesis polymerization (ROMP) [7,47]. Substrates subjected to either approach includes but not limited to graphene [69], titanium [70], iron oxide (Fe_3O_4) [71], and gold [72]. The “grafting from” approach (Figure 2.15 a) involves a substrate modified with a

catechol-functionalized initiator followed by surface-initiated polymerization of monomers. On the other hand, the “grafting to” approach (Figure 2.15 b) involves polymerizing monomers using a catechol-functionalized initiator (protected or unprotected) and subsequently using it to modify surfaces of choice.

2.3 Living Free Radical Polymerization

Due to its applicability, versatility and low cost, free radical polymerization (FRP) has been employed to generate polymers of high molecular weight at the commercial scale. However, it is notorious for giving rise to polymers to high polydispersity indexes (PDI > 1.5) [73] and high viscosity in tandem. This can be explained by looking at Scheme 2.1.

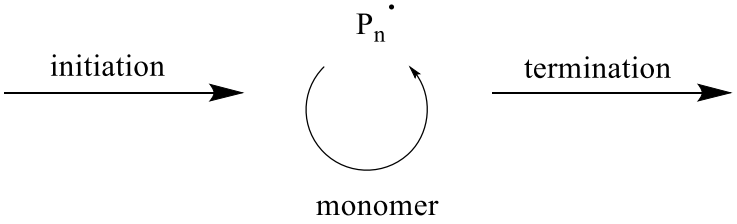

Scheme 2.1 Conventional free radical polymerization [73].

In a conventional free radical polymerization, polymeric chains are formed continuously, propagated, and are terminated by radical–radical reaction. The high molecular weight (MW) of chains formed in the early stages of the reaction is due to the steady-state concentration of propagating species being around 10^{-7} M, and individual chains grow for 5–10 s before terminating [73]. To overcome such issues, living free radical polymerization (LFRP) is of high regard. The term “living” implies a linear increase of molecular weight as a function of monomer(s) conversion. In an ideal living polymerization, all chains are initiated at the start of the reaction and grow at the same rate with the absence of the termination step. Thus, living radical polymerization is only possible in the presence of reagents that react with the propagating radicals by reversible deactivation or reversible chain transfer [73]. Up to this date, three commonly used LFRPs include nitroxide-mediated polymerization (NMP), atom transfer radical

polymerization (ATRP) and reversible addition-fragmentation chain transfer (RAFT) polymerization [74]. Of the three listed LFRPs, RAFT can control chain growth via reversible chain transfer to generate polymers to controlled complex structures [75].

2.4 RAFT Polymerization

RAFT polymerization is a LFRP developed in 1998 at the Commonwealth Scientific and Industrial Research Organization (CSIRO) located in Australia [76]. Advantages wise, RAFT offers its compatibility towards a huge library of monomers including but not limited to styrenes [77], acrylates [78], acrylamides [79], methacrylates [80], methacrylamides [79], vinyl esters [81], and vinyl amides [82]. Additionally, RAFT can be performed under mild temperatures, tolerate the polarity of unprotected functional groups on monomers, using many common solvents (aqueous, protic, or non-protic). Furthermore, RAFT can be performed using the same conditions as a conventional free radical polymerization, plus the introduction of a chain transfer agent (CTA), also known as the RAFT agent. Given these advantages, RAFT can be done in various modes of free radical polymerization such as bulk, solution, suspension, emulsion and microemulsion [73]. Because of RAFT, making polymers with architectures with defined structure such as blocks [83], stars [73], combs [84], grafts [47], and gradients [85] is possible.

2.5 References

[1] Mighty Mussels Have Industrial Strength, NPR.Org. (n.d.). https://www.npr.org/templates/story/story.php?storyId=124319594 (accessed August 17, 2020).

[2] G. Westwood, T.N. Horton, J.J. Wilker, Simplified Polymer Mimics of Cross-Linking Adhesive Proteins, Macromolecules. 40 (2007) 3960–3964. https://doi.org/10.1021/ma0703002.

[3] S.C.T. Nicklisch, J.H. Waite, Mini-review: The role of redox in Dopa-mediated marine adhesion, Biofouling. 28 (2012) 865–877. https://doi.org/10.1080/08927014.2012.719023.

[4] M. Rahimnejad, W. Zhong, Mussel-inspired hydrogel tissue adhesives for wound closure, RSC Advances. 7 (2017) 47380–47396. https://doi.org/10.1039/C7RA06743G.

[5] H.G. Silverman, F.F. Roberto, Understanding Marine Mussel Adhesion, Mar Biotechnol. 9 (2007) 661–681. https://doi.org/10.1007/s10126-007-9053-x.

[6] A.H. Hofman, I.A. van Hees, J. Yang, M. Kamperman, Bioinspired Underwater Adhesives by Using the Supramolecular Toolbox, Advanced Materials. 30 (2018) 1704640. https://doi.org/10.1002/adma.201704640.

[7] P.K. Forooshani, B.P. Lee, Recent approaches in designing bioadhesive materials inspired by mussel adhesive protein, Journal of Polymer Science Part A: Polymer Chemistry. 55 (2017) 9–33. https://doi.org/10.1002/pola.28368.

[8] Q. Lin, D. Gourdon, C. Sun, N. Holten-Andersen, T.H. Anderson, J.H. Waite, J.N. Israelachvili, Adhesion mechanisms of the mussel foot proteins mfp-1 and mfp-3, Proc Natl Acad Sci U S A. 104 (2007) 3782–3786. https://doi.org/10.1073/pnas.0607852104.

[9] C.V. Benedict, J.H. Waite, Composition and ultrastructure of the byssus of Mytilus edulis, Journal of Morphology. 189 (1986) 261–270. https://doi.org/10.1002/jmor.1051890305.

[10] L.M. Rzepecki, K.M. Hansen, J.H. Waite, Characterization of a Cystine-Rich Polyphenolic Protein Family from the Blue Mussel Mytilus edulis L, The Biological Bulletin. (2016). https://doi.org/10.2307/1542413.

[11] K.J. Coyne, X.-X. Qin, J.H. Waite, Extensible Collagen in Mussel Byssus: A Natural Block Copolymer, Science. 277 (1997) 1830–1832. https://doi.org/10.1126/science.277.5333.1830.

[12] H. Zhao, N.B. Robertson, S.A. Jewhurst, J.H. Waite, Probing the Adhesive Footprints of Mytilus californianus Byssus, J. Biol. Chem. 281 (2006) 11090–11096. https://doi.org/10.1074/jbc.M510792200.

[13] J. Yu, Antioxidant is a Key Factor in Mussel Protein Adhesion, in: J. Yu (Ed.), Adhesive Interactions of Mussel Foot Proteins, Springer International Publishing, Cham, 2014: pp. 31–41. https://doi.org/10.1007/978-3-319-06031-6_4.

[14] K.M. Gray, E. Kim, L.-Q. Wu, Y. Liu, W.E. Bentley, G.F. Payne, Biomimetic fabrication of information-rich phenolic-chitosan films, Soft Matter. 7 (2011) 9601–9615. https://doi.org/10.1039/C1SM05293D.

[15] C. Ghobril, M.W. Grinstaff, The chemistry and engineering of polymeric hydrogel adhesives for wound closure: a tutorial, Chem. Soc. Rev. 44 (2015) 1820–1835. https://doi.org/10.1039/C4CS00332B.

[16] J.H. Waite, M.L. Tanzer, Polyphenolic Substance of Mytilus edulis: Novel Adhesive Containing L-Dopa and Hydroxyproline, Science. 212 (1981) 1038–1040. https://doi.org/10.1126/science.212.4498.1038.

[17] J. Schnurrer, C.-M. Lehr, Mucoadhesive properties of the mussel adhesive protein, International Journal of Pharmaceutics. 141 (1996) 251–256. https://doi.org/10.1016/0378-5173(96)04625-X.

[18] W.M. Chirdon, W.J. O'Brien, R.E. Robertson, Adsorption of catechol and comparative solutes on hydroxyapatite, Journal of Biomedical Materials Research Part B: Applied Biomaterials. 66B (2003) 532–538. https://doi.org/10.1002/jbm.b.10041.

[19] W. Zhang, R. Wang, Z. Sun, X. Zhu, Q. Zhao, T. Zhang, A. Cholewinski, F. (Kuo) Yang, B. Zhao, R. Pinnaratip, P.K. Forooshani, B.P. Lee, Catechol-functionalized hydrogels: biomimetic design, adhesion mechanism, and biomedical applications, Chem. Soc. Rev. 49 (2020) 433–464. https://doi.org/10.1039/C9CS00285E.

[20] J. Saiz-Poseu, J. Mancebo-Aracil, F. Nador, F. Busqué, D. Ruiz-Molina, The Chemistry behind Catechol-Based Adhesion, Angewandte Chemie International Edition. 58 (2019) 696–714. https://doi.org/10.1002/anie.201801063.

[21] J.H. Waite, Nature's underwater adhesive specialist, International Journal of Adhesion and Adhesives. 7 (1987) 9–14. https://doi.org/10.1016/0143-7496(87)90048-0.

[22] J.H. Waiter, Reverse Engineering of Bioadhesion in Marine Mussels, Annals of the New York Academy of Sciences. 875 (1999) 301–309. https://doi.org/10.1111/j.1749-6632.1999.tb08513.x.

[23] S. Das, N.R.M. Rodriguez, W. Wei, J.H. Waite, J.N. Israelachvili, Peptide Length and Dopa Determine Iron-Mediated Cohesion of Mussel Foot Proteins, Advanced Functional Materials. 25 (2015) 5840–5847. https://doi.org/10.1002/adfm.201502256.

[24] W. Zhao, Y. Wang, Coacervation with surfactants: From single-chain surfactants to gemini surfactants, Advances in Colloid and Interface Science. 239 (2017) 199–212. https://doi.org/10.1016/j.cis.2016.04.005.

[25] W. Wei, L. Petrone, Y. Tan, H. Cai, J.N. Israelachvili, A. Miserez, J.H. Waite, An Underwater Surface-Drying Peptide Inspired by a Mussel Adhesive Protein, Advanced Functional Materials. 26 (2016) 3496–3507. https://doi.org/10.1002/adfm.201600210.

[26] Adaptive synergy between catechol and lysine promotes wet adhesion by surface salt displacement | Science, (n.d.). https://science-sciencemag-org.proxy1.lib.uwo.ca/content/349/6248/628 (accessed November 30, 2020).

[27] M.V. Rapp, G.P. Maier, H.A. Dobbs, N.J. Higdon, J.H. Waite, A. Butler, J.N. Israelachvili, Defining the Catechol–Cation Synergy for Enhanced Wet Adhesion to Mineral Surfaces, J. Am. Chem. Soc. 138 (2016) 9013–9016. https://doi.org/10.1021/jacs.6b03453.

[28] J. Yu, W. Wei, E. Danner, R.K. Ashley, J.N. Israelachvili, J.H. Waite, Mussel protein adhesion depends on interprotein thiol-mediated redox modulation, Nature Chemical Biology. 7 (2011) 588–590. https://doi.org/10.1038/nchembio.630.

[29] S. Bahri, C.M. Jonsson, C.L. Jonsson, D. Azzolini, D.A. Sverjensky, R.M. Hazen, Adsorption and Surface Complexation Study of L-DOPA on Rutile (α-TiO2) in NaCl

Solutions, Environ. Sci. Technol. 45 (2011) 3959–3966. https://doi.org/10.1021/es1042832.

[30] M. Vega-Arroyo, P.R. LeBreton, T. Rajh, P. Zapol, L.A. Curtiss, Density functional study of the TiO2–dopamine complex, Chemical Physics Letters. 406 (2005) 306–311. https://doi.org/10.1016/j.cplett.2005.03.029.

[31] S.-C. Li, L.-N. Chu, X.-Q. Gong, U. Diebold, Hydrogen Bonding Controls the Dynamics of Catechol Adsorbed on a TiO2(110) Surface, Science. 328 (2010) 882–884. https://doi.org/10.1126/science.1188328.

[32] J.H. Waite, Mussel adhesion – essential footwork, Journal of Experimental Biology. 220 (2017) 517–530. https://doi.org/10.1242/jeb.134056.

[33] B.P. Lee, A. Narkar, R. Wilharm, Effect of metal ion type on the movement of hydrogel actuator based on catechol-metal ion coordination chemistry, Sensors and Actuators B: Chemical. 227 (2016) 248–254. https://doi.org/10.1016/j.snb.2015.12.038.

[34] C.J. Sun, A. Srivastava, J.R. Reifert, J.H. Waite, Halogenated DOPA in a Marine Adhesive Protein, The Journal of Adhesion. 85 (2009) 126–138. https://doi.org/10.1080/00218460902782188.

[35] M. Cencer, M. Murley, Y. Liu, B.P. Lee, Effect of Nitro-Functionalization on the Cross-Linking and Bioadhesion of Biomimetic Adhesive Moiety, Biomacromolecules. 16 (2015) 404–410. https://doi.org/10.1021/bm5016333.

[36] E. Amstad, A.U. Gehring, H. Fischer, V.V. Nagaiyanallur, G. Hähner, M. Textor, E. Reimhult, Influence of Electronegative Substituents on the Binding Affinity of Catechol-Derived Anchors to Fe3O4 Nanoparticles, J. Phys. Chem. C. 115 (2011) 683–691. https://doi.org/10.1021/jp1109306.

[37] B.K. Ahn, Perspectives on Mussel-Inspired Wet Adhesion, J. Am. Chem. Soc. 139 (2017) 10166–10171. https://doi.org/10.1021/jacs.6b13149.

[38] B.P. Lee, J.L. Dalsin, P.B. Messersmith, Synthesis and Gelation of DOPA-Modified Poly(ethylene glycol) Hydrogels, Biomacromolecules. 3 (2002) 1038–1047. https://doi.org/10.1021/bm025546n.

[39] B.P. Lee, K. Huang, F. Nelson Nunalee, K.R. Shull, P.B. Messersmith, Synthesis of 3,4-dihydroxyphenylalanine (DOPA) containing monomers and their co-polymerization with PEG-diacrylate to form hydrogels, Journal of Biomaterials Science -- Polymer Edition. 15 (2004) 449–464. https://doi.org/10.1163/156856204323005307.

[40] H. Lee, B.P. Lee, P.B. Messersmith, A reversible wet/dry adhesive inspired by mussels and geckos, Nature. 448 (2007) 338–341. https://doi.org/10.1038/nature05968.

[41] B.P. Lee, C.-Y. Chao, F.N. Nunalee, E. Motan, K.R. Shull, P.B. Messersmith, Rapid Gel Formation and Adhesion in Photocurable and Biodegradable Block

Copolymers with High DOPA Content, Macromolecules. 39 (2006) 1740–1748. https://doi.org/10.1021/ma0518959.

[42] S.S. More, R. Vince, Design, Synthesis and Biological Evaluation of Glutathione Peptidomimetics as Components of Anti-Parkinson Prodrugs, J. Med. Chem. 51 (2008) 4581–4588. https://doi.org/10.1021/jm800239v.

[43] S.-B. Lee, C. González-Cabezas, K.-M. Kim, K.-N. Kim, K. Kuroda, Catechol-Functionalized Synthetic Polymer as a Dental Adhesive to Contaminated Dentin Surface for a Composite Restoration, Biomacromolecules. 16 (2015) 2265–2275. https://doi.org/10.1021/acs.biomac.5b00451.

[44] W. Ma, Y. Higaki, A. Takahara, Superamphiphobic Coatings from Combination of a Biomimetic Catechol-Bearing Fluoropolymer and Halloysite Nanotubes, Advanced Materials Interfaces. 4 (2017) 1700907. https://doi.org/10.1002/admi.201700907.

[45] Z. Liu, B.-H. Hu, P.B. Messersmith, Convenient synthesis of acetonide-protected 3,4-dihydroxyphenylalanine (DOPA) for Fmoc solid-phase peptide synthesis, Tetrahedron Letters. 49 (2008) 5519–5521. https://doi.org/10.1016/j.tetlet.2008.07.052.

[46] B.-H. Hu, P.B. Messersmith, Protection of 3,4-dihydroxyphenylalanine (DOPA) for Fmoc solid-phase peptide synthesis, Tetrahedron Letters. 41 (2000) 5795–5798. https://doi.org/10.1016/S0040-4039(00)00957-6.

[47] N. Patil, C. Jérôme, C. Detrembleur, Recent advances in the synthesis of catechol-derived (bio)polymers for applications in energy storage and environment, Progress in Polymer Science. 82 (2018) 34–91. https://doi.org/10.1016/j.progpolymsci.2018.04.002.

[48] D.G. Barrett, G.G. Bushnell, P.B. Messersmith, Mechanically Robust, Negative-Swelling, Mussel-Inspired Tissue Adhesives, Advanced Healthcare Materials. 2 (2013) 745–755. https://doi.org/10.1002/adhm.201200316.

[49] N. Holten-Andersen, A. Jaishankar, M. Harrington, D.E. Fullenkamp, G. DiMarco, L. He, G.H. McKinley, P.B. Messersmith, K.Y.C. Lee, Metal-coordination: Using one of nature's tricks to control soft material mechanics, J Mater Chem B Mater Biol Med. 2 (2014) 2467–2472. https://doi.org/10.1039/C3TB21374A.

[50] Q. Wei, T. Becherer, P.-L.M. Noeske, I. Grunwald, R. Haag, A Universal Approach to Crosslinked Hierarchical Polymer Multilayers as Stable and Highly Effective Antifouling Coatings, Advanced Materials. 26 (2014) 2688–2693. https://doi.org/10.1002/adma.201304737.

[51] S. Kim, J.-M. Moon, J.S. Choi, W.K. Cho, S.M. Kang, Mussel-Inspired Approach to Constructing Robust Multilayered Alginate Films for Antibacterial Applications, Advanced Functional Materials. 26 (2016) 4099–4105. https://doi.org/10.1002/adfm.201600613.

[52] C. Fan, J. Fu, W. Zhu, D.-A. Wang, A mussel-inspired double-crosslinked tissue adhesive intended for internal medical use, Acta Biomaterialia. 33 (2016) 51–63. https://doi.org/10.1016/j.actbio.2016.02.003.

[53] C.J. Ochs, T. Hong, G.K. Such, J. Cui, A. Postma, F. Caruso, Dopamine-Mediated Continuous Assembly of Biodegradable Capsules, Chem. Mater. 23 (2011) 3141–3143. https://doi.org/10.1021/cm201390e.

[54] M. Lee, Y. Kim, J.H. Ryu, K. Kim, Y.-M. Han, H. Lee, Long-term, feeder-free maintenance of human embryonic stem cells by mussel-inspired adhesive heparin and collagen type I, Acta Biomaterialia. 32 (2016) 138–148. https://doi.org/10.1016/j.actbio.2016.01.008.

[55] J. Lee, K.C. Yoo, J. Ko, B. Yoo, J. Shin, S.-J. Lee, D. Sohn, Hollow hyaluronic acid particles by competition between adhesive and cohesive properties of catechol for anticancer drug carrier, Carbohydrate Polymers. 164 (2017) 309–316. https://doi.org/10.1016/j.carbpol.2017.02.009.

[56] Z. Liu, P. Yao, Injectable shear-thinning xanthan gum hydrogel reinforced by mussel-inspired secondary crosslinking, RSC Adv. 5 (2015) 103292–103301. https://doi.org/10.1039/C5RA17246B.

[57] M. Shin, S.-G. Park, B.-C. Oh, K. Kim, S. Jo, M.S. Lee, S.S. Oh, S.-H. Hong, E.-C. Shin, K.-S. Kim, S.-W. Kang, H. Lee, Complete prevention of blood loss with self-sealing haemostatic needles, Nature Materials. 16 (2017) 147–152. https://doi.org/10.1038/nmat4758.

[58] M.J. Sever, J.J. Wilker, Synthesis of peptides containing DOPA (3,4-dihydroxyphenylalanine), Tetrahedron. 57 (2001) 6139–6146. https://doi.org/10.1016/S0040-4020(01)00601-9.

[59] M. Yu, T.J. Deming, Synthetic Polypeptide Mimics of Marine Adhesives, Macromolecules. 31 (1998) 4739–4745. https://doi.org/10.1021/ma980268z.

[60] H.J. Meredith, J.J. Wilker, The Interplay of Modulus, Strength, and Ductility in Adhesive Design Using Biomimetic Polymer Chemistry, Advanced Functional Materials. 25 (2015) 5057–5065. https://doi.org/10.1002/adfm.201501880.

[61] L.Q. Xu, D. Pranantyo, Y.X. Ng, S.L.-M. Teo, K.-G. Neoh, E.-T. Kang, G.D. Fu, Antifouling Coatings of Catecholamine Copolymers on Stainless Steel, Ind. Eng. Chem. Res. 54 (2015) 5959–5967. https://doi.org/10.1021/acs.iecr.5b00171.

[62] I. Louzao, C. Sui, K. Winzer, F. Fernandez-Trillo, C. Alexander, Cationic polymer mediated bacterial clustering: Cell-adhesive properties of homo- and copolymers, European Journal of Pharmaceutics and Biopharmaceutics. 95 (2015) 47–62. https://doi.org/10.1016/j.ejpb.2015.05.026.

[63] Y.-G. Jia, X.X. Zhu, Nanocomposite hydrogels of LAPONITE® mixed with polymers bearing dopamine and cholic acid pendants, RSC Adv. 6 (2016) 23033–23037. https://doi.org/10.1039/C5RA26316F.

[64] T.A. Jones, J.J. Wilker, Influences of Phosphates on the Adhesion of a Catechol-Containing Polymer, ACS Appl. Polym. Mater. 2 (2020) 4632–4639. https://doi.org/10.1021/acsapm.0c00699.

[65] C.R. Matos-Pérez, J.D. White, J.J. Wilker, Polymer Composition and Substrate Influences on the Adhesive Bonding of a Biomimetic, Cross-Linking Polymer, J. Am. Chem. Soc. 134 (2012) 9498–9505. https://doi.org/10.1021/ja303369p.

[66] M.A. North, C.A. Del Grosso, J.J. Wilker, High Strength Underwater Bonding with Polymer Mimics of Mussel Adhesive Proteins, ACS Appl. Mater. Interfaces. 9 (2017) 7866–7872. https://doi.org/10.1021/acsami.7b00270.

[67] J.D. White, J.J. Wilker, Underwater Bonding with Charged Polymer Mimics of Marine Mussel Adhesive Proteins, Macromolecules. 44 (2011) 5085–5088. https://doi.org/10.1021/ma201044x.

[68] C.R. Matos-Pérez, J.J. Wilker, Ambivalent Adhesives: Combining Biomimetic Cross-Linking with Antiadhesive Oligo(ethylene glycol), Macromolecules. 45 (2012) 6634–6639. https://doi.org/10.1021/ma300962d.

[69] J. Luo, F. Zhao, X. Fei, X. Liu, J. Liu, Mussel inspired preparation of polymer grafted graphene as a bridge between covalent and noncovalent methods, Chemical Engineering Journal. 293 (2016) 171–181. https://doi.org/10.1016/j.cej.2016.02.057.

[70] B.-Y. Yu, J. Zheng, Y. Chang, M.-C. Sin, C.-H. Chang, A. Higuchi, Y.-M. Sun, Surface Zwitterionization of Titanium for a General Bio-Inert Control of Plasma Proteins, Blood Cells, Tissue Cells, and Bacteria, Langmuir. 30 (2014) 7502–7512. https://doi.org/10.1021/la500917s.

[71] W. Zhao, Q. Ye, H. Hu, X. Wang, F. Zhou, Fabrication of binary components based on a poly(ionic liquid) through “grafting” and “clicking” and their synergistic antifouling activity, RSC Adv. 5 (2015) 100347–100353. https://doi.org/10.1039/C5RA23391G.

[72] D.J. Phillips, G.-L. Davies, M.I. Gibson, Siderophore-inspired nanoparticle-based biosensor for the selective detection of Fe3+, J. Mater. Chem. B. 3 (2014) 270–275. https://doi.org/10.1039/C4TB01501K.

[73] G. Moad, E. Rizzardo, S.H. Thang, Living Radical Polymerization by the RAFT Process, Aust. J. Chem. 58 (2005) 379–410. https://doi.org/10.1071/CH05072.

[74] R.B. Grubbs, R.H. Grubbs, 50th Anniversary Perspective: Living Polymerization—Emphasizing the Molecule in Macromolecules, Macromolecules. 50 (2017) 6979–6997. https://doi.org/10.1021/acs.macromol.7b01440.

[75] R. Gu, Synthesis and Characterization of Graphene-Polymer Nanocomposites via Reversible Addition-Fragmentation Chain-Transfer Polymerization, (n.d.) 113.

[76] J. Chiefari, Y.K. (Bill) Chong, F. Ercole, J. Krstina, J. Jeffery, T.P.T. Le, R.T.A. Mayadunne, G.F. Meijs, C.L. Moad, G. Moad, E. Rizzardo, S.H. Thang, Living Free-Radical Polymerization by Reversible Addition−Fragmentation Chain Transfer: The RAFT Process, Macromolecules. 31 (1998) 5559–5562. https://doi.org/10.1021/ma9804951.

[77] J.M. Lee, O.H. Kim, S.E. Shim, B.H. Lee, S. Choe, Reversible Addition-Fragmentation Chain Transfer (RAFT) Bulk Polymerization of Styrene: Effect of R-Group Structures of Carboxyl Acid Group Functionalized RAFT Agents, 2005.

[78] W. Zhao, G. Gody, S. Dong, P.B. Zetterlund, S. Perrier, Optimization of the RAFT polymerization conditions for the in situ formation of nano-objects via dispersion polymerization in alcoholic medium, Polym. Chem. 5 (2014) 6990–7003. https://doi.org/10.1039/C4PY00855C.

[79] B.A. Chalmers, A. Alzahrani, G. Hawkins, F. Aldabbagh, Efficient synthesis and RAFT polymerization of the previously elusive N-[(cycloalkylamino)methyl]acrylamide monomer class, Journal of Polymer Science Part A: Polymer Chemistry. 55 (2017) 2123–2128. https://doi.org/10.1002/pola.28607.

[80] J. Hui, Z. Dong, Y. Shi, Z. Fu, W. Yang, Reversible-deactivation radical polymerization of chloroprene and the synthesis of novel polychloroprene-based block copolymers by the RAFT approach, RSC Adv. 4 (2014) 55529–55538. https://doi.org/10.1039/C4RA08715A.

[81] J. Hwang, H.-C. Lee, M. Antonietti, B.V.K.J. Schmidt, Free radical and RAFT polymerization of vinyl esters in metal–organic-frameworks, Polym. Chem. 8 (2017) 6204–6208. https://doi.org/10.1039/C7PY01607G.

[82] K. Nakabayashi, H. Mori, Recent progress in controlled radical polymerization of N-vinyl monomers, European Polymer Journal. 49 (2013) 2808–2838. https://doi.org/10.1016/j.eurpolymj.2013.07.006.

[83] S. Moulay, Recent Trends in Mussel-Inspired Catechol-Containing Polymers (A Review), Oriental Journal of Chemistry. 34 (2018) 1153–1197.

[84] X. Zhang, X. Lian, L. Liu, J. Zhang, H. Zhao, Synthesis of Comb Copolymers with Pendant Chromophore Groups Based on RAFT Polymerization and Click Chemistry and Formation of Electron Donor−Acceptor Supramolecules, Macromolecules. 41 (2008) 7863–7869. https://doi.org/10.1021/ma801405j.

[85] X. Guo, T. Zhang, Y. Wu, W. Shi, B. Choi, A. Feng, S.H. Thang, Synthesis of CO2-responsive gradient copolymers by switchable RAFT polymerization and their controlled self-assembly, Polym. Chem. 11 (2020) 6794–6802. https://doi.org/10.1039/D0PY01109F.

Chapter 3

3 Synthesis of Poly (3,4-dihydroxy-co-styrene) Derivatives and their Potential as Denture Adhesives.

3.1 Abstract

Nine catechol containing copolymers (P1A-P3C) were prepared by free radical polymerization of 3,4-dimethoxystyrene (3,4 DMS) and different styrene derivatives followed by deprotection using BBr_3 and acidic work-up. ^{1}H-NMR, ^{13}C-NMR, and FTIR confirmed successful deprotection. TGA results indicate all protected copolymers, P1A-P to P3C-P (except P3B-P) have one stage decomposition at around 400 ^{o} C regardless of substitution or monomer percentage. With regards to DSC, the order of glass transition temperature is P3-P > P2-P > P1-P. P1A-P3C were added to denture adhesive formulations (F1-F7) and combined with control and PBS to generate F(P)-C-PBS for lap shear. All formulations were ≥ 5 kPa which satisfies ISO 10873. Control-PBS had the highest shear stress of 16.55 kPa at pH 2 compared to Poligrip. However, except for control-PBS and F1(P1A)-C-PBS, other formulations did not follow the trend of pH effect on adhesion due to poor uniformity. F6(P3C)-C-PBS had a reverse pH effect on shear stress and F7(P1C)-C-PBS remained consistent through out pH change. The FTIR of control-PBS, F1(P1A)-C-PBS, F6(P3C)-C-PBS, and F7(P1C)-C-PBS was taken to investigate their hydrogen bonding, however it was not enough to explain their resulted shear stress.

3.2 Introduction: Poly (3,4-dihydroxy-co-styrene)

Marine mussels, experts in underwater surface adhesions, have provided structural inspiration for developing underwater adhesion technologies. The production of proteins and polypeptide containing DOPA moieties is challenging and costly [1]. Within the literature, the mussel- inspired synthetic polymer p(3,4-dihydroxy-co-styrene) (p(3,4-DHS-co-sty)) shown in Figure 3.1 have shown promising adhesive abilities underwater [1–5].

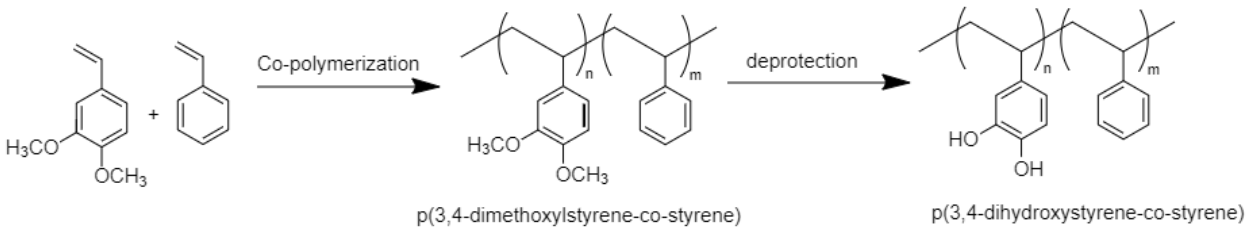

Figure 3.1 Synthesis of p(3,4-dihydroxystyrene-co-styrene).

Advantage of this polymeric structure include accessibility of starting materials, low cost, no monomer synthesis, scalable synthesis and reported to be non-toxic [6]. P-(3,4-DHS-co-Sty) is prepared by co-polymerizing the monomers 3,4-dimethoxystyrene (3,4-DMS) and styrene (sty) to form p(3,4-dimethoxystyrene-co-styrene) (p(3,4-DMS-co-sty)) followed by deprotection of the methoxy groups. A polystyrene backbone is used in place of a polypeptide to provide thermal stability, hydrophobicity, and retardation of oxidation. The catechol unit provided by 3,4-DHS mimics the side-chain containing DOPA of the mussel protein which is responsible for adhesion through crosslinking [1,5], whereas styrene serves by contributing itself as a hydrophobic component to repel water and reduce catechol oxidation [7,8]. Other factors that enhance the adhesion performance include 3,4-DMS to styrene compositions, molecular weight, choice of oxidizing agents, curing time, and curing temperature [1,2,4,5,9].

3.2.1 Poly (3,4-dihydroxystyrene/styrene-alt-maleic acid) as a Denture Adhesive

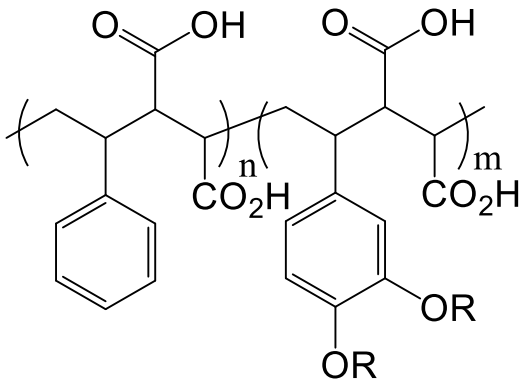

Figure 3.2 P(DHS/S-alt-MA) when R=H, and P(DMS/S-alt-MA) when R=Me.

The dental field has developed adhesives that not only function in the moist oral cavity but also make active use of saliva in the achievement of their adhesive properties [9,10]. Utilization of denture adhesives has increased over the years for prosthetic purposes [11,12] to improve fitting, comfort, and chewing of dentures [13–15]. Denture adhesives must provide temporary adhesion between the denture and the oral mucosa [16]. Gill et al. [10] synthesized a analogous structure of p(3,4-DMS-co-S) by incorporating maleic acid into the chain resulting in poly (3,4-dihydroxystyrene/styrene-alt-maleic acid) (p(DHS/S-alt-MA)) with broad dispersity indexes. The p(DHS/S-alt-MA) was compared and evaluated against the common active ingredient PMVEMA for its performance for denture fixation. Through lap shear experiment using polymethyl methacrylate (PMMA): PMMA slides and mixing adhesive formulation with deionized (DI) water (or mucin solution), it revealed p(DHS/S-alt-MA) adhesion exceeds PMVEMA, but both are outperformed by poly (3,4-dimethoxystyrene/styrene-alt-maleic acid) (p(DMS/S-alt-MA)). When one of the PMMA slides was replaced with a tissue mimetic material, p(DHS/S-alt-MA) adhesion was higher than p(DMS/S-alt-MA) when its formulation was mixed with DI water or mucin by 50 wt %.

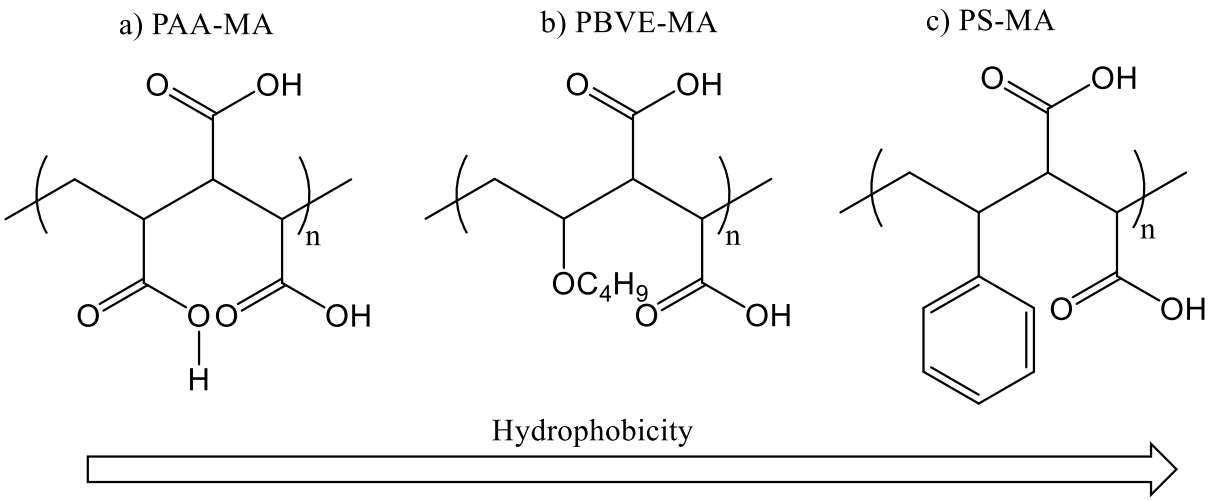

Figure 3.3 Structures of a) PAA-MA, b) PBVE-MA, c) PS-MA and their hydrophobicity.

In another literature, Gill et al. [17] derivatized PMVEMA yielding the hydrophilic polyacrylic acid-maleic acid (PAA-MA), along with the two hydrophobic polymers poly butyl vinyl ether-maleic acid (PBVE-MA) and polystyrene-maleic acid (PS-MA). Like

p(DHS/S-alt-MA), all were compared and evaluated against PVMEMA. The lap shear experiment (PMMA: PMMA) revealed the adhesion strength in the order PBVE-MA > PS-MA > PMVEMA > PAA-MA. This stress the importance of hydrophobic ingredients in the formulation of denture adhesives. Variations of P(3,4-DMS-co-sty) by replacing styrene with a para-substituted styrene has yet to be reported in the literature. The replacement of the hydrogen with a more hydrophobic functional group such as methyl (Me) and tert-butyl (tBu) increase the water repellency of the polymer backbone. It is expected to enhance adhesion on substrates with moisture or submerged underwater.

3.3 Experimental Section

3.3.1 Materials

Boron tribromide (BBr_3, ≥ 99.99%, Sigma Aldrich), hydrochloric acid (HCl), sodium hydroxide (NaOH), sodium chloride (NaCl, 99%), petrolatum (Walmart), mineral oil (light, Sigma Aldrich), sodium carboxymethylcellulose (NaCMC, M_w ~ 250000, degree of substitution 0.9, Sigma Aldrich), poly(methyl vinyl ether-alt-maleic acid) (PMVEMA, M_w ~216,000, Sigma Aldrich), potassium chloride (KCl, 99%), calcium chloride dihydrate ($CaCl_2.2H_2O$), sodium dihydrogen phosphate dihydrate ($NaH_2PO_4.2H_2O$, Sigma Aldrich), sodium sulfide nonahydrate ($Na_2S.9H_2O$ Sigma Aldrich), phosphate buffer solution (PBS, pH 7.2, Ward's Science), acetone-d (99.9%, Sigma Aldrich) and chloroform-d (Cambridge, 99.8%) were used as received. All organic solvents used: dichloromethane (DCM, ≥ 99.8%), dimethylformamide (DMF, 99%), methanol (MeOH, ≥ 99.8%), and toluene (≥ 99.5%) were purchased from Caledon Labs. DCM and toluene were uploaded and dispensed from MB-SPS and dried with molecular sieves (3 Å). 2,2′-Azobis(2-methylpropionitrile) (98%, AIBN, Sigma Aldrich) was recrystallized in methanol and stored at -4^{o}C prior to usage. 3,4-dimethoxystyrene (3,4-DMS, 99 %, Sigma Aldrich) was washed with 10% NaOH, distilled water, and brine to remove the inhibitor tert-butylcatechol (TBC), dried with $MgSO_4$ overnight before placing in cold storage. Styrene (sty, ≥ 99%, Sigma Aldrich), 4-methylstyrene (4ms, 98%, Alfa Aesar), and 4-tert-butylstyrene (4tbs, 94%, Alfa Aesar) was passed through a prepacked column inhibitor remover (*tert*-butylcatechol, Scientific Polymer), sealed, and stored at -20^{o}C

before use. Plexiglass substrates were purchased from Western University's University Machine Shop.

3.3.2 Synthesis of Poly (3,4-dimethoxystyrene-co-styrene) (P1A-P - P1C-P)

In a Schlenk tube equipped with a stir bar, varying amounts of styrene and 3,4-dimethoxystyrene (see Table 3.1) were added to AIBN (89 mg; 0.54 mmol), and toluene (2 ml). The mixture was purged with nitrogen for 20 minutes before placing into an oil bath (70^{o}C) and stirred overnight (18 hours). Upon completion, toluene (8ml) was added to the mixture and then precipitated in MeOH (90 ml) with stirring, transferred onto vacuum filtration, washed with MeOH (3 x 50 ml) and dried for 2 hours. The polymer was re-dissolved in DCM (10 ml), precipitated in MeOH (90 ml), and further washed with MeOH (3 x 50 ml) before placing in vacuum oven overnight.

3.3.3 Synthesis of Poly (3,4-dimethoxystyrene-co-4-methylstyrene) (P2A-P - P2C-P)

Synthesis and purification procedures are same as 3.3.2. See Table 3.1 for monomers in the feed.

3.3.4 Synthesis of Poly (3,4-dimethoxystyrene-co-4-tert-butylstyrene) (P3A-P – P3C-P)

Synthesis and purification procedures are same as 3.3.2. See Table 3.1 for monomers in the feed.

3.3.5 Deprotection of P1A-P - P1C-P

In a typical reaction, approximately 0.6 – 0.8g of P1-P samples were dissolved in anhydrous DCM (10 ml) and purged with nitrogen for 20 minutes. The mixture was placed into an ice bath (20 min) and BBr_3 in DCM (2 mmol equivalent of catechol) was added with a syringe before letting the reaction stir in room temperature overnight (18 hours). MeOH (1 ml) was added to quench the BBr_3, followed by stirring (15 min). Afterwards, the mixture was poured into 0.12 M HCl (80 ml) with stirring (15 min) to work-up which generated a white cluster as a result. The HCl was decanted and fresh HCl

solution was added to repeat the process twice more. The white cluster was dissolved with acetone, dried with reduced pressure, and stored in the vacuum oven overnight.

3.3.6 Deprotection of P2A-P - P2C-P

Deprotection and purification procedure is same as 3.3.5.

3.3.7 Deprotection of P3A-P - P3C-P

Deprotection and purification procedure is same as 3.3.5.

3.3.8 Preparation of Denture Adhesive Formulations

All formulations were made according to Gill [10,17]. By weight percentage, denture adhesive formulations contain petrolatum (29%), mineral oil (17%), NaCMC (24%), PMVEMA (22.5%), and copolymer (7.5%). The PMVEMA was crushed into fine powder using pestle and mortar. Petrolatum and mineral oil were mixed using vortex for 2 minutes. NaCMC, PMVEMA and copolymers were added to the resulting mixture and placed on vortex again for 2 minutes. A spatula was used to disperse the solid particles into entire mixture before placing on vortex again for 4 minutes. All formulations were placed in the refrigerator before lap shear testing. Upon testing, the control was added to dilute the formulations followed by the addition of PBS of desired pH at a ratio of 1:1:0.5 by weight to generate further latter formulations Fn(P)-C-PBS-pH.

3.3.9 Preparation of Artificial Saliva

The artificial saliva was prepared according to Fallahi's article [18]. In a 1L plastic bottle, KCl (0.4019g), NaCl (0.4006g), $CaCl_2.2H_2O$ (0.9063g), $NaH_2PO_4.2H_2O$ (0.6915g), $Na_2S.9H_2O$ (5 mg) and urea (1.0010 g) was added and diluted with distilled water (1L). The artificial saliva was placed in the refrigerator prior to use. The pH was adjusted using 1M HCl or 1M NaOH solution.

3.3.10 Thermogravimetric Analysis (TGA)

Thermal stability was determined using SDT Q600. The system was operated using nitrogen and vacuum. The sample pan was tared with the reference pan within the TGA

several times to ensure readings are stable. The sample pan was filled with 10-20 mg of polymer samples. All samples were heated from room temperature up to 600 ^{o}C using a heat flow of 10 ^{o}C/min. The sample pan was cleansed using flame torch, followed by sonication in water then acetone, finally with flame once more.

3.3.11 Differential Scanning Calorimetry (DSC)

The glass transition temperatures (T_g's) were determined using DSC Q200 V24.10 Build 122 Module DSC Standard Cell FC. About 5-10 mg of polymer samples were measured into Tzero Aluminum pans and sealed. Nitrogen flow was 50 mL/min. Heating and cooling rate of 10 ^{o}C/ min were used for heating-cooling-heating cycle from 20 – 250 ^{o} C.

3.3.12 Gel Permeation Chromatography (GPC)

Molecular weights (M_w, M_n) and dispersity values (Đ) of the synthesized copolymer samples were measured by a Polymer Laboratories PL-GPC 220 gel permeation chromatography equipped with a triple detector array: a refractive index detector, a bridge viscometer (PL-BV 400HT), and two light scattering detectors (low angle 15^{o} and right angle 90^{o}, 658 nm). THF solvent stabilized with BHT (250 ppm) was used as the mobile phase at a flow rate of 1.0 mL/min. Three Agilent PLgel 10 μm Mixed-B (300 × 7.5 mm) columns were employed to separate the samples at 30^{o}C, which were calibrated using a narrow polystyrene standard (MW: 205 kDa, Đ: 1.05).

3.3.13 Lap Shear Testing

Plexiglass pieces were cleansed by submerging into deionized water, stored in oven at 37 ^{o}C overnight, then dried. Approximately 200 mg of control-PBS added formulations was measured onto the plexiglass on 16 x 22 mm area and covered with another plexiglass. A 200g weight was used to press onto the glued plexiglasses. The glued area of the specimens was stabilized using binder clips and properly orientated using 24x22 mm plexiglasses when loading onto Instron 3345 (Norwood, MA, USA) equipped with 50 N load cell (Model 2519-102). All control-PBS formulations at pH 2, 7, and 10 had 5

specimens each and was pulled at 5 mm/min to measure the shear stress, shear strain and shear modulus.

3.3.14 Fourier Transformation – Infrared Spectroscopy (FTIR)

FTIR spectra was recorded at a resolution of 4 cm^{-1} over 64 scans using Nicolet 6700 equipped with a smart diamond ATR (attenuated total reflection) 0 to 4000 cm^{-1} using air as the background. For the effect of pH, PBS of desired pH was used as the background.

3.3.15 Statistical Analysis

Statistical analysis was conducted by 2way Anova and Tukey multiple comparative tests at p = 0.05. The statistical software used is Prism 6.

3.4 Results and Discussion

3.4.1 Free Radical Copolymerization of P1A-P – P3C-P and their Deprotection (P1A-P3C)

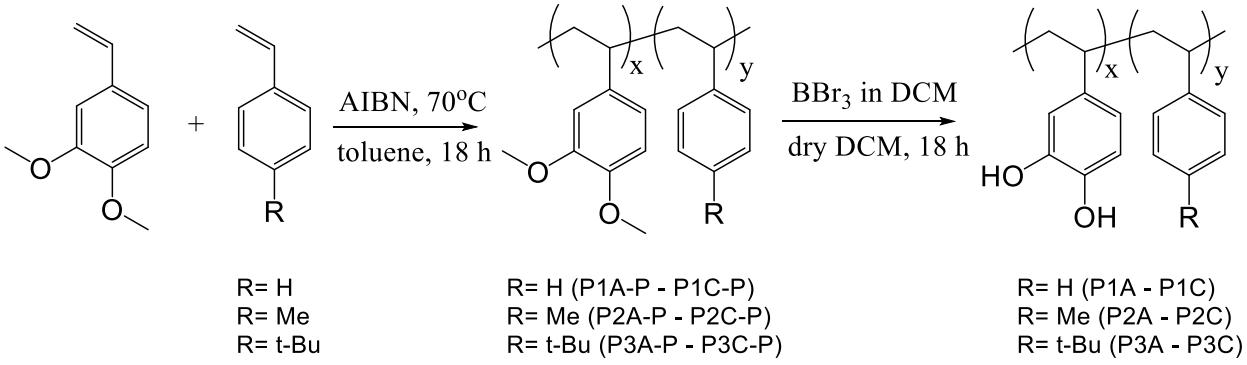

Scheme 3.1 Free radical polymerization of P1A-P – P3C-P followed by deprotection using BBr_3 (P1A-P3C).

In this work, 3 sets of co-polymers with different styrene derivatives of varying ratios were made by free radical polymerization using AIBN followed by deprotection using BBr_3 (Scheme 3.1). Previously, P1A-P series were prepared using anionic polymerization via n-butyl lithium, however the process requires a strictly clean system [19]. Using AIBN (0.27 M) at 70 ° C for 18 hours gave high monomer conversions. The final monomer compositions of 3,4 DMS ($F_{3,4\ DMS}$) and styrene derivatives ($F_{4\text{-R-styrene}}$)

was obtained by equations (3-1) and (3-2) respectively using ^{1}H-NMR. The 6.00 is number of dimethoxy protons from 3,4 DMS in the polymer used as a reference for calculation.

$$F_{3,4\ DMS} = \frac{6.00}{6.00 + Area\ of\ aromatic\ region}\ x\ 100\% \qquad (3\text{-}1)$$

$$F_{4-R-styrene} = 1 - F_{3,4\ DMS} \qquad (3\text{-}2)$$

On Table 3.1, P1-P and P3-P chain compositions are like their monomer feed ratios whereas P2-P set differed (except P2C). The difference in P2-P set could indicate a preference of the 4ms to react with itself to form homopolymers of poly(4ms). The polydispersity index (Đ) was obtained using gel permeation chromatography (GPC) using the protected copolymers to avoid crosslinking [1]. As a result, the Đ of P1-P and P2-P sets are similar (except for P2C-P) close to 1.5 which is Flory's most probable distribution without living polymerization techniques [20] whereas the P3-P set is broadest.

Table 3.1 Final composition, molecular weights, and polydispersity indexes of P1A-P to P3C-P.

R	Name	$f_{4\text{-R-styrene}}$	$f_{3,4\text{-DMS}}$	$F_{4\text{-R-styrene}}$	$F_{3,4\text{-DMS}}$	M_n (kDa)	M_w (kDa)	Đ
	P1A-P	70	30	72	28	11.3	17.8	1.58
H	P1B-P	80	20	81	19	10.0	15.4	1.54
	P1C-P	90	10	90	10	8.0	12.4	1.55
	P2A-P	70	30	69	31	11.9	17.5	1.47
Me	P2B-P	80	20	73	27	12.2	19.0	1.56
	P2C-P	90	10	82	18	11.9	17.9	1.50
	P3A-P	70	30	70	30	27.1	113.8	4.20
t-Bu	P3B-P	80	20	76	24	24.2	99.2	4.10
	P3C-P	90	10	88	12	28.9	161.8	5.60

The broad Đ of P3-P set can be attributed to chain transfer mentioned by Qiu and Matyjaszewski [21] where the generated polymer's Đ may increase after its initial decrease due to t-butyl's electron donating nature. T-butyl stabilizes the styryl radical making it react faster and generating heavier polymer chains before termination. This effect is greater in free radical compared to ATRP considering it is a non-controlled reaction. P3B-P has the highest Đ within the set due to its high 4-tert-butyl styrene content in the feed. Using GPC, P1A-P, P2A-P and P3A-P were compared, and it can be seen P1A-P and P2A-P elute at same time whereas P3A-P elutes earlier and broader than the other two (Figure 3.4). Possible modes of chain transfer leading to P3-Ps' high Đ may include transfer to solvent (Figure 3.5 a), initiator (Figure 3.5b) or to neighbouring polymer chains (Figure 3.5 c) [21]. It is more likely to chain transfer to monomers or polymers given toluene and AIBN have been constant through out all synthetic procedures.

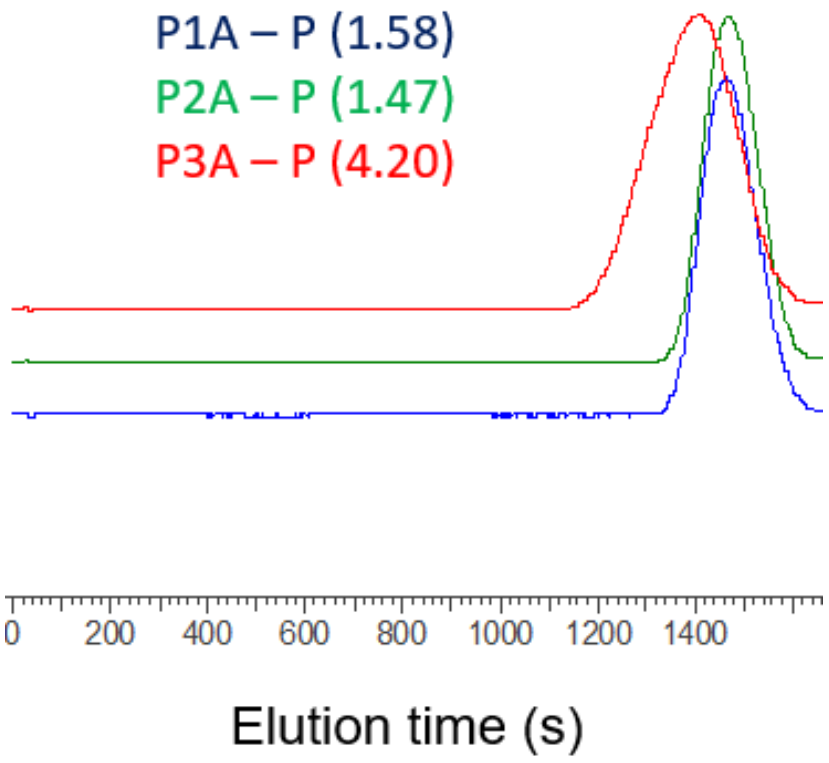

Figure 3.4 GPC curves of P1A - P, P2A - P, and P3A - P.

a) To solvent (toluene)

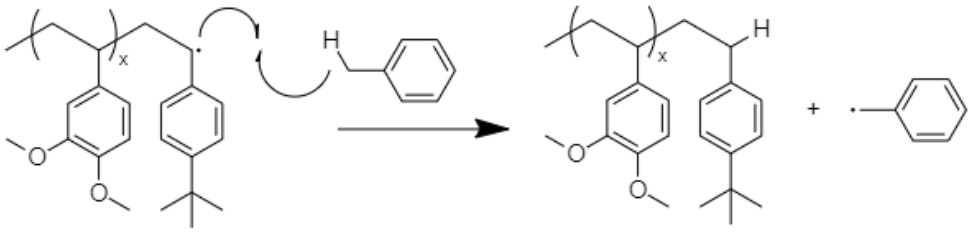

b) To initiator (AIBN)

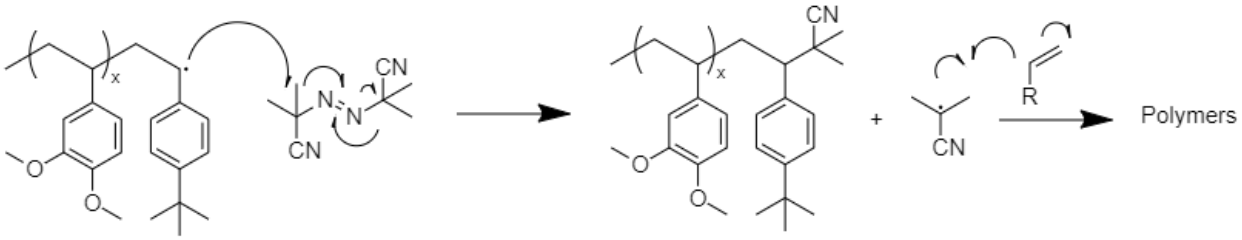

c) To neighbouring polymer

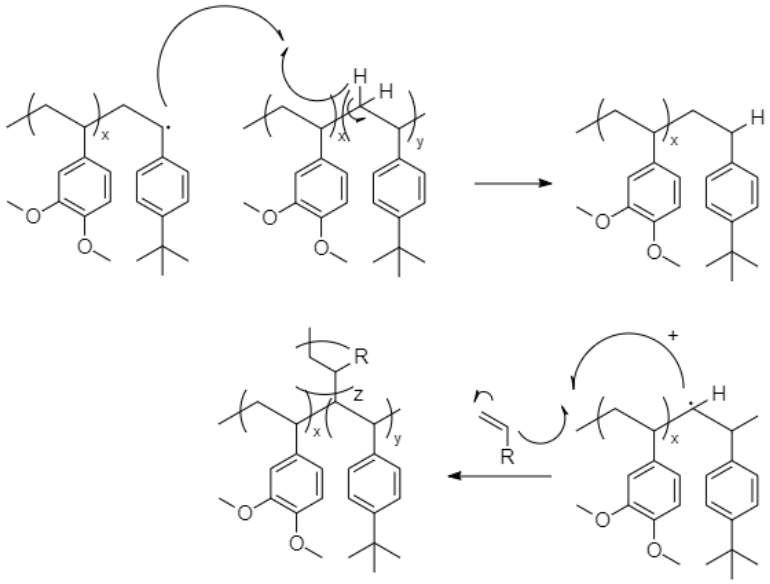

Figure 3.5 Possible modes of chain transfer leading to P3-Ps' high Đ a) transfer to solvent b) to initiator or c) to neighbouring polymer chains.

To obtain the catechol copolymers P1A-P3C, P1A-P – P3C-P were treated with BBr_3 in DCM, in anhydrous DCM. The deprotection process requires inert, cold, and dry

environment given BBr_3's volatility and violent reaction upon contact with any hydroxyl-containing species. For brief, ^{1}H-NMR confirmed the success of the deprotection reaction for P1B-P (Figure 3.6), P2B-P (Figure 3.7), and P3B-P (Figure 3.8) as the methoxy protons at 3.80 – 3.50 ppm are not present. However, FTIR revealed P1B, P2B, and P3B have small O-H stretch present (Figure 3.9) within 3400-3200 cm^{-1} [22] and raised the concern whether the catechol units have oxidized. To confirm, a ^{13}C-NMR between P3A-P and P3A was conducted (Figure 3.10). The spectrum revealed the carbons labeled "c" and "b" on P3A-P was in the same position on P3A (c' and b'), thus no oxidation occurred. Suppose oxidation occurred, the C=O signal would appear at 180 ppm. For further confirmation, GPC of P3A-P and P3A were compared (Figure 3.11). As a result, P3A shows tailing before the high molecular weight polymers elute indicating crosslinking which is only possible for the deprotected form.

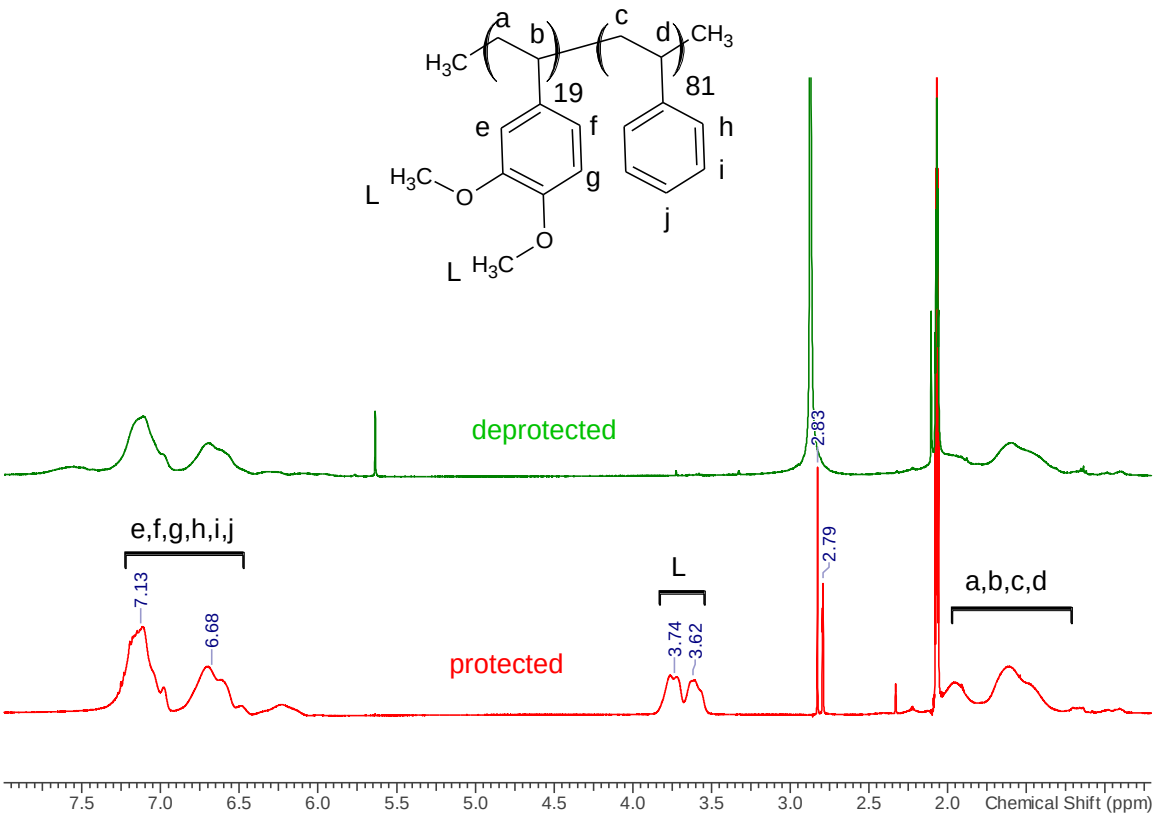

Figure 3.6 ^{1}H-NMR of P1B-P in acetone-d_6 before and after deprotection.

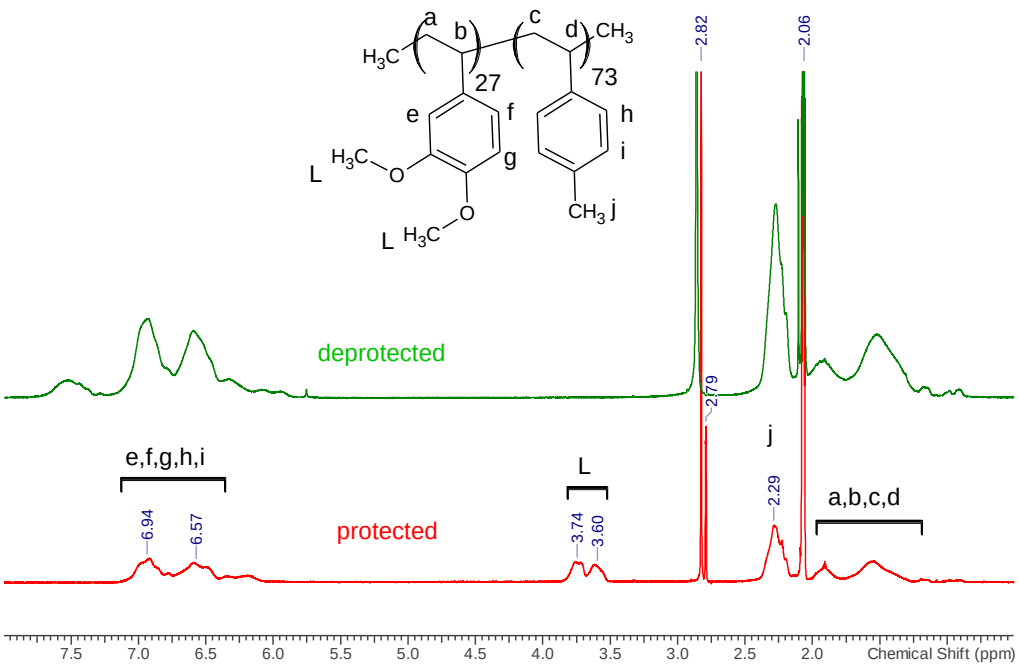

Figure 3.7 ^{1}H-NMR of P2B-P in acetone-d_6 before and after deprotection.

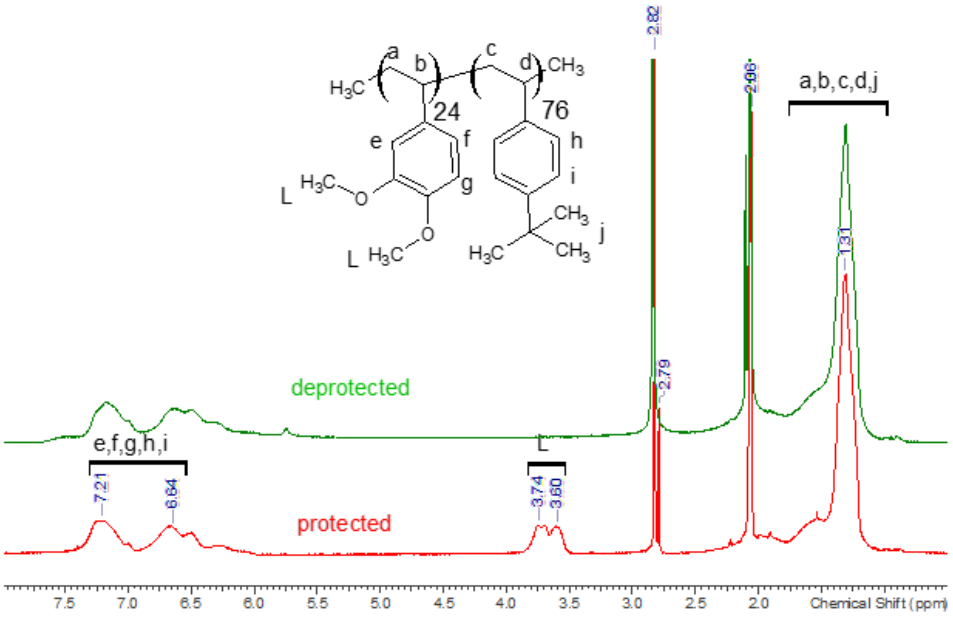

Figure 3.8 ^{1}H-NMR of P3B-P in acetone-d_6 before and after deprotection.

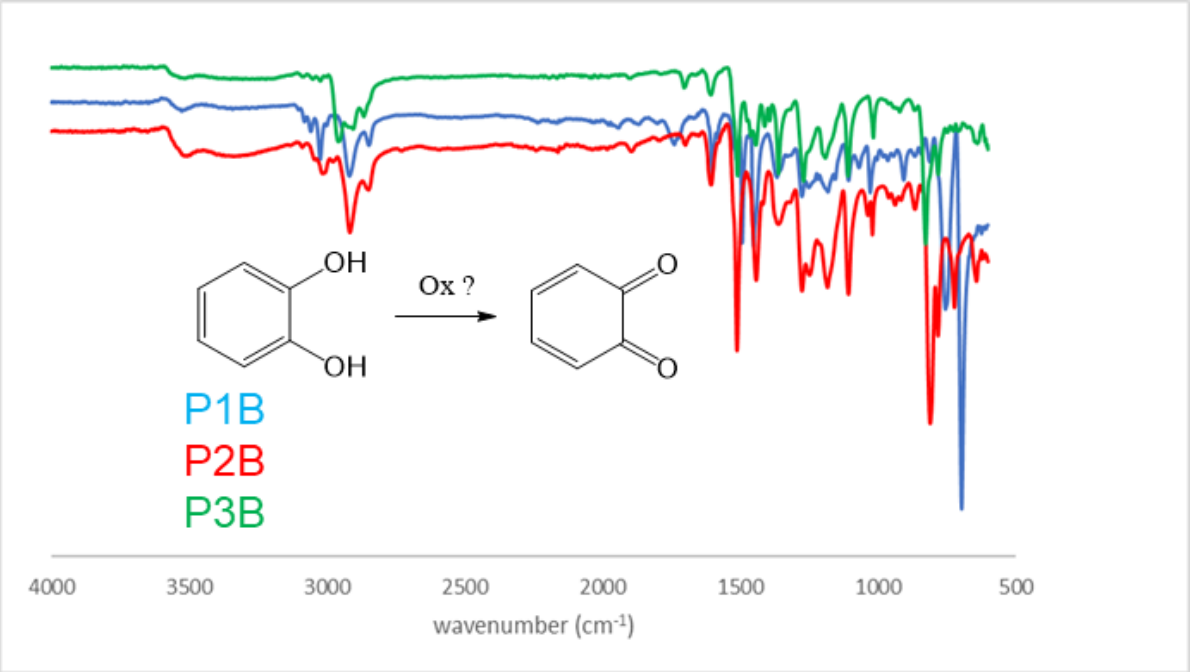

Figure 3.9 FTIR of P1B (blue), P2B (red) and P3B (green).

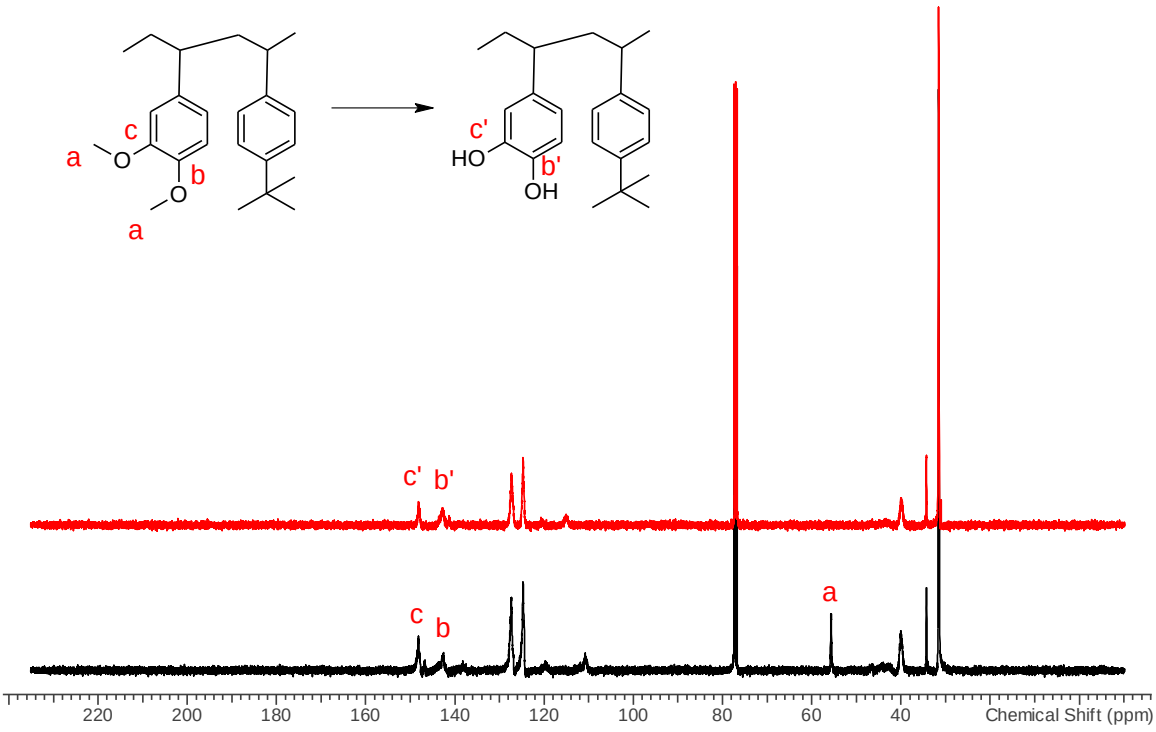

Figure 3.10 ^{13}C-NMR of P3A-P (black) and P3A (red).

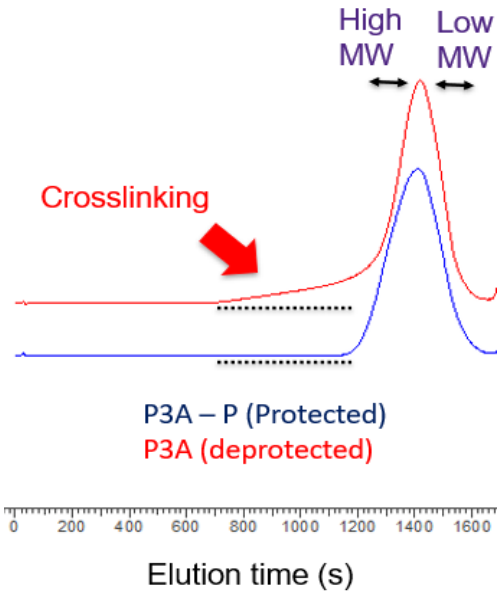

Figure 3.11 GPC of P3A-P and P3A.

3.4.2 TGA and DSC

Thermal stability of P1A-P to P3C-P (except P3B-P) was determined using SDT Q600 where all samples were heated from room temperature up to 600 ^{o}C using a heat flow of 10 ^{o}C/min. The thermographs for each polymer set are shown in Figure 3.12 along with their decomposition temperatures (T_d) on Table 3.2.

Table 3.2 Thermal decomposition of P1A-P to P3C-P.

R	Name	$F_{4\text{-R-styrene}}$	$F_{3,4\text{-DMS}}$	T_d
	P1A-P	72	28	405.6
H	P1B-P	81	19	402.0
	P1C-P	90	10	406.2
	P2A-P	69	31	400.2
Me	P2B-P	73	27	403.8
	P2C-P	82	18	399.0
	P3A-P	70	30	400.2
t-Bu	P3B-P	76	24	403.2
	P3C-P	88	12	n/a

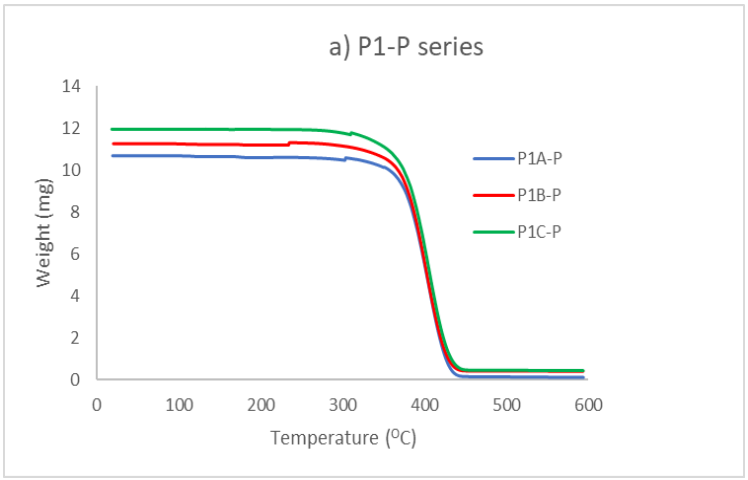

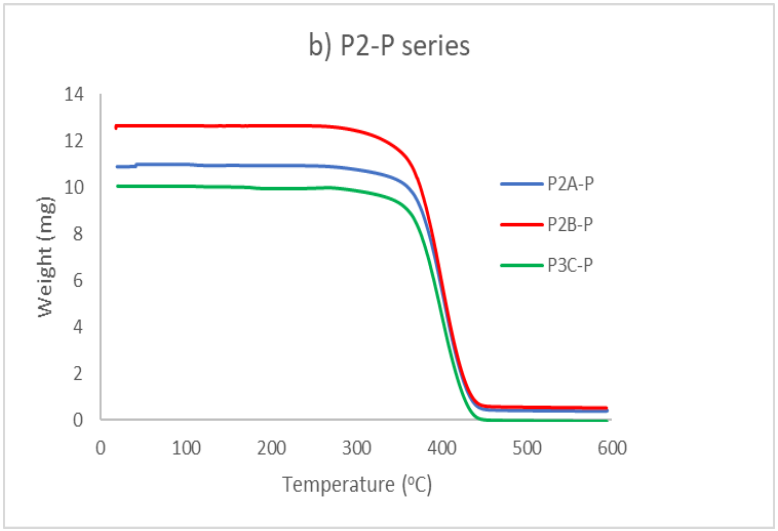

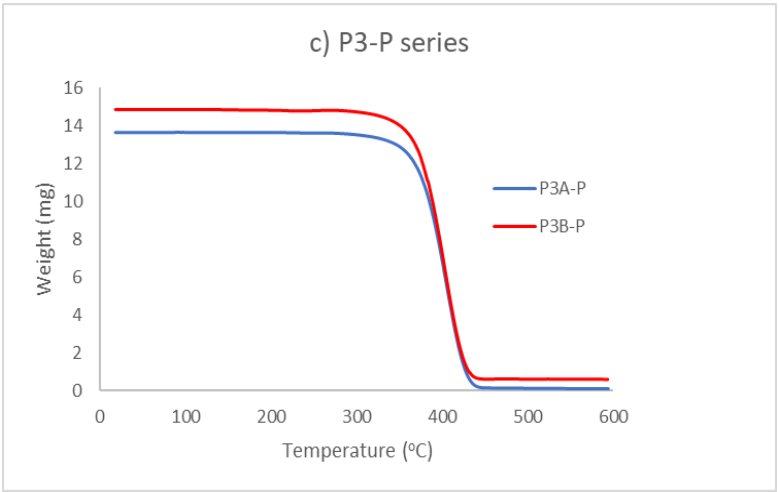

Figure 3.12 The thermographs for a) P1-P series, b) P2-P series and c) P3-P) series.

From the thermograms, all polymers have one stage of decomposition which indicates scission of the main chain. Also, all polymers have identical thermal stability up to approximately 400 ^{o}C regardless of monomer composition, styrene substitution, or molecular weight. With regards to the P1-P and P2-P series, this result aligns with experiments conducted by Senocak et al. (polystyrene and poly(4ms)) [23] and Rincon (poly(4-methoxylstyrene)) [24] using the same heating rate of 10 ^{o}C/min. It was expected for the P3-P series to have higher thermal stabilities given tert-butyl is a heavier pendant group, followed by their high molecular weights provided by GPC. The similarity of the thermal stability of P3-P series suggests the chain transfer did not form any branched polymers, while having similar repeating units as the other series.

The glass transition temperatures (T_g's) for P1A-P to P3C-P were determined using DSC Q200. Only the protected polymers were analyzed as the supposed deprotected polymers can undergo heat-induced crosslinking [1]. Heating and cooling rate of 10 ^{o}C/ min were used for heating-cooling-heating cycle from 20 – 250 ^{o}C. The first heating and cooling were used to remove any prior thermal history of residing solvents. Table 3.3 lists all T_g of the DSC curves (Figure 3.13) for P1A-P to P3C-P and the results align with what was hypothesized to be P3-P > P2-P >P1-P.

Table 3.3 Glass transition temperatures of P1A-P to P3C-P.

R	Name	$F_{4\text{-R-styrene}}$	$F_{3,4\text{-DMS}}$	T_g
	P1A-P	72	28	91.4
H	P1B-P	81	19	92.0
	P1C-P	90	10	95.4
	P2A-P	69	31	95.7
Me	P2B-P	73	27	96.4
	P2C-P	82	18	99.8
	P3A-P	70	30	123.6
t-Bu	P3B-P	76	24	125.2
	P3C-P	88	12	136.6

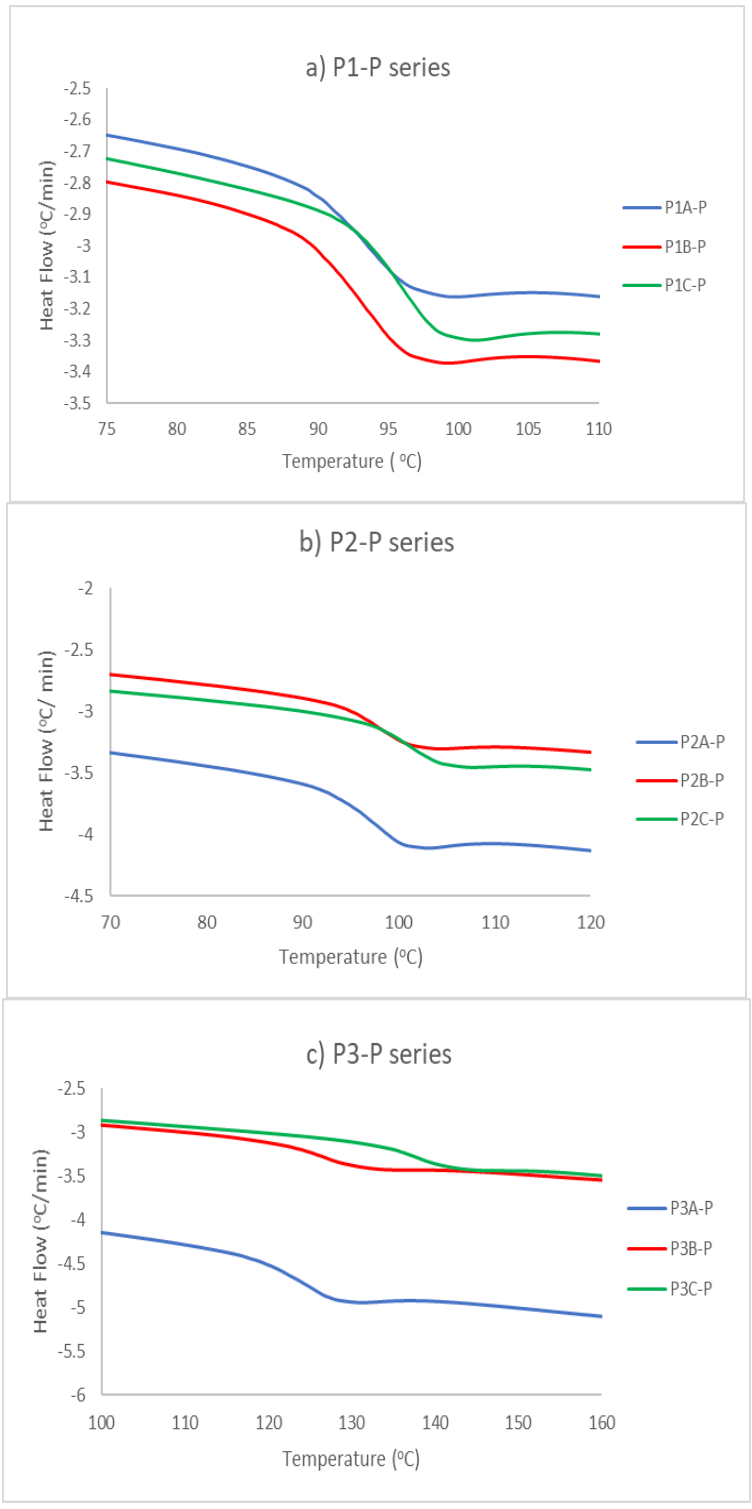

Figure 3.13 DSC curves for a) P1-P series, b) P2-P series and c) P3-P) series.

This result can be explained by regarding the structures of polystyrene, poly (4-methyl-styrene) and poly (4-tert-butyl-styrene). According to Kunal et al. [25], any substituted

polystyrene exhibits greater T_g values at comparable chain lengths. It is important to note T_g values relate to the polymer's segmental motion which is dependent on its backbone stiffness and side groups. Poly (4-tert-butyl-styrene) has the highest T_g (144 ^{o} C) amongst the set due to its bulk size which requires more energy to allow segmental motion, followed by poly (4-methyl-styrene) (104 ^{o} C), then polystyrene (100 ^{o} C). All synthesized co-polymers have lower T_g values compared to their respective homopolymers as the methoxy groups contribute their pendant nature and increasing its content further lowers T_g.

3.4.3 Lap Shear Testing

Table 3.4 Denture adhesive formulations.

Formulation	Petrolatum (g)	Mineral Oil (mL)	NaCMC (g)	PMVEMA (g)	Copolymer (g)
Control	7.55	5.28	6.25	7.81	0
F1 (P1A)	0.65	0.46	0.54	0.50	0.17
F2 (P2A)	1.10	0.77	0.91	0.85	0.28
F3 (P3A)	1.18	0.82	0.97	0.91	0.30
F4 (P3B)	0.82	0.57	0.68	0.64	0.21
F5 (P2C)	1.70	1.19	1.40	1.32	0.44
F6 (P3C)	1.18	0.83	0.98	0.92	0.31
F7 (P1C)	1.16	0.82	0.97	0.91	0.30

The control formulation was made using hydrophobic compounds petrolatum, and mineral oil along with hydrophilic compounds NaCMC and PMVEMA. The formulations (F1-F7 listed on Table 3.4) have 7.5% of the PMVEMA replaced with deprotected copolymers. The hydrophilic compounds absorb and maintains water to enhance adhesion whereas the hydrophobic compounds prevent excessive swelling and dissolution of the paste [18,26]. The artificial saliva (pH ~5.55) contains the listed materials (3.3.9) to mimic the electrolytes and odor. However, upon increasing pH with 1M NaOH lead to formation of calcium hydroxide at pH 7 which is not favorable, thus leading to the use of PBS as a replacement for simulating saliva. It was realized that the control and the commercial denture adhesive Poligrip are adhesives upon contact with

saliva or other aqueous medium. This was necessary considering the control was granular due to PMVEMA. Prior to the lap shear experiments of formulations F1-F7, a trial test, following Fallahi [18] with modifications, consist of 5 specimens where plexiglasses were glued with control formula mixed with 50% distilled water followed by soaking in 100 ml of PBS (pH 7) for 10 min at room temperature. As a result, the formula dissolved, and the surviving specimens provided average lap shear of 3.5 kPa which is below standard for denture adhesives according to ISO 10873 (5 kPa). Therefore, it was suggested that all formulations were to be mixed with 50% PBS by weight to advance. The formulations F1-F7 were topped with the control due to limited copolymers in stock. To ensure enough formulation for lap shear, each formulation was mixed with the control followed by addition of PBS of desired pH at a ratio of 1:1:0.5 by weight to generate the test formulations F(P)-C-PBS. All F(P)-C-PBS formulations were vortexed, stirred with spatula and allowed to rest for 10 minutes to allow mixture to equilibrate. When performing lap shear, the force is parallel between the two glued plexiglasses. Lap shear is represented by equation 3-3 where τ is ultimate shear stress (kPa), F is force (N) applied, and A is the area (mm^2) covered with the adhesive.

$$\tau = \frac{F}{A} \qquad \textbf{(3-3)}$$

The shear stress, shear strain and shear modulus (MPa) were recorded. To allow specimens to be glued and remain parallel, a binder clip was attached to the glued area followed by proper reorientation using squared plexiglasses (Figure 3.14) when loading onto the Instron. Sequentially, the binder clips were removed prior to pulling to generate a stress-strain curve (Figure 3.15).

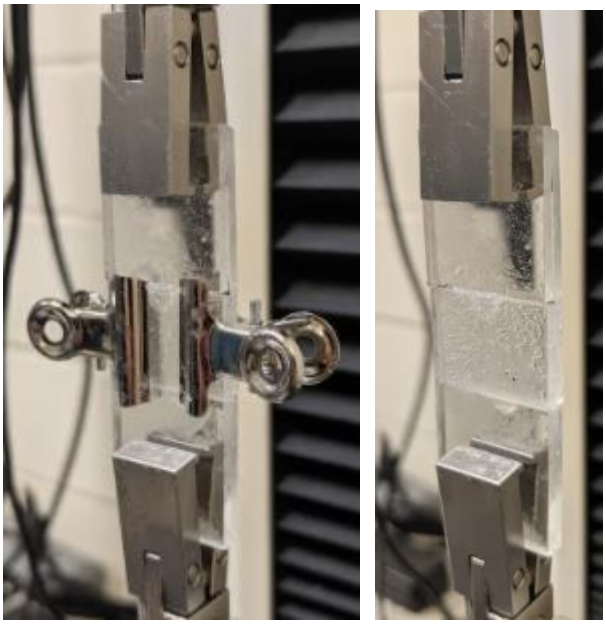

Figure 3.14 Example of a specimen loaded onto Instron being stabilized with binder clips (left) and removal of binder clips upon shearing (right).

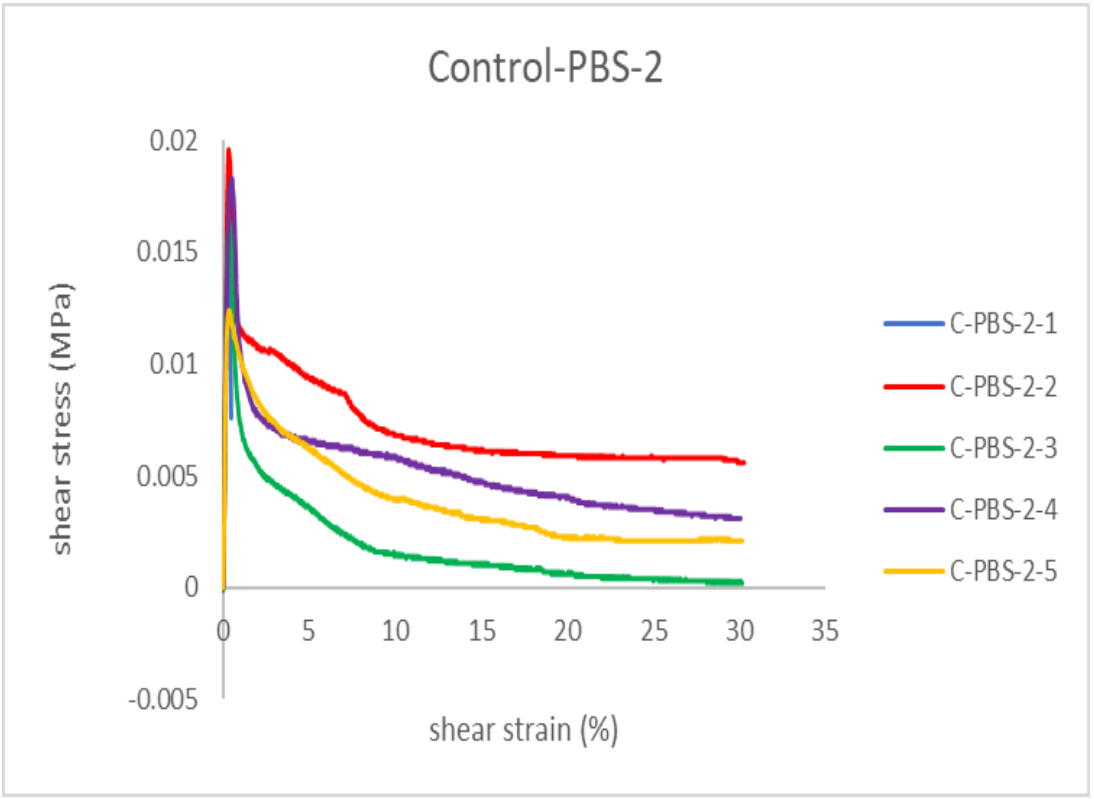

Figure 3.15 Stress-Strain curve of Control-PBS-2.

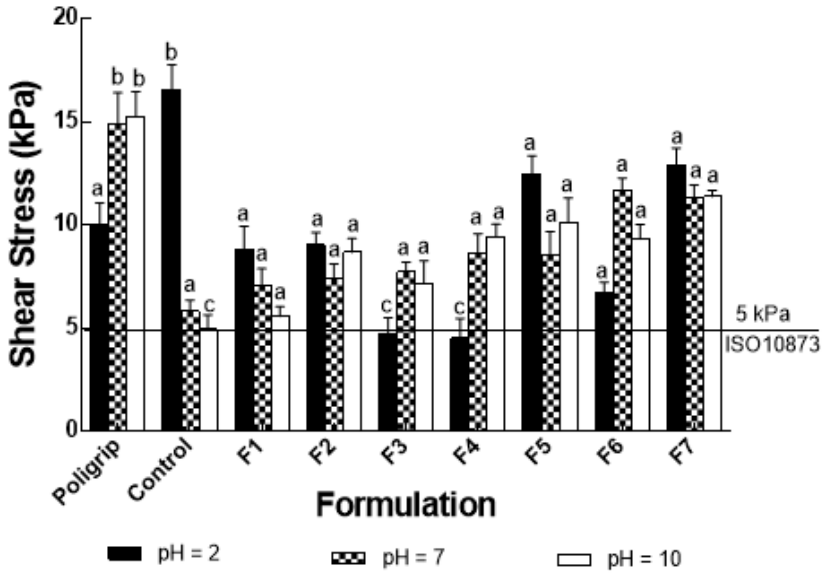

Figure 3.16 Effect of composition and pH on shear stress of experimental adhesives. F1 = F1(P1A)-C-PBS, F2 = F2(P2A)-C-PBS, F2 = F3(P3A)-C-PBS, F4 = F4(P3B)-C-PBS, F5(P2C)-C-PBS, F6 = F6(P3C)-C-PBS, F7 = F7(P1C)-C-PBS. Similar letters mean the groups are not significantly different at $p > 0.05$.

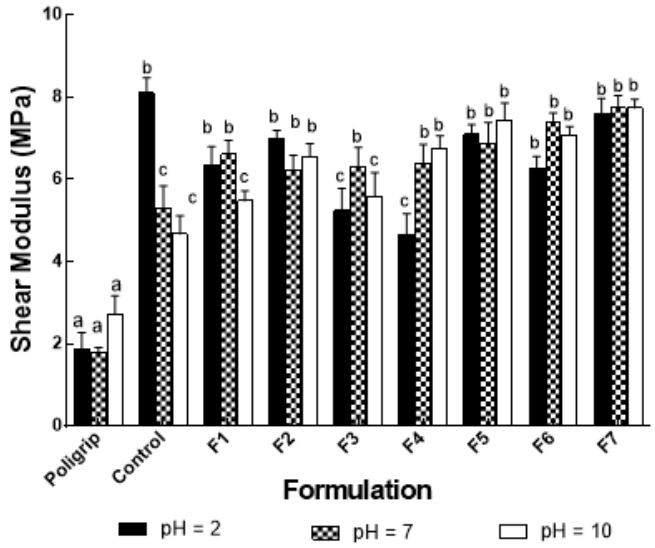

Figure 3.17 Effect of composition and pH on shear modulus of experimental adhesives. F1 = F1(P1A)-C-PBS, F2 = F2(P2A)-C-PBS, F2 = F3(P3A)-C-PBS, F4 = F4(P3B)-C-PBS, F5(P2C)-C-PBS, F6 = F6(P3C)-C-PBS, F7 = F7(P1C)-C-PBS. Similar letters mean the groups are not significantly different at $p > 0.05$.

The denture bases are made from polyacrylates, most commonly poly methyl methacrylate (PMMA). PMMA have advantages such as simple processing techniques, inexpensive fabrications, and ease of repair [28–30]. Knowing the effect of pH on adhesion is important as oral environment's pH change with food intake. Acidic food or beverages (eg. citrous fruits or soda) decreases pH whereas alkaline food or beverages (eg. soy, herbs, vegetables) increases pH. The shear stresses and moduli for Poligrip-PBS, control-PBS, and F(P)-C-PBS formulations are shown on Figure 3.16 and 3.17, respectively. All shears are around ≥ 5 kPa. With the exceptions of control-PBS and F1(P1A)-C-PBS, Poligrip-PBS and the other formulations did not follow the trend as reported by Fallahi [18]. It was expected for all formulations to lower adhesion at increasing pH. The control exceeds Poligrip in acidic conditions. Poligrip should have followed the trend reported in [18], however the material had difficulty spreading uniformly on the plexiglass. Replacing the PMVEMA with synthetic copolymers reduces adhesion because of their immiscibility with entire formulation. Adhesion is expected to be greatest at pH 2, because the PMVEMA forms hydrogen bond which repels water that slows swelling of the paste. On the other hand, at pH 10, the PMVEMA gets deprotonated which attracts more water causing faster swelling leading to degradation of paste. Also, the presence of negative electrostatic repulsion charges and neutralization with Na+ ions prevent hydrogen bonding which consequently reduces adhesion. Another possible explanation of the unfollowed trend is some copolymers were not properly mixed uniformly. Figure 3.18 shows polymer solids on the glued plexiglass which takes up space within the area of interest, thus giving rise to various shear results. One last possible error could attribute from improper removal of the adhesive from the manufacturing covers that came with the plexiglass. This can alter the surface chemistry of the plexiglass and affect its interaction with the formulations.

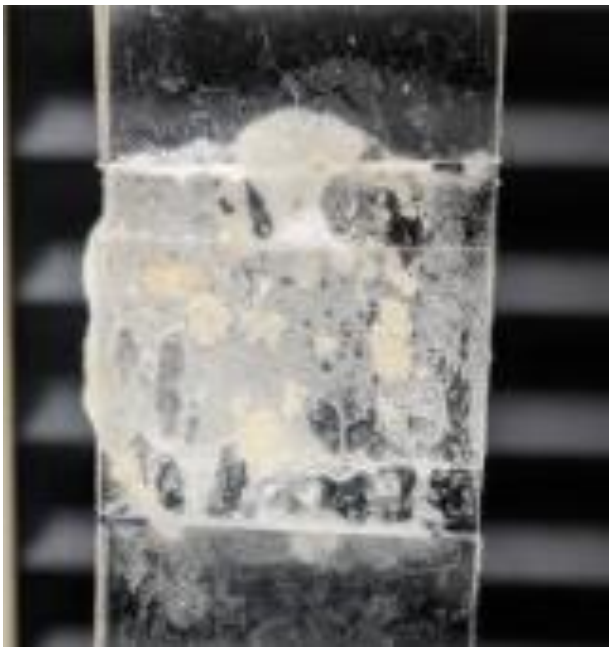

Figure 3.18 Polymer solids on the shear area of F4 (P3B)-C-PBS-2 specimen.

Asides from control-PBS and F1(P1A)-C-PBS, the unusual trends worth investigating were F6(P3C)-C-PBS and F7(P1C)-C-PBS. F6(P3C)-C-PBS. From Figure 3.16, it appears F6(P3C)-C-PBS had a reverse pH effect whereas F7(P1C)-C-PBS remained consistent through out pH change. To explain such phenomena, FTIR was implemented to see the effect of pH on hydrogen bonding. Attention was turned to the C=O (Figure 3.19a) and O-H (Figure 3.19b) stretches specifically. Of the four formulations, only F1(P1A)-C-PBS's C=O stretch had small increasing wavenumbers from acidic to basic conditions Fallahi [18]. It was expected for control-PBS to have the same trend given it had no co-polymer. F7(P1C)-C-PBS had similar C=O stretches at pH 2 and 7 but slightly higher at 10. F6(P3C)-C-PBS's trend cannot be explained from Figure 3.14a as the FTIR on all pH's show nothing unusual. Lastly, the effect in pH had no effect for O-H stretches in the four formulations. Overall, FTIR alone cannot explain the adhesion trend of all formulations. Despite some small changes in the C=O stretch, it is insufficient to confirm the effect of hydrogen bonding on adhesion. This suggest additional work such as swelling test, scanning electron microscopy, and rheology is necessary to better understand the adhesion of these formulations.

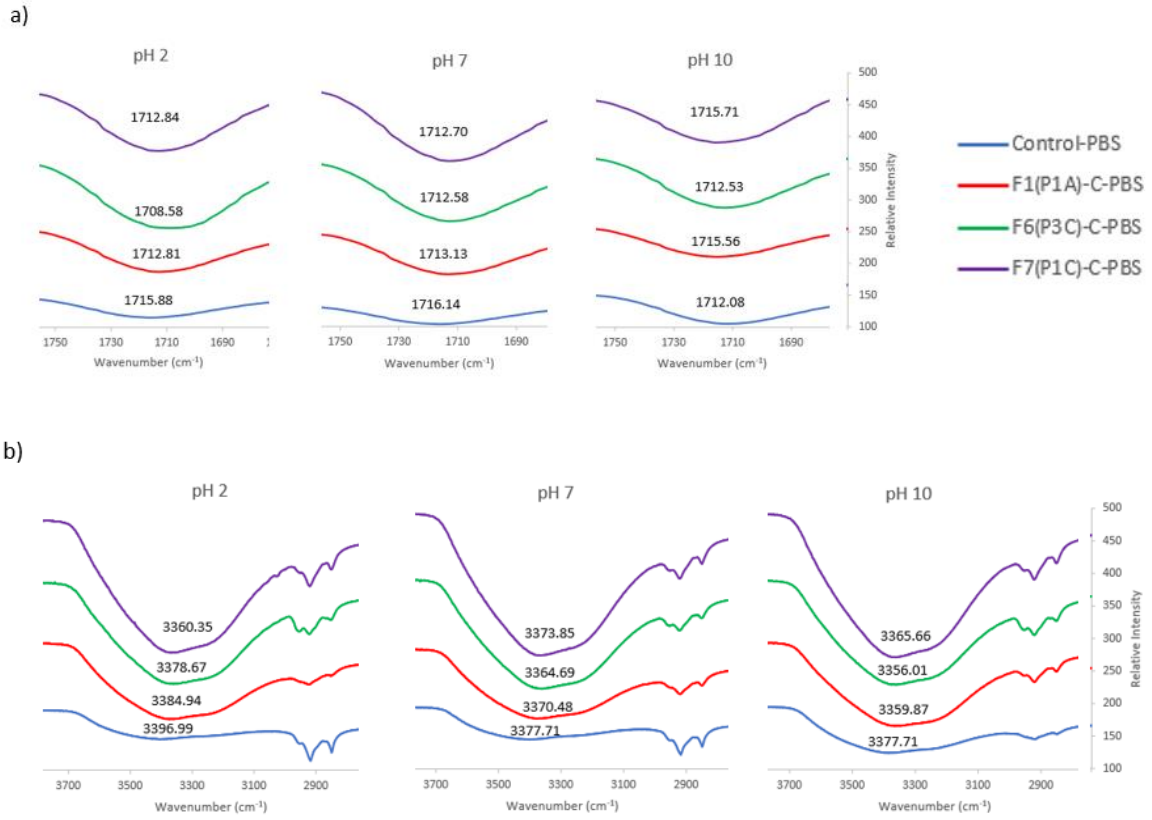

Figure 3.19 FTIR showing a) C=O and b) O-H stretches for Control-PBS, F1(P1A)-C-PBS, F6(P3C)-C-PBS, and F7(P1C)-C-PBS at different pH.

3.5 Statistical Analysis

Figure 3.16 suggests pH does not affect F1, F2, F5, F6 and F7 (labelled “a”)’s shear stress value. Only the control showed direct pH effect on its shear stress. Poligrip, F3 and F4 appeared to have significant difference at pH 2. The groups labeled “c” were equal or less then 5 kPA. These results can be attributed to the steric interactions within the copolymer caused by the electron donating functional groups. Regarding the shear modulus in Figure 3.17, Poligrip, F2, F5, F6 and F7’s modulus is not effected by pH. Both the control and F4 have significant difference at pH 2. Lastly, F3 has significant difference at pH 7.

3.6 Conclusion

Nine catechol containing copolymers (P1A-P3C) were synthesized and characterized. ^{1}H-NMR, ^{13}C-NMR, and FTIR confirmed successful deprotection. GPC results show P1-P and P2-P sets have narrow distribution according to Flory's most probable distribution whereas P3-P set have a broader distribution of molecular weight. TGA results indicate all protected copolymers P1A-P to P3C-P (except P3B-P) have one stage decomposition at around 400 ^{o} C regardless of substitution or monomer percentage. With regards to DSC, the order of glass transition temperature is P3-P > P2-P > P1-P due to substitution and size of pendant functional group. P1A-P3C were added to denture adhesive formulations (F1-F7) and combined with control and PBS to generate F(P)-C-PBS formulations for lap shear due to limited quantity. Lap shear results of all formulations were ≥ 5 kPa which satisfies ISO 10873. However, except for control-PBS and F1(P1A)-C-PBS, other formulations did not follow the trend of pH effect on adhesion due to poor uniformity. F6(P3C)-C-PBS had a reverse pH effect on shear stress and F7(P1C)-C-PBS remained consistent throughout pH change. F7(P1C)-C-PBS's consistent shear stress can be a strong asset for denture adhesives, especially for those with diet concerns. The control-PBS, F1(P1A)-C-PBS, F6(P3C)-C-PBS, and F7(P1C)-C-PBS had their hydrogen bonding properties investigated by FTIR however it was not enough to explain their resulted shear stress. Overall, additional experiments such as swelling test, scanning electron microscopy, and rheology needs to be done to better understand these formulations' adhesive nature. Lastly, the cytotoxicity of the P1 copolymer series have been determined in [6], it is important to evaluate P2 and P3 also if they were to be deployed for wet adhesion applications.

3.7 References

[1] G. Westwood, T.N. Horton, J.J. Wilker, Simplified Polymer Mimics of Cross-Linking Adhesive Proteins, Macromolecules. 40 (2007) 3960–3964. https://doi.org/10.1021/ma0703002.

[2] C.R. Matos-Pérez, J.D. White, J.J. Wilker, Polymer Composition and Substrate Influences on the Adhesive Bonding of a Biomimetic, Cross-Linking Polymer, J. Am. Chem. Soc. 134 (2012) 9498–9505. https://doi.org/10.1021/ja303369p.

[3] C. Leng, Y. Liu, C. Jenkins, H. Meredith, J.J. Wilker, Z. Chen, Interfacial Structure of a DOPA-Inspired Adhesive Polymer Studied by Sum Frequency Generation Vibrational Spectroscopy, Langmuir. 29 (2013) 6659–6664. https://doi.org/10.1021/la4008729.

[4] H.J. Meredith, C.L. Jenkins, J.J. Wilker, Enhancing the Adhesion of a Biomimetic Polymer Yields Performance Rivaling Commercial Glues, Advanced Functional Materials. 24 (2014) 3259–3267. https://doi.org/10.1002/adfm.201303536.

[5] M.A. North, C.A. Del Grosso, J.J. Wilker, High Strength Underwater Bonding with Polymer Mimics of Mussel Adhesive Proteins, ACS Appl. Mater. Interfaces. 9 (2017) 7866–7872. https://doi.org/10.1021/acsami.7b00270.

[6] M.J. Brennan, H.J. Meredith, C.L. Jenkins, J.J. Wilker, J.C. Liu, Cytocompatibility studies of a biomimetic copolymer with simplified structure and high-strength adhesion, Journal of Biomedical Materials Research Part A. 104 (2016) 983–990. https://doi.org/10.1002/jbm.a.35633.

[7] A.H. Hofman, I.A. van Hees, J. Yang, M. Kamperman, Bioinspired Underwater Adhesives by Using the Supramolecular Toolbox, Advanced Materials. 30 (2018) 1704640. https://doi.org/10.1002/adma.201704640.

[8] Q. Lu, E. Danner, J.H. Waite, J.N. Israelachvili, H. Zeng, D.S. Hwang, Adhesion of mussel foot proteins to different substrate surfaces, Journal of The Royal Society Interface. 10 (2013) 20120759. https://doi.org/10.1098/rsif.2012.0759.

[9] J.E. Méndez Silva, C.C. Madrid Troconis, L.R. Tirado Amador, SALIVA AND ALTERNATIVE ADHESIVE SYSTEMS FOR COMPLETE DENTURES, Revista Facultad de Odontología Universidad de Antioquia. 25 (2013) 208–218.

[10] S.K. Gill, N. Roohpour, P.D. Topham, B.J. Tighe, Tunable denture adhesives using biomimetic principles for enhanced tissue adhesion in moist environments, Acta Biomaterialia. 63 (2017) 326–335. https://doi.org/10.1016/j.actbio.2017.09.004.

[11] A.J. Coates, Usage of denture adhesives, Journal of Dentistry. 28 (2000) 137–140. https://doi.org/10.1016/S0300-5712(99)00046-9.

[12] Y. Kulak, M. Özcan, A. Arikan, Subjective Assessment by Patients of the Efficiency of Two Denture Adhesive Pastes, Journal of Prosthodontics. 14 (2005) 248–252. https://doi.org/10.1111/j.1532-849X.2005.00049.x.

[13] S. Papadiochou, I. Emmanouil, I. Papadiochos, Denture adhesives: A systematic review, The Journal of Prosthetic Dentistry. 113 (2015) 391-397.e2. https://doi.org/10.1016/j.prosdent.2014.11.001.

[14] J.E. Grasso, Denture adhesives, Dental Clinics. 48 (2004) 721–733. https://doi.org/10.1016/j.cden.2004.04.002.

[15] J.K. Rendell, T. Gay, J.E. Grasso, R.A. Baker, J.L. Winston, THE EFFECT OF DENTURE ADHESIVE: ON MANDIBULAR MOVEMENT DURING CHEWING, The Journal of the American Dental Association. 131 (2000) 981–986. https://doi.org/10.14219/jada.archive.2000.0316.

[16] X. Guo, F. Deng, L. Li, R.K. Prud'homme, Synthesis of Biocompatible Polymeric Hydrogels with Tunable Adhesion to both Hydrophobic and Hydrophilic Surfaces, Biomacromolecules. 9 (2008) 1637–1642. https://doi.org/10.1021/bm800142z.

[17] S.K. Gill, N. Roohpour, Y. An, J.E. Gautrot, P.D. Topham, B.J. Tighe, Hydrophobic and hydrophilic effects on water structuring and adhesion in denture adhesives, Journal of Biomedical Materials Research Part A. 106 (2018) 1355–1362. https://doi.org/10.1002/jbm.a.36341.

[18] A. Fallahi, N. Khadivi, N. Roohpour, A.M. Middleton, M. Kazemzadeh-Narbat, N. Annabi, A. Khademhosseini, A. Tamayol, Characterization, mechanistic analysis and improving the properties of denture adhesives, Dental Materials. 34 (2018) 120–131. https://doi.org/10.1016/j.dental.2017.09.015.

[19] H. Hirohara, K. Takaya, N. Ise, A Study of the Effect of Impurities in Living Anionic Polymerization, Macromolecules. 4 (1971) 288–290. https://doi.org/10.1021/ma60021a005.

[20] J.B.P. Soares, The Use of Instantaneous Distributions in Polymerization Reaction Engineering, Macromolecular Reaction Engineering. 8 (2014) 235–259. https://doi.org/10.1002/mren.201300173.

[21] J. Qiu, K. Matyjaszewski, Polymerization of Substituted Styrenes by Atom Transfer Radical Polymerization, Macromolecules. 30 (1997) 5643–5648. https://doi.org/10.1021/ma9704222.

[22] J.M.G. Cowie, V. Arrighi, Polymers: chemistry and physics of modern materials, CRC Press, Boca Raton, 2008. //catalog.hathitrust.org/Record/009464216.

[23] D.A. Lukyanov, R.V. Apraksin, A.N. Yankin, P.S. Vlasov, O.V. Levin, E.G. Tolstopjatova, V.V. Kondratiev, Synthesis and electrochemical properties of poly(3,4-dihydroxystyrene) and its composites with conducting polymers, Synthetic Metals. 256 (2019) 116151. https://doi.org/10.1016/j.synthmet.2019.116151.

[24] A. Şenocak, C. Alkan, A. Karadağ, Thermal Decomposition and a Kinetic Study of Poly(Para-Substituted Styrene)s, AJAC. 07 (2016) 246–253. https://doi.org/10.4236/ajac.2016.73021.

[25] A. Rincon, I.C. McNeill, Thermal degradation of blends of polystyrene and poly-4-methoxystyrene with bisphenol A polycarbonate, Polymer Degradation and Stability. 40 (1993) 343–348. https://doi.org/10.1016/0141-3910(93)90140-E.

[26] K. Kunal, C.G. Robertson, S. Pawlus, S.F. Hahn, A.P. Sokolov, Role of Chemical Structure in Fragility of Polymers: A Qualitative Picture, Macromolecules. 41 (2008) 7232–7238. https://doi.org/10.1021/ma801155c.

[27] H. Kano, T. Kurogi, T. Shimizu, M. Nishimura, H. Murata, Viscosity and adhesion strength of cream-type denture adhesives and mouth moisturizers, Dental Materials Journal. 31 (2012) 960–968. https://doi.org/10.4012/dmj.2012-004.

[28] M. Nakhaei, H. Dashti, R. Barazandeh, N. Teimouri, Shear Bond Strength of Acrylic Denture Teeth to PMMA and Polyamide Denture Base Materials, Journal of Dental Materials and Techniques. 7 (2018) 19–24. https://doi.org/10.22038/jdmt.2017.10003.

[29] C. Machado, E. Sanchez, S.S. Azer, J.M. Uribe, Comparative study of the transverse strength of three denture base materials, Journal of Dentistry. 35 (2007) 930–933. https://doi.org/10.1016/j.jdent.2007.09.006.

[30] S.B. Patil, B.H. Naveen, N.P. Patil, Bonding acrylic teeth to acrylic resin denture bases: a review, Gerodontology. 23 (2006) 131–139. https://doi.org/10.1111/j.1741-2358.2006.00129.x.

Chapter 4

4 Reactivity Ratios of 3,4-Dimethoxystyrene and Para-Substituted Styrene in Free Radical Copolymerization

4.1 Abstract

Free radical polymerization of 3,4 - DMS and para-substituted styrene derivatives were performed using AIBN in toluene-d_8 at 70 ^{o} C and studied under *in-situ* NMR for first time. Reactivity ratios were calculated using NLLS (Mayo-Lewis and Meyer-Lowry method) and LLS (K-T method), which showed similar results. The reactivity ratio of 3,4 – DMS and styrene was $r_{3,4\text{-DMS}} = 1.55$ and $r_{styrene} = 0.84$ (Meyer-Lowry), $r_{3,4\text{-DMS}} = 1.53 \pm 0.06$ and $r_{styrene} = 0.89 \pm 0.04$ (Mayo-Lewis) and provided $r_{3,4\text{-DMS}} = 1.57 \pm 0.05$ and $r_{styrene} = 0.90 \pm 0.04$ (K.T). Furthermore, the reactivity ratio of 3,4 – DMS and 4ms was $r_{3,4\text{-DMS}} = 1.43$ and $r_{4ms} = 0.76$ (Meyer-Lowry), $r_{3,4\text{-DMS}} = 1.31 \pm 0.07$ and $r_{4ms} = 0.72 \pm 0.04$ (Mayo-Lewis) and $r_{3,4\text{-DMS}} = 1.30 \pm 0.06$ and $r_{4ms} = 0.71 \pm 0.04$ (K.T). Lastly, the reactivity ratio between 3,4 – DMS and 4-tbs was $r_{3,4\text{-DMS}} = 1.93$ and $r_{4tbs} = 1.07$ (Meyer-Lowry), $r_{3,4\text{-DMS}} = 1.73 \pm 0.08$ and $r_{4tbs} = 1.00 \pm 0.05$ (Mayo-Lewis) and $r_{3,4\text{-DMS}} = 1.72 \pm 0.08$ and $r_{4tbs} = 0.98 \pm 0.06$ (K.T). All calculated reactivity ratios suggest the para-substitution have minor effect on its value and all copolymers adopt a random chain sequence.

4.2 Introduction

A copolymerization reaction consists of two monomers M_1 and M_2 where four propagation reactions may occur, as either monomer can be added to the last propagating ends M_1* and M_2*. The rate constant k determines the compositional profile. The reactivity ratios, r_1 and r_2, is the measurement of both M_1 and M_2's preference for insertion into the growing polymer [1] and is defined by equation 4-5.

$$M_1^* + M_1 \xrightarrow{k11} M_1M_1^*$$

$$M_1^* + M_2 \xrightarrow{k12} M_1M_2^*$$

$$M_2^* + M_2 \xrightarrow{k22} M_2M_2^*$$

$$M_2^* + M_1 \xrightarrow{k21} M_2M_1^*$$

$$r_1 = \frac{k11}{k12} \text{ and } r_2 = \frac{k22}{k21} \quad (4\text{-}1)$$

Copolymerization of M_1 and M_2 can produce a copolymer of 3 unique sequences block, alternating or random (Figure 4.1). The sequence of M_1 and M_2 in the chain and compositional heterogeneity greatly influence the chemical and physical properties of the copolymer [2]. Therefore, determining the reactivity ratios of M_1 and M_2 allows prediction of copolymer composition the structure [3].

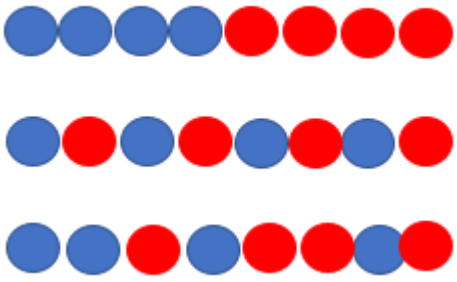

Figure 4.1 Possible chain sequences of copolymers are block (top), alternating (middle) or random (bottom).

The calculation method for reactivity ratios are categorized into non-linear least squares (NLLS) method and linear least squares (LLS) method [2]. Common LLS methods include Finemann-Ross (F-R) and Kelen-Tüdös (K-T) [2,4]. The F-R equation (eq 4-2) can determine reactivity ratios through the linear plot of G versus H using known M_1 quantity in the feed (f_1) and in the polymer composition (F_1). The slope and intercept provide r_1 and r_2, respectively.

$$G = r_1H - r_2 \qquad (4\text{-}2)$$

$$G = \frac{f_1(2F_1-1)}{F_1(1-f_1)} \qquad (4\text{-}3)$$

$$H = \frac{f_1^2(1-F_1)}{F_1(1-f_1)^2} \qquad (4\text{-}4)$$

Suppose monomer concentrations are too high or too low, this will introduce bias in the F-R equation. To avoid bias, Kelen and Tüdös introduced an arbitrary constant α to distribute the data more evenly [5] and yielding the K-T equation (eq 4-5).

$$\eta = [r_1 + \frac{r_2}{\alpha}]\mu - \frac{r_2}{\alpha} \qquad (4\text{-}5)$$

$$\alpha = \sqrt{H_{min}H_{max}} \qquad (4\text{-}6)$$

$$\eta = \frac{G}{\alpha+H} \qquad (4\text{-}7)$$

$$\mu = \frac{H}{\alpha+H} \qquad (4\text{-}8)$$

Plotting η verses μ yields r_1 and r_2 using the slope and intercept. In 1987, O'Driscoll and Reilly reported the LLS method distorts the error distribution resulting in poor estimates [6]. The NLLS method using the famous Mayo–Lewis equation (eq 4-9) is more accurate and statistically sound [2,7].

$$F_1 = \frac{r_1 f_1^2 + f_1(1-f_1)}{r_1 f_1^2 + 2f_1(1-f_1) + r_2(1-f_1)^2} \tag{4-9}$$

$$F_1 = \frac{d[M_1]}{d[M_1] + d[M_2]} \tag{4-10}$$

$$f_1 = \frac{[M_1]}{[M_1] + [M_2]} \tag{4-11}$$

Meyer and Lowry integrated the Mayo−Lewis equation into the Meyer−Lowry equation (eq 4-12) [2] which can be directly fit by means of the NLLS method which was recommended by Lynd et al. for accurate experimental computation of reactivity ratios [8].

$$X_{n,t=t} = 1 - \left(\frac{f_{1,t=t}}{f_{1,t=0}}\right)^{\frac{r_2}{1-r_2}} \times \left(\frac{1-f_{1,t=t}}{1-f_{1,t=0}}\right)^{\frac{r_1}{1-r_1}} \times \left(\frac{(2-r_1-r_2)f_{1,t=t} + r_2 - 1}{(2-r_1-r_2)f_{1,t=0} + r_2 - 1}\right)^{\frac{(r_1 r_2 - 1)}{(1-r_1)(1-r_2)}} \tag{4-12}$$

$$X_{n,t} = 1 - \frac{m_{1,t} + m_{2,t}}{m_{1,t=0} + m_{2,t=0}} \tag{4-13}$$

A plethora of $F_1 - f_1$ data determined experimentally is needed by both the LLS and the NLLS methods using the Mayo–Lewis equation. Two concerns regarding this technique are 1) approximate F_1 introduces experimental errors and 2) it requires extensive experimental effort to run the copolymerization at a series of feed compositions. One advantage using Meyer-Lowry equation is it does not require $F_1 - f_1$ data but rather

dependent on $X_{n.}$ - f_1 values which avoids approximate F_1 and experimental errors altogether.

4.2.1 Reactivity Ratio Determination by In-Situ NMR

With the advent of *in situ* spectroscopies such as ^{1}H NMR and FTIR, obtaining a series of $F_1 - f_1$ data in a single *in situ* experiment is possible and making extensive experimental endeavors less cumbersome [2,9]. However, *in-situ* FTIR struggles with distinguishing peaks between the monomer and the copolymer. In this case, NMR is preferred for its greater selectivity, resolution, and sensitivity towards variations compared to FTIR [10]. The most notable feature of *in-situ* NMR is monitoring real-time concentration of individual monomers and the continuously forming copolymer in tandem throughout a single run [11]. For efficient use of *in-situ* NMR, it is important that 1) the copolymerization reaction rate needs to be lower than scanning rate, 2) the monomer and copolymer's peaks are distinguishable from each other, and 3) the copolymer is soluble in the selected deuterium solvent [12]. The sequence prediction of M_1 and M_2 with reactivity ratios is summarized on Table 4.1.

Table 4.1 Summary of reactivity ratios and their corresponding chain sequences.

r_1	r_2	Sequence
=1	=1	Random
>1	<1	
~0	~0	Alternating
>1	>1	Block

In 1968, Lau and Burns copolymerized 2,6 dimethoxystyrene (2,6-DMS) and styrene using free radical and computed their reactivity ratios to be $r_{2,6\text{-DMS}} = 0.55 \pm 0.001$ and $r_{styrene} = 0.98 \pm 0.04$ respectively using Mayo-Lewis suggesting alternating sequence [13]. In a more recent work, Leibig et al. took 4-vinylcatechol acetonide (4-VCA) or 3-vinylcatechol acetonide (3-VCA) and performed carbanionic copolymerization with styrene. Using K-T equation, the reactivity ratios for 4-VCA: styrene were $r_{4\text{-VCA}} = 0.24$; $r_{styrene} = 4.0$ and for 3-VCA: styrene were $r_{3\text{-VCA}} = 2.4$; $r_{styrene} = 0.48$ [14]. However, both works never stressed the importance of LLS or NLLS. In the previous chapter, 3,4 –

dimethoxystyrene (3,4 – DMS) and other substituted styrene have been copolymerized using free radical approach. 3,4 – DMS, a commercially available precursor for preparing mussel-inspired copolymers, and its reactivity ratios with substituted styrene have not been reported in the literature. Knowing their reactivity ratios can allow better understanding of their structure and physical properties. This chapter will focus on computing reactivity ratios of 3,4 – DMS and various substituted styrene via KT, Mayo – Lewis and Meyer – Lowry with the aid of *in-situ* NMR.

4.3 Experimental Section

4.3.1 Materials

Sodium hydroxide (NaOH), sodium chloride (NaCl, 99%), toluene-d_8 (99.6 %, Sigma Aldrich), and dimethylformamide (DMF, Caledon) were used as received. 2,2′-Azobis(2-methylpropionitrile) (98%, AIBN, Aldrich) was recrystallized in methanol and stored at -4^{o}C prior to use. 3,4-dimethoxystyrene (3,4-DMS, 99 %, Sigma Aldrich) was placed in a separatory funnel and washed with 10% NaOH, distilled water, and brine to remove the inhibitor tert-butylcatechol (TBC), dried with $MgSO_4$ overnight before placing in cold storage. Styrene (sty, ≥ 99%, Sigma Aldrich), 4-methylstyrene (4ms, 98%, Alfa Aesar), and 4-tert-butylstyrene (4tbs, 94%, Alfa Aesar) was passed through a prepacked column inhibitor remover (TBC, Scientific Polymer), sealed, and stored at -20 ^{o} C before use.

4.3.2 Copolymerization

Copolymerization was performed by *in situ* NMR spectroscopy according to our previously published methods [2,15]. The copolymerization of 3,4 - DMS and selected substituted styrene was done in toluene-d_8 or where AIBN and DMF were used as the initiator and the internal reference, respectively. In a typical experiment, the predetermined amounts of 3,4 -DMS and substituted styrene, AIBN, and DMF (Table 4.2) were dissolved in toluene-d_8 in an NMR tube by using a vortex mixer. The mixture was then purged with nitrogen for 20 min to remove dissolved oxygen. The amounts of monomers were also further determined by ^{1}H NMR based on the amount of internal reference DMF. The reaction was performed in the NMR tube in the NMR spectrometer

at 70 ° C. The NMR instrument was programmed to collect one ^{1}H NMR spectrum every 5 min for 13 h.

4.3.3 Characterization

The copolymerization process was detected *in situ* by a Varian INOVA 600 at 70 °C. The ^{1}H NMR spectra of the monomers' mixture before and after *in situ* copolymerization were collected at 25 °C and 70 °C. All chemical shifts were referenced to tetramethylsilane (0.0 ppm). ACD Spectrus Processor was used for analyzing the ^{1}H NMR spectra. MATLAB is used compute reactivity ratios.

4.4 Results and Discussion

Upon exposure to heat, free radicals produced by AIBN initiated the copolymerization of 3.4- DMS and the substituted styrene. The vinyl group on each monomer contributed to the formation of the hydrocarbon backbone (Scheme 4.1). The list of *in-situ* NMR experiments is summarized on Table 3.2 at 70 ° C in 1 ml toluene-d_8.

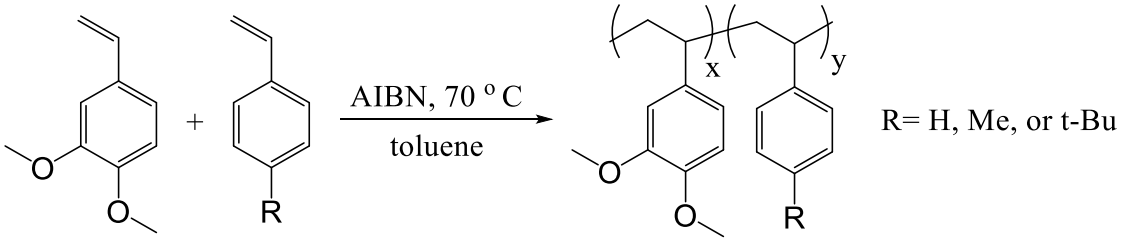

Scheme 4.1 Copolymerization of 3,4 -DMS and substituted styrene derivatives using AIBN and toluene-d_8 during in-situ NMR.

Table 4.2 List of in-situ NMR experiments conducted in this chapter using toluene-d_8 in 70 ^{o} C for 13 hours.

Exp	3,4 – DMS (mg)	4-R-Styrene (mg)	R	AIBN (mg)	DMF (mg)
1	43.00	30.00	H	2.58	17.25
2	25.48	37.07	H	2.66	17.55
3	62.87	14.56	H	2.59	16.23
4	37.34	32.72	Me	2.65	19.20
5	24.92	41.66	Me	2.63	19.73
6	58.27	19.77	Me	2.65	15.37
7	41.60	45.20	t-Bu	2.56	18.30
8	28.30	61.90	t-Bu	2.69	17.18
9	59.48	28.64	t-Bu	2.56	19.03

As mentioned in the introduction, *in-situ* ^{1}H-NMR analysis for reactivity ratio determination in copolymerization has been proved to be efficient and less cumbersome. DMF was added to the mixture to monitor the changes of each monomer and AIBN during the copolymerization process. DMF characteristic peaks do not overlap with other characteristic peaks and is inert throughout the entire run. The characteristic peaks of DMF in toluene-d_8 spectra are 2.13, 2.43 and 7.65 ppm. As an example, the ^{1}H-NMR spectrums of the copolymerization mixture for Exp 1 before and after 10 h are shown in Figure 4.2.

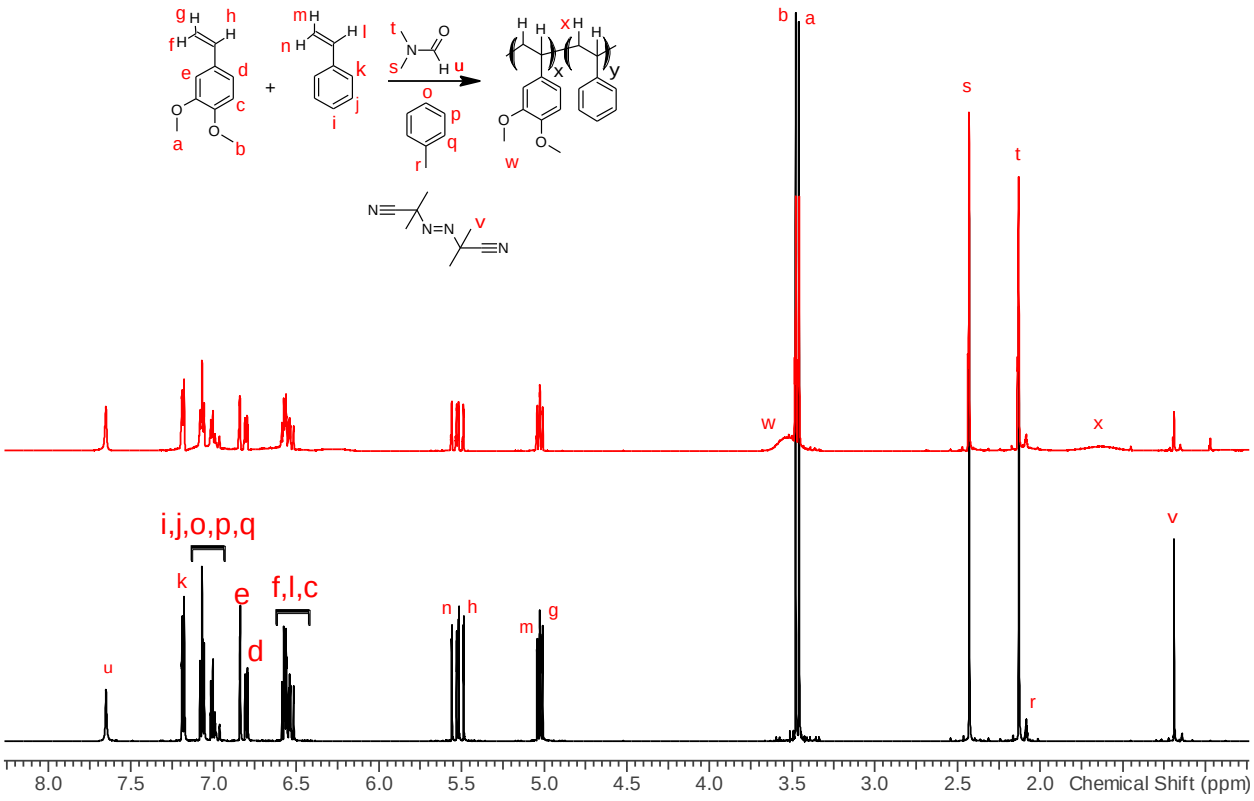

Figure 4.2 ^{1}H-NMR spectrums of the copolymerization mixture for Exp 1 before and after 10 hours in toluene-d_8 at 70 ^{o} C.

Other important characteristic peaks include the two vinyl groups on both 3,4 – DMS (6.64, 5.59, 5.11 ppm) and styrene (6.57, 5.61, 5.09 ppm) plus AIBN at 1.16 ppm. As time progresses, the peak labeled “x” indicates the formation of the aliphatic polymer backbone. The peak labeled “w” indicates 3,4 – DMS is being added to the backbone, the sharp peaks at the start become shorter and broader.

To determine the moles of the monomers over time, characteristic peaks of 3,4 – DMS (5.59 ppm) and styrene (5.61 ppm) were integrated by referencing the integration of DMF (7.65 ppm). These protons were easily defined and did not overlap with other peaks. The integration values of both monomers decreased over time, while “x” and “w” peaks increased. The reaction profiles of Exp 1-3 from 0 – 600 minutes were integrated using every 15 min intervals and the monomer consumptions are shown in Figure 4.3.

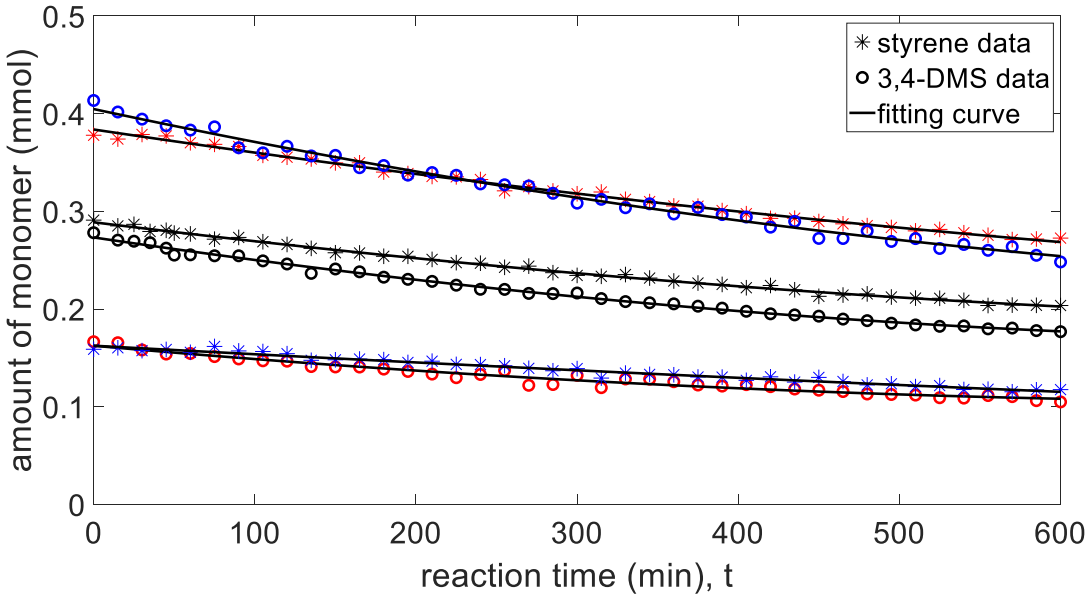

Figure 4.3 Consumption profile of styrene (∗) and 3,4-dimethoxystyrene (o) with reaction time for the copolymerization at 70 °C in toluene-d_8. Three sets of experiments are identified as three different colors: Exp 1 (black), Exp 2 (red) and Exp 3 (blue).

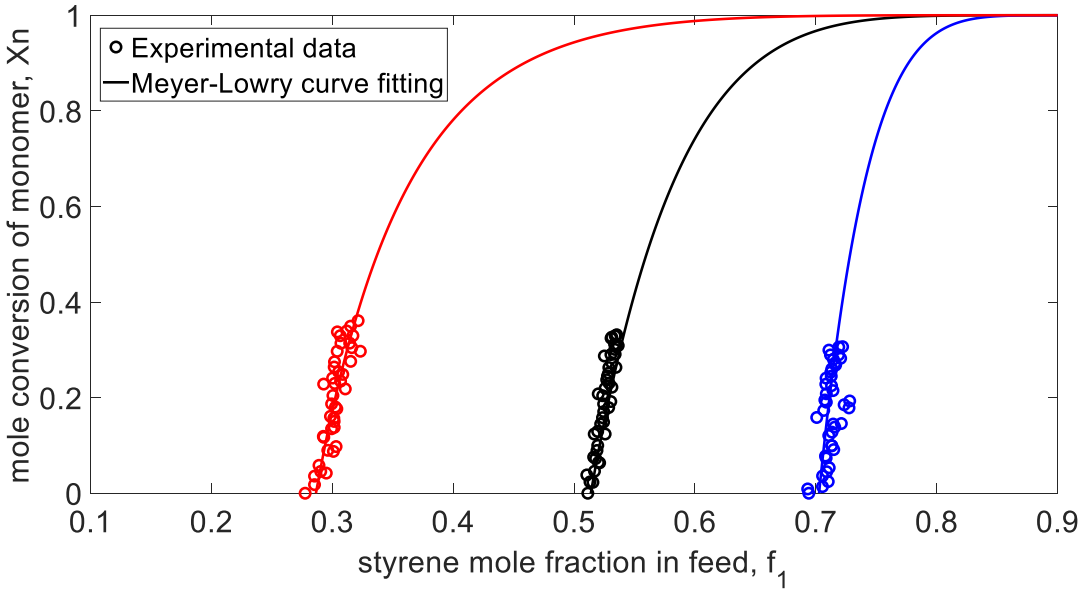

Figure 4.4 Fitting curves by the Meyer-Lowry method using the data from three sets of in situ NMR experiments for the copolymerization of styrene and 3,4-dimethoxystyrene at 70 °C in toluene-d_8. Exp 1 (black), Exp 2 (red) and Exp 3 (blue).

All experimental data in Figure 4.3 lie close to the fitting curve generated by MATLAB. Using the fitting curve, the mole fraction of styrene in the feed ($f_{1,t}$) and total mole conversion ($X_{n,t}$) at any time can be calculated using equations 4-15 and 4-17 respectively. Both $f_{1,t}$ and $X_{n,t}$ values allow the construction of the Meyer-Lowry fitting curves via NLLS method shown in Figure 4.4 for Exp 1-3. Using all three Meyer-Lowy fitting curves, the calculated reactivity ratios for 3,4 -DMS and styrene are $r_{3,4\text{-DMS}} = 1.55$ and $r_{styrene} = 0.84$. In addition to having both $f_{1,t}$ and $X_{n,t}$, it is possible to obtain mole fraction (F_1) of styrene in the copolymer using numerical solution differential method (NSD) (eq 4-14).

$$F_{1,t} = f_{1,t} - (1 - X_{n,t})\frac{df_1}{dX_n} \qquad (4\text{-}14)$$

After obtaining a set of $F_{1,t}$ - $f_{1,t}$, the fitting curve by NLLS method of Mayo-Lewis (eq 4-13) can be plotted (Figure 4.5). The NLLS method of Meyer-Lowry (eq 4-16) was also plotted for comparison and both curves are identical with experimental data fitting along them. Having $F_{1,t}$ - $f_{1,t}$ values on the fitting curve, computing reactivity ratios using NLLS of Mayo-Lewis is $r_{3,4\text{-DMS}} = 1.53 \pm 0.06$ and $r_{styrene} = 0.89 \pm 0.04$ whereas using LLS of K-T provided $r_{3,4\text{-DMS}} = 1.57 \pm 0.05$ and $r_{styrene} = 0.90 \pm 0.04$.

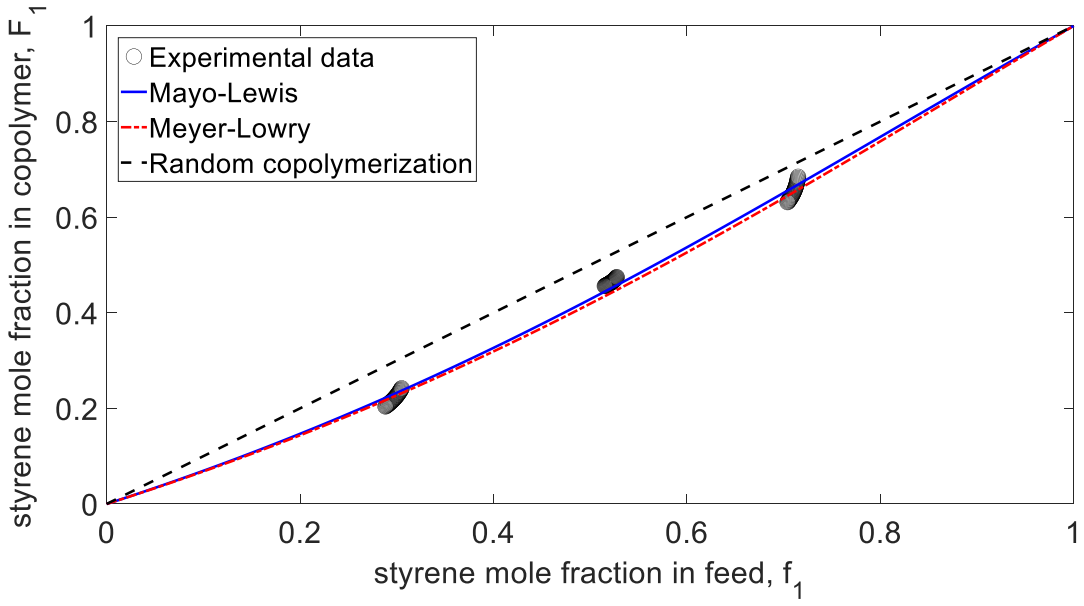

Figure 4.5 Fitting curve by the Mayo-Lewis method and compared with the Meyer-Lowry method, using the data from Exp 1-3 in-situ NMR experiments for the copolymerization of styrene and 3,4-dimethoxystyrene at 70 °C in toluene-d_8.

The same approach was applied to calculate the reactivity ratios for Exp 4-9. Figures 4.6 to Figure 4.14 shows the ^{1}H-NMR spectrums, reaction profiles, Meyer-Lowry fitting curve, and Mayo-Lewis fitting curves for Exp 4-9. Finally, all reactivity ratios of Exp 1-9 using K-T, Mayo-Lewis, and Meyer-Lowry are summarized on Table 4.3. Although the 4-methylstyrene had the lowest value, its not significantly different from styrene and 4-tert-butylstyrene, suggesting para-substitution had little affect on reactivity ratio. Figure 4.15 compares the Mayo-Lewis curves of the three sets of reactivity ratios, and it can be seen they all adopt random polymeric sequence.

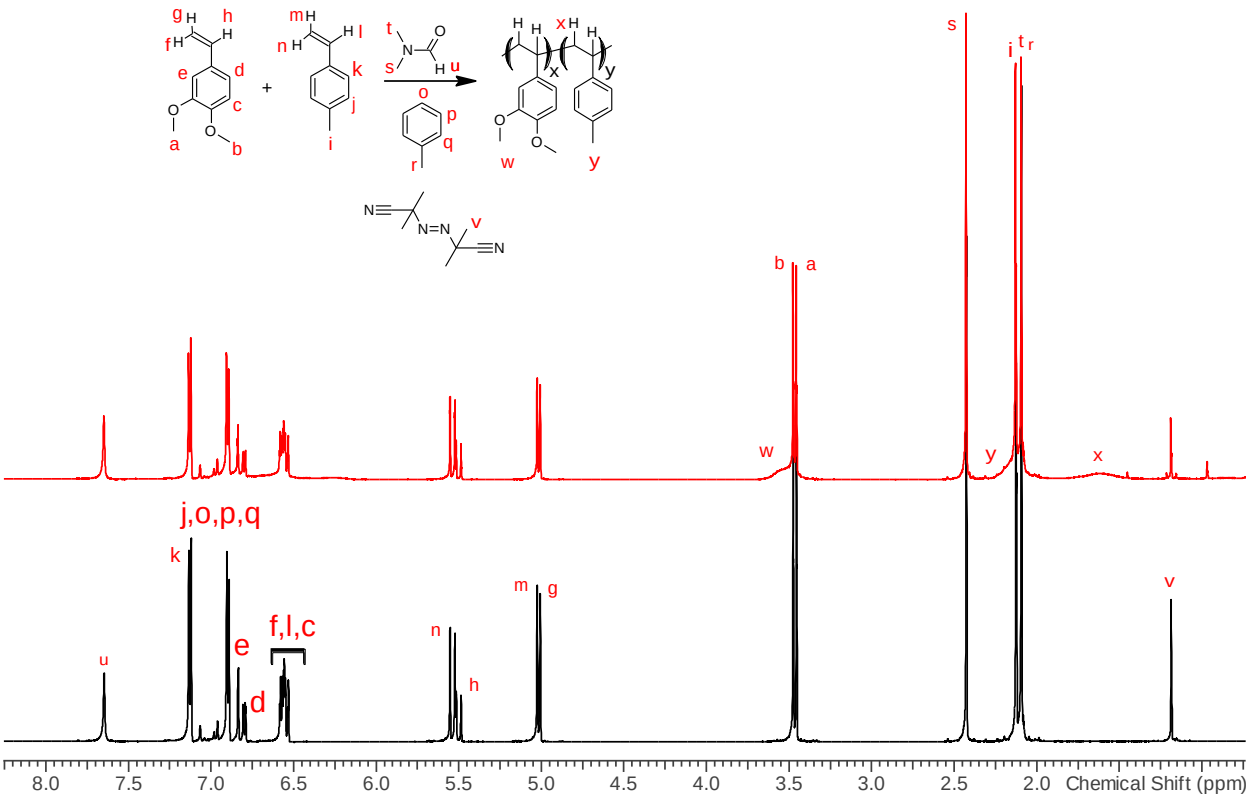

Figure 4.6 ^{1}H-NMR spectrums of the copolymerization mixture for Exp 4 before and after 10 hours in toluene-d_8 at 70 ^{o} C.

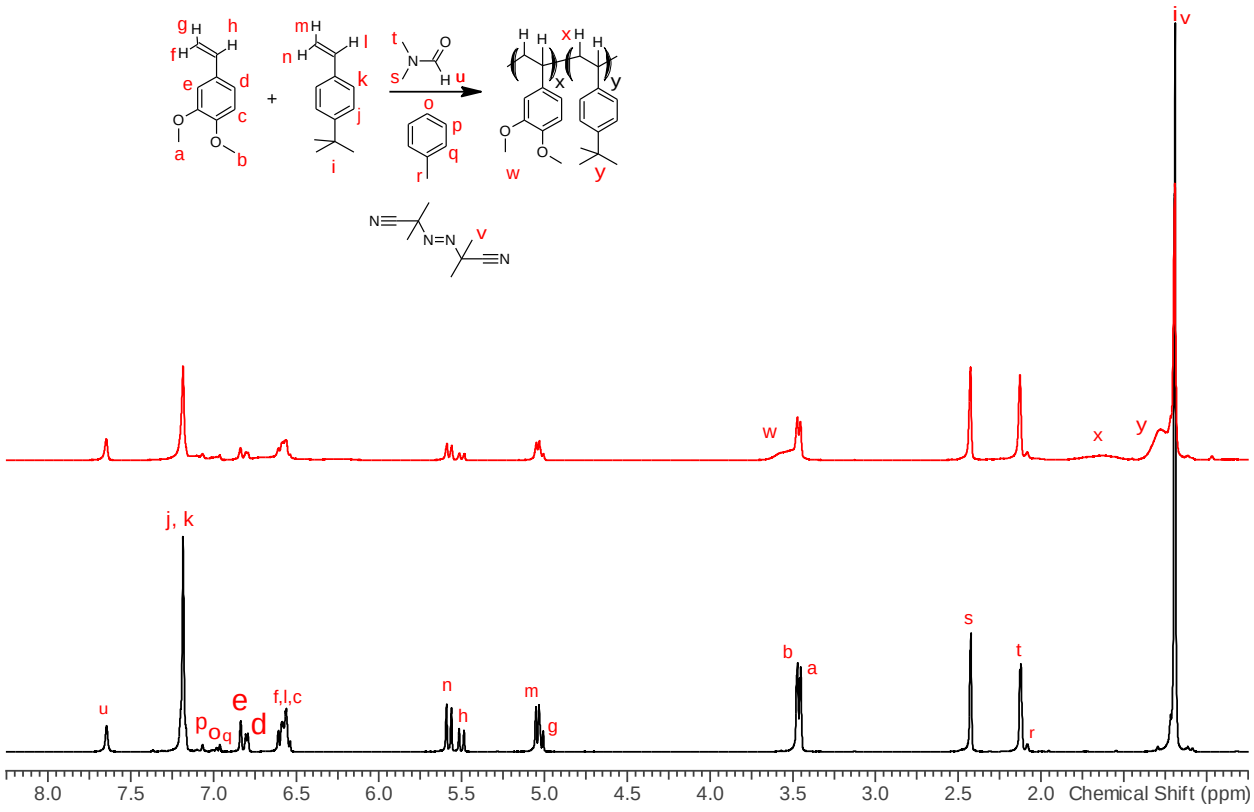

Figure 4.7 ^{1}H-NMR spectrums of the copolymerization mixture for Exp 7 before and after 10 hours in toluene-d_8 at 70 ^{o} C.

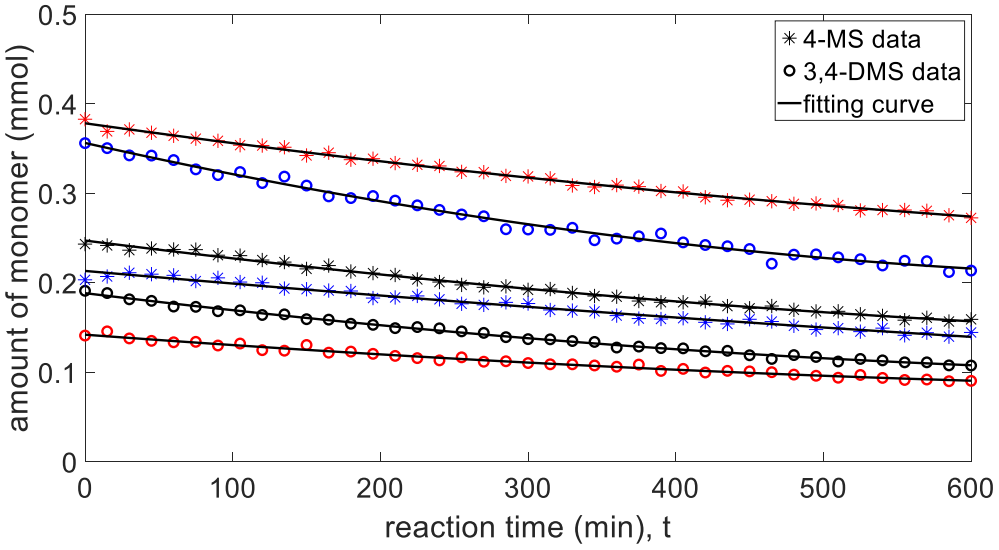

Figure 4.8 Consumption profile of 4-methylstyrene (∗) and 3,4-dimethoxystyrene (o) with reaction time for the copolymerization at 70 °C in toluene-d_8. Three sets of experiments are identified as three different colors: Exp 4 (black), Exp 5 (red), Exp 6 (blue).

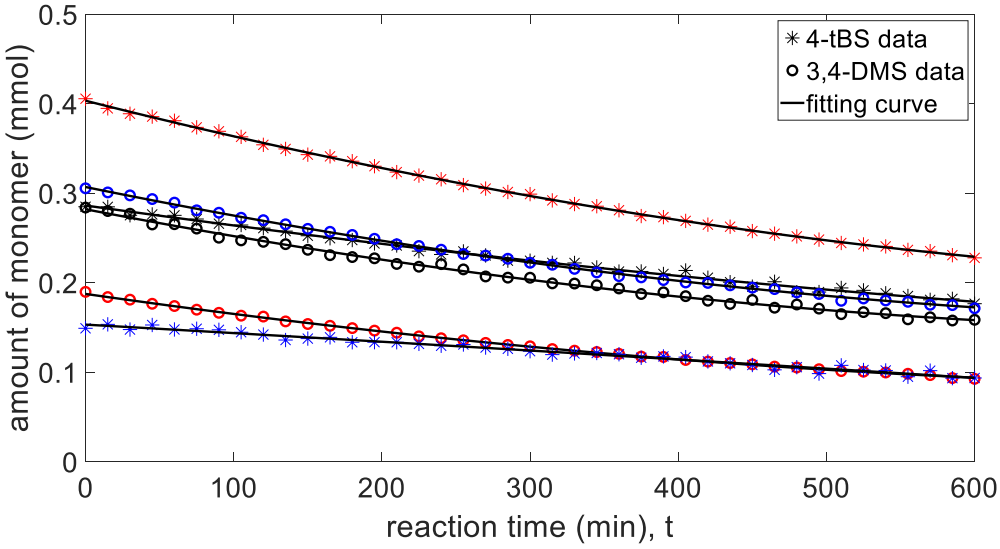

Figure 4.9 Consumption profile of 4-tert-butylstyrene (∗) and 3,4-dimethoxystyrene (o) with reaction time for the copolymerization at 70 °C in toluene-d_8. Three sets of experiments are identified as three different colors: Exp 7 (black), Exp 8 (red), Exp 9 (blue).

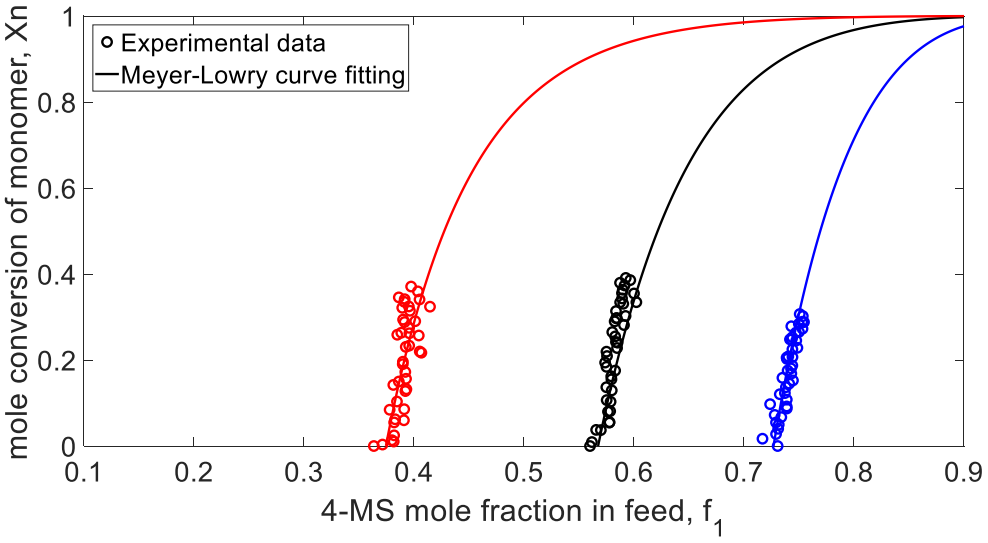

Figure 4.10 Fitting curves by the Meyer-Lowry method using the data from three sets of in situ NMR experiments for the copolymerization of 4-methylstyrene and 3,4-dimethoxystyrene at 70 °C in toluene-d_8. Exp 4 (black), Exp 5 (red), Exp 6 (blue).

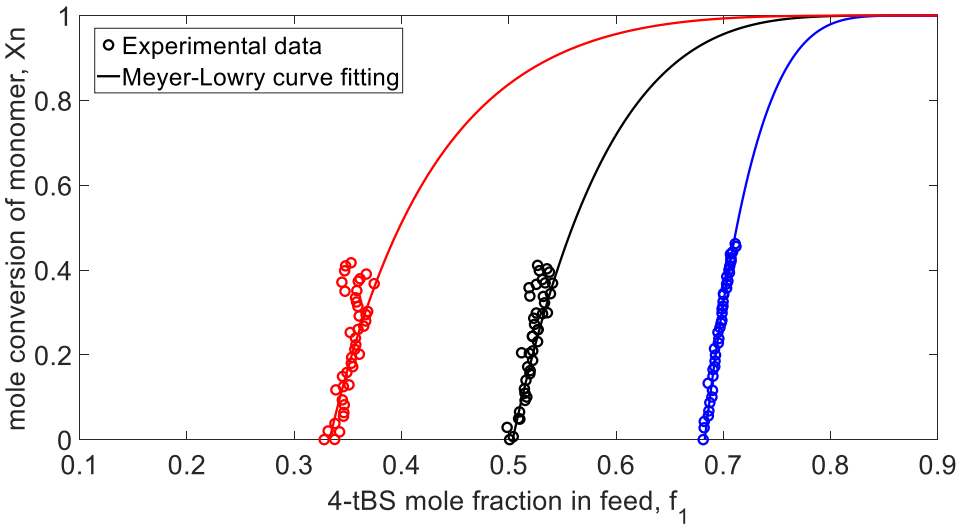

Figure 4.11 Fitting curves by the Meyer-Lowry method using the data from three sets of in situ NMR experiments for the copolymerization of 4-tert-butylstyrene and 3,4-dimethoxystyrene at 70 °C in toluene-d_8. Exp 7 (black), Exp 8 (red), Exp 9 (blue).

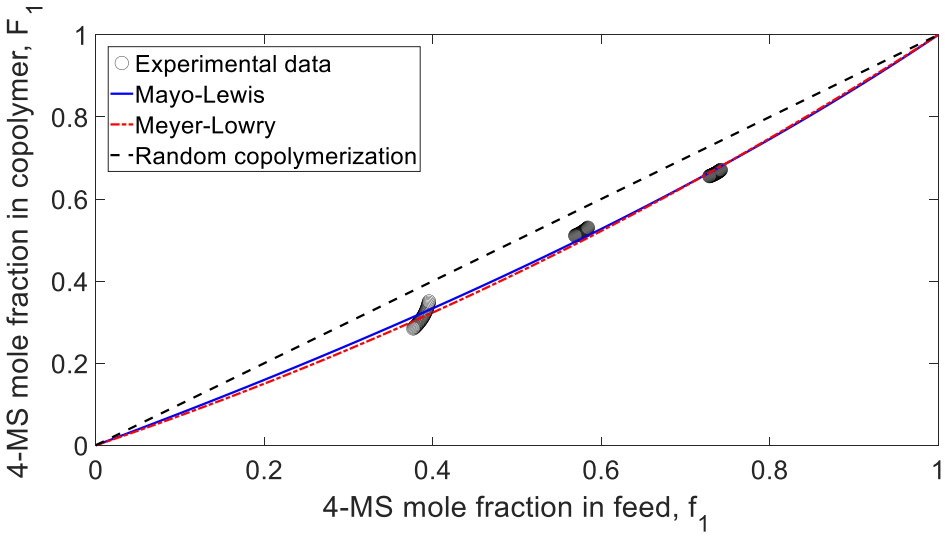

Figure 4.12 Fitting curve by the Mayo-Lewis method and compared with that by the Meyer-Lowry method, using the data from three sets of in situ NMR experiments for the copolymerization of 4-methylstyrene and 3,4-dimethoxystyrene at 70 °C in toluene-d_8.

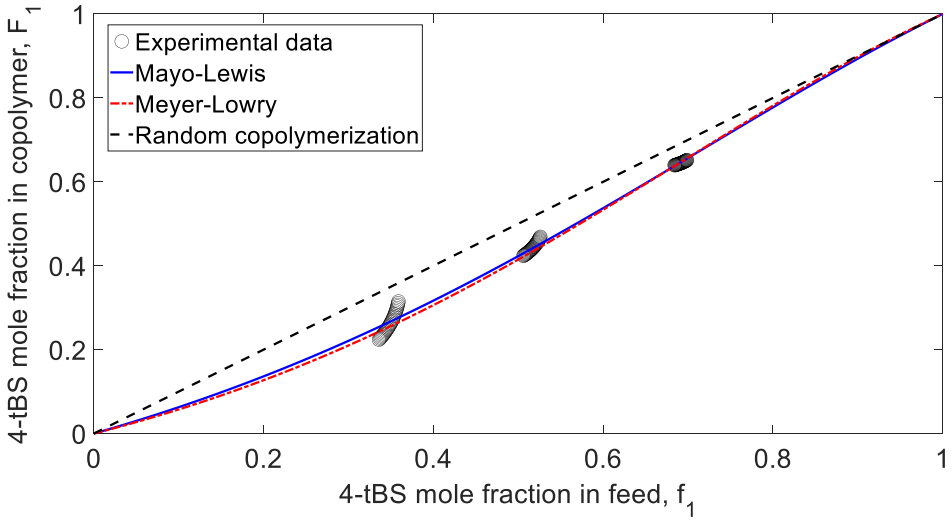

Figure 4.13 Fitting curve by the Mayo-Lewis method and compared with that by the Meyer-Lowry method, using the data from three sets of in situ NMR experiments for the copolymerization of 4-tert-butylstyrene and 3,4-dimethoxystyrene at 70 °C in toluene-d_8.

Table 4.3 Summary of Reactivity Ratios of all monomers from in-situ NMR.

Methods	Styrene and 3,4-DMS		4-MS and 3,4-DMS		4-tBS and 3,4-DMS	
	$r_{styrene}$	$r_{3,4\text{-DMS}}$	$r_{4\text{-MS}}$	$r_{3,4\text{-DMS}}$	$r_{4\text{-tBS}}$	$r_{3,4\text{-DMS}}$
Meyer-Lowry	0.84	1.55	0.76	1.43	1.07	1.93
Mayo-Lewis	0.89±0.04	1.53±0.06	0.72±0.04	1.31±0.07	1.00±0.05	1.73±0.08
Kelen-Tudos	0.90±0.04	1.57±0.05	0.71±0.04	1.30±0.06	0.98±0.06	1.72±0.08

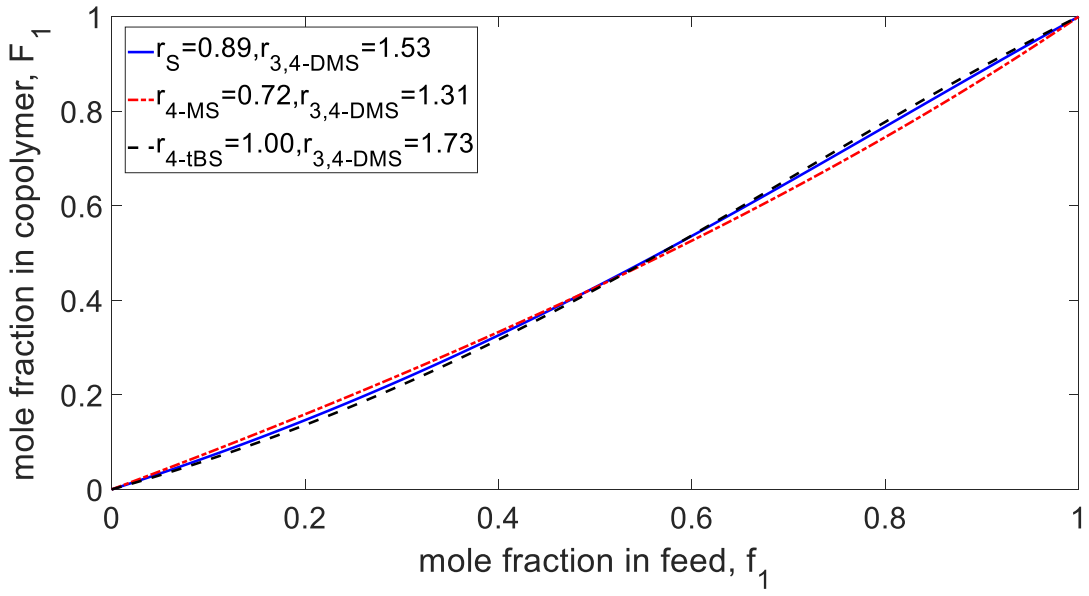

Figure 4.14 Comparison of F_1 versus f_1 curves for the three sets of reactivity ratios using NLLS of Mayo-Lewis.

Comparing to Lau and Burns and, Leibig et al.'s work, it is suggested the position of methoxy groups, and type of ether protection influences the reactivity ratio values of both monomers involved. The $r_{3,4\text{-DMS}} > r_{2,6\text{-DMS}}$ in free radical polymerization because the methoxy groups in the 3,4 position does not impede polymerization compared to the 2,6 position. Comparing 3,4 – DMS to 4VCA and 3VCA, the order of reactivity ratio is $r_{3VCA} > r_{3,4\text{-DMS}} > r_{4VCA}$ using K-T. In Leibig et al.'s work [16], the effect of bridged-ether position on reactivity in anionic polymerization was supported by ^{13}C-NMR showing

difference β-carbon shifts. These shifts reflect the charge distribution in the vinyl group. A higher chemical shift corresponds to a more positive charge at the β-carbon and thus making the monomer more susceptible to carbanions. The $r_{styrene}$ values computed in this work by free radical polymerization is not significantly lower than the value computed by Lau and Burns ($r_{styrene}$ =0.98) [13] but falls in between $r_{styrene}$ = 0.48 (3VCA) and 4.0 (4VCA) by Leibig et al. [16]. However, since all work had different variables such as monomer structure, reaction temperature, polymerization method, and solvent, these comparisons are not conclusive. Lastly, regarding the reactivity ratios of 4ms and 4tbs, these values are the first within this studied system and more work needs to be done to better understand the structure-reactivity relationship.

4.5 Conclusion

Free radical polymerization of 3,4 - DMS and para-substituted styrene derivatives were performed using AIBN in toluene-d_8 at 70 ° C and studied under *in-situ* NMR. Reactivity ratios were calculated using NLLS (Mayo-Lewis and Meyer-Lowry method) and LLS (K-T method), which showed similar results. The reactivity ratio of 3,4 – DMS and styrene was $r_{3,4\text{-DMS}}$ = 1.55 and $r_{styrene}$ = 0.84 (Meyer-Lowry), $r_{3,4\text{-DMS}}$ = 1.53 ± 0.06 and $r_{styrene}$ = 0.89 ± 0.04 (Mayo-Lewis) and $r_{3,4\text{-DMS}}$ = 1.57 ± 0.05 and $r_{styrene}$ = 0.90 ± 0.04 (K.T). Furthermore, the reactivity ratio of 3,4 – DMS and 4ms was $r_{3,4\text{-DMS}}$ = 1.43 and r_{4ms} = 0.76 (Meyer-Lowry), $r_{3,4\text{-DMS}}$ = 1.31 ± 0.07 and r_{4ms} = 0.72 ± 0.04 (Mayo-Lewis) and $r_{3,4\text{-DMS}}$ = 1.30 ± 0.06 and r_{4ms} = 0.71 ± 0.04 (K.T). Lastly, the reactivity ratio between 3,4 – DMS and 4-tbs was $r_{3,4\text{-DMS}}$ = 1.93 and r_{4tbs} = 1.07 (Meyer-Lowry), $r_{3,4\text{-DMS}}$ = 1.73 ± 0.08 and r_{4tbs} = 1.00 ± 0.05 (Mayo-Lewis) and $r_{3,4\text{-DMS}}$ = 1.72 ± 0.08 and r_{4tbs} = 0.98 ± 0.06 (K.T). All calculated reactivity ratios suggest the para-substitution have minor effect on its value and all copolymers adopt random chain sequence. However, this work only focused on changing the monomer concentration in the feed, therefore it is important to consider other factors such as temperature and solvent. Changing temperature affects the rate of monomer consumption whereas changing the solvent affects how monomers and radicals are solvated in the system. Doing so allows better understanding on how these focused monomers will react and how they become copolymers with their unique structure and properties.

4.6 References

[1] Reactivity Ratio - an overview | ScienceDirect Topics, (n.d.). https://www.sciencedirect.com/topics/engineering/reactivity-ratio (accessed March 26, 2021).

[2] Y. Liu, W.Z. Xu, P.A. Charpentier, Reactivity Ratios of MMA and N,N-Dimethyl-N-{2-[(2-methylprop-2-enoyl)oxy]ethyl}undecane-1-aminium Bromide in Thermal and UV Initiation Copolymerization, Ind. Eng. Chem. Res. 59 (2020) 8965–8973. https://doi.org/10.1021/acs.iecr.9b06413.

[3] J.M. Ting, T.S. Navale, F.S. Bates, T.M. Reineke, Precise Compositional Control and Systematic Preparation of Multimonomeric Statistical Copolymers, ACS Macro Lett. 2 (2013) 770–774. https://doi.org/10.1021/mz4003112.

[4] M. Fineman, S.D. Ross, Linear method for determining monomer reactivity ratios in copolymerization, Journal of Polymer Science. 5 (1950) 259–262. https://doi.org/10.1002/pol.1950.120050210.

[5] T. Kelen, F. TÜd[Otilde]s, Analysis of the Linear Methods for Determining Copolymerization Reactivity Ratios. I. A New Improved Linear Graphic Method, Journal of Macromolecular Science: Part A - Chemistry. 9 (1975) 1–27. https://doi.org/10.1080/00222337508068644.

[6] A. Habibi, E. Vasheghani-Farahani, M.A. Semsarzadeh, K. Sadaghiani, Monomer reactivity ratios for lauryl methacrylate–isobutyl methacrylate in bulk free radical copolymerization, Polymer International. 52 (2003) 1434–1443. https://doi.org/10.1002/pi.1238.

[7] M. Zhang, E.M. Carnahan, T.W. Karjala, P. Jain, Theoretical Analysis of the Copolymer Composition Equation in Chain Shuttling Copolymerization, Macromolecules. 42 (2009) 8013–8016. https://doi.org/10.1021/ma9018685.

[8] N.A. Lynd, R.C. Ferrier, B.S. Beckingham, Recommendation for Accurate Experimental Determination of Reactivity Ratios in Chain Copolymerization, Macromolecules. 52 (2019) 2277–2285. https://doi.org/10.1021/acs.macromol.8b01752.

[9] W.Z. Xu, P.A. Charpentier, FTIR Study Measuring the Monomer Reactivity Ratios for Ethylene−Vinyl Acetate Polymerization in Supercritical CO2, Ind. Eng. Chem. Res. 48 (2009) 1384–1390. https://doi.org/10.1021/ie801275g.

[10] W. Zhang, J. Allgaier, R. Zorn, S. Willbold, Determination of the Compositional Profile for Tapered Copolymers of Ethylene Oxide and 1,2-Butylene Oxide by In-situ-NMR, Macromolecules. 46 (2013) 3931–3938. https://doi.org/10.1021/ma400166n.

[11] M. Abdollahi, M. Sharifpour, A new simple procedure to calculate monomer reactivity ratios by using on-line 1H NMR kinetic experiments: Copolymerization system

with greater difference between the monomer reactivity ratios, Polymer. 48 (2007) 25–30. https://doi.org/10.1016/j.polymer.2006.11.010.

[12] A.-R. Mahdavian, M. Abdollahi, H.R. Bijanzadeh, Kinetic study of radical polymerization. III. Solution polymerization of acrylamide by 1H-NMR, Journal of Applied Polymer Science. 93 (2004) 2007–2013. https://doi.org/10.1002/app.20649.

[13] W.Y. Lau, C.M. Burns, Polymerization behavior of 2,6-dimethoxystyrene, Can. J. Chem. 47 (1969) 2057–2060. https://doi.org/10.1139/v69-330.

[14] D. Leibig, A.-K. Lange, A. Birke, H. Frey, Capitalizing on Protecting Groups to Influence Vinyl Catechol Monomer Reactivity and Monomer Gradient in Carbanionic Copolymerization, Macromolecular Chemistry and Physics. 218 (2017) 1600553. https://doi.org/10.1002/macp.201600553.

[15] J. Feng, O.O. Oyeneye, W.Z. Xu, P.A. Charpentier, In-Situ NMR Measurement of Reactivity Ratios for Copolymerization of Methyl Methacrylate and Diallyl Dimethylammonium Chloride, Ind. Eng. Chem. Res. 57 (2018) 15654–15662. https://doi.org/10.1021/acs.iecr.8b04033.

[16] D. Leibig, A.H.E. Müller, H. Frey, Anionic Polymerization of Vinylcatechol Derivatives: Reversal of the Monomer Gradient Directed by the Position of the Catechol Moiety in the Copolymerization with Styrene, Macromolecules. 49 (2016) 4792–4801. https://doi.org/10.1021/acs.macromol.6b00831.

Chapter 5

5 Conclusion and Future Works

5.1 Conclusion

In Chapter 3, nine catechol containing copolymers were synthesized using 3,4 – DMS and different para-substituted styrene derivatives with free radical polymerization. Deprotection of the methoxy groups were carried out using BBr_3. The protected and deprotected copolymers were characterized using ^{1}H-NMR, FTIR, GPC, TGA, and DSC. The copolymers were added to the denture formulations subjected to lap shear experiments. The summarized results of this chapter are listed as follows:

- ^{1}H-NMR, ^{13}C-NMR and FTIR confirmed successful free radical polymerization and deprotection of the methoxy groups.

- GPC of all protected copolymers P1-P and P2-P show they have molecular weight distribution close to 1.5 (based on Flory's most probable dispersity), whereas the P3-P series had a broad distribution attributing to the t-butyl group.

- TGA results of all protected copolymers P1A-P to P3C-P (except P3B-P) have one stage decomposition at around 400 ^{o} C regardless of substitution or monomer percentage.

- DSC results of all protected copolymers P1A-P to P3C-P show the order of glass transition temperature is P3-P > P2-P > P1-P due to substitution and size of pendant functional group.

- The copolymers P1A-P3C (except P1B and P2B) were added to denture adhesive formulations (F1-F7) and combined with control and PBS to generate F(P)-C-PBS formulations for lap shear. Lap shear results of all formulations were around ≥ 5 kPa, satisfying ISO 10873. Only Control-PBS and F1(P1A)-C-PBS followed pH effect on adhesion. F6(P3C)-C-PBS had a reverse pH effect on shear stress and

F7(P1C)-C-PBS remained consistent through out pH change. FTIR alone could not explain their adhesion results.

In Chapter 4, free radical polymerization of 3,4 - DMS and para-substituted styrene derivatives were performed using AIBN in toluene-d_8 at 70 ^{o} C and studied under *in-situ* NMR. Reactivity ratios were calculated using NLLS (Mayo-Lewis and Meyer-Lowry method) and LLS (K-T method), and they suggest the copolymers have random sequence. The reactivity ratios of 3,4 – DMS and selected styrene derivative were the following:

- 3,4 – DMS and styrene: $r_{3,4\text{-DMS}} = 1.55$ and $r_{styrene} = 0.84$ (Meyer-Lowry); $r_{3,4\text{-DMS}} = 1.53 \pm 0.06$ and $r_{styrene} = 0.89 \pm 0.04$ (Mayo-Lewis); $r_{3,4\text{-DMS}} = 1.57 \pm 0.05$ and $r_{styrene} = 0.90 \pm 0.04$ (K.T).

- 3,4 – DMS and 4ms: $r_{3,4\text{-DMS}} = 1.43$ and $r_{4ms} = 0.76$ (Meyer-Lowry); $r_{3,4\text{-DMS}} = 1.31 \pm 0.07$ and $r_{4ms} = 0.72 \pm 0.04$ (Mayo-Lewis); $r_{3,4\text{-DMS}} = 1.30 \pm 0.06$ and $r_{4ms} = 0.71 \pm 0.04$ (K.T).

- 3,4 – DMS and 4tbs: $r_{3,4\text{-DMS}} = 1.93$ and $r_{4tbs} = 1.07$ (Meyer-Lowry), $r_{3,4\text{-DMS}} = 1.73 \pm 0.08$ and $r_{4tbs} = 1.00 \pm 0.05$ (Mayo-Lewis) and $r_{3,4\text{-DMS}} = 1.72 \pm 0.08$ and $r_{4tbs} = 0.98 \pm 0.06$ (K.T).

5.2 Future Work and Recommendations

In Chapter 3, the copolymers had a small degree of crosslinking upon deprotection, this may have resulted as the HCl solution was open to the atmosphere. Another explanation can be the presence of dissolved oxygen in the acetone used to dissolve the polymer. One possible method to prevent this outcome can be conducting the deprotection of the copolymers in a closed system where it is oxygen free and solvent-grade acetone. The GPC indicated all copolymers have polydispersity indexes ≥ 1.50. To make the distribution narrower, RAFT polymerization can be applied. RAFT polymerization was the aim originally, however styrene systems, especially the derivatives having electron donating groups, requires more time to generate enough copolymers. Also, RAFT reagents are costly and comes in limited quantity, it is more

efficient to synthesize them given the starting materials are affordable. Structurally, maleic acid can be incorporated into the poly (3,4-DMS-co-styrene) chain to allow better miscibility in denture adhesive formulations. With regards to the lap shear testing, asides from pH, temperature also changes during a meal, which need to be considered while testing glued specimens. The specimens made only consisted of plexiglass which simulated the denture material, polyvinyl alcohol can be used to simulate skin. FTIR alone cannot explained lap shear results at different pH, other experimental work such as rheology, scanning electron microscopy, and swelling test needs to be done on formulations to better understand the physical properties of the formulations. Rheological properties can provide a measurement of cohesion of soft materials. In this work, all specimens showed cohesive failure and rheology can affirm the outcome of the lap shear testing. Swelling test, in conjunction with FTIR, will provide more insight of how PBS of different pH effect the rate of liquid adsorption of the adhesive formulations. Scanning electron microscopy can provide morphologic information such as pore size which contributes to how the formulation interacts with the substrates of interest. Lastly, the P2 and P3 catechol copolymer structures were synthesized for first time and it is vital to conduct their cytotoxicity test if they are to be deployed for wet adhesion applications. Like before, all formulations must be ≥ 5 kPa to satisfy ISO 10873 using American Standard Test Method (ASTM) F2255-5.

In Chapter 4, the *in-situ* NMR studies only had changes in monomer feed while keeping temperature and solvent constant. Other factors such as temperature and solvent polarity are important. The polarity of the solvent can affect how the monomers and radicals self-assemble in the mixture which effects chain formation. The temperature controls how much monomer is converted as a function of time. Knowing how these parameters affect reactions can provide more information when generating fitting curves using NLLS or LLS methods to build confidence towards experimental data. Lastly, the kinetic studies between 3,4 DMS and substituted styrene derivatives were studied for first time, it is worth exploring other DMS structures such as 2,6-DMS, and 2,3-DMS, plus 4-VCA and 3-VCA in the same FRP conditions for better comparison and contrast of reactivity ratios.

Curriculum Vitae

Name:	Vincent Ying Wun Kong
Post-secondary Education and Degrees:	Simon Fraser University Burnaby, BC, Canada 2007-2013 BSc in Chemistry The University of Western Ontario London, Ontario, Canada 2018-2021 MESc in CBE
Related Work Experience	Quality Assurance Technician AG Hair Cosmetics April 2014 – July 2014 Manufacturing Chemist Glustitch Inc. Sept 2014 – Sept 2018